Multi-GNSS Hybridization for precise positioning

Georgia Katsigianni

Université Fédérale
Toulouse Midi-Pyrénées

THÈSE

En vue de l'obtention du

DOCTORAT DE L'UNIVERSITÉ DE TOULOUSE

Délivré par l'Université Toulouse 3 - Paul Sabatier

Présentée et soutenue par

Georgia KATSIGIANNI

Le 15 novembre 2019

hybridation multi-GNSS pour le positionnement précis

Ecole doctorale : **SDU2E - Sciences de l'Univers, de l'Environnement et de l'Espace**

Spécialité : **Sciences de la Terre et des Planètes Solides**

Unité de recherche :
GET - Geosciences Environnement Toulouse

Thèse dirigée par
Felix PEROSANZ et Sylvain LOYER

Jury

M. Pierre BRIOLE, Rapporteur
M. Urs HUGENTOBLER, Rapporteur
M. Laurent MOREL, Examinateur
M. Guillaume RAMILLIEN, Examinateur
M. Felix PEROSANZ, Directeur de thèse
M. Sylvain LOYER, Co-directeur de thèse

Multi-GNSS Hybridization for Precise Positioning

Thesis Dissertation

of

Georgia Katsigianni

Toulouse, 2019

Acknowledgements

The present doctoral dissertation was prepared from research conducted during the academic years from November 2016 to November 2019 under the supervision of Dr. HDR Felix Perosanz and Dr. Sylvain Loyer. Financial support was shared by Centre National d'Etudes Spatiales (CNES) and Collecte Localisation Satellites (CLS Group). This thesis was prepared for the Doctoral School (Ecole Doctorale-ED) of "Geosciences, Astrophysics, Space and Environmental Sciences" ("Sciences de l' Univers, de l' Environnement et de l' Espace"-SDUEE) at Paul Sabatier University (Toulouse III).

First and foremost, I would like to deeply thank my two supervisors Felix Perosanz and Sylvain Loyer for giving me the opportunity to work on this PhD topic, for their valuable support and guidance and for our perfect cooperation during the whole time of my studies.

Secondly, I would like to acknowledge Flavien Mercier (CNES), Alvaro Santamaria (CRNS), Jean-Charles Marty (CNES), Jean-Michel Lemoine (CNES), Miriam Zoulida (CNRS), Mini Gupta (CNRS), Adrien Mezerette (CLS), Laetitia Versini (CLS) and Térence Desclaux (CLS) for their help, cooperation and for our fruitful discussions and exchange of ideas.

To the members of the Jury, Pierre Briole (ENS), Urs Hugentobler (TUM) and Laurent Morel (CNAM), I would like to give my gratitude for their willingness to read and examine my work and for their objective judgement. Additionally, I show appreciation to the members of my thesis committee Jean-François Crétaux (LEGOS/CNES), Paul Rebischung (LAREG/IGN), Flavien Mercier (CNES) and Alvaro Santamaria (CNRS) that followed my progress every year and gave me their advice.

I am also very grateful for the support of all my colleagues from CNES, CLS, CNRS and GET-OMP for their positive mood, humor and kindness. They all made my stay in 'The Pink City' during these three years very pleasant.

Last but not least, I would like to express my deepest gratitude to my family and to my fiancé Sean. Although they were very far away from me during these years, they were always giving their faith, support and patience. Finally, thanks to all my friends for their encouragement.

I thank you all!

Gina

Abstract in English

GNSS are widely used for precise positioning applications of geosciences and especially space geodesy. So far, mainly the existing GPS was extensively used for scientific applications. With the arrival of the new European Galileo system it became imperative to include the new system in the studies and check the new capabilities that it will bring as a system alone and as combined together with the others in a Multi-GNSS processing.

The CNES/CLS analysis center of the IGS is weekly calculating GNSS (GPS, GLONASS and Galileo) products that can be taken from any kind of user to perform precise positioning. A way to achieve the best accuracy possible is to resolve the unknown integer ambiguities of the phase measurements. Up until now, the CNES/CLS was performing ambiguity resolution to the GPS system using the zero-difference method. In this way they are able to deliver precise satellite orbits and precise clock products with phase fixed ambiguities.

The goal of this work was to implement and validate if the method can be also applied for the Galileo system. The method applied from the CNES/CLS is consisting of two further steps. The first one is the resolution of the Wide-Lane ambiguities. The Galileo Wide-Lane satellite biases have been proven to be stable over long periods of time. In addition, there is homogeneity in the way they are observed from different types of receivers. These findings were used and the Wide-Lane biases were successfully resolved with nearly 100% success rate percentage.

The second step of zero-difference method is the Narrow-Lane ambiguity resolution. This step was executed for the Galileo system together with the GPS system in a Multi-GNSS Precise Orbit Determination processing. Galileo ambiguity fixing success percentage is around 93%, nearly similar to the one of the GPS system. The integer property of the Galileo phase clocks is demonstrated. Both orbit overlaps and orbit validation using SLR validation methods showed that ambiguity resolution improves mainly in the normal and the along track direction. Galileo orbit overlaps in 3D RMS showed an improvement of around 50%, from around 7 cm to 3.5 cm. The results of this work were used by the CNES/CLS IGS AC that has announced the delivery of weekly Galileo precise orbits, clocks and Wide-Lane satellite biases. A new method is also introduced on how to compare ambiguity resolution results for a common overlapping period. This method is also used to speculate the agreement and the disagreement between two different daily solutions.

Finally, it was examined the post-processed kinematic PPP and PPP-AR using Galileo-only, GPS-only and Multi-GNSS (GPS + Galileo) constellations. The interest was to validate the accuracy for each GNSS system individually but also of their combination. Results showed that Galileo-only positioning accuracy is nearly at the same level of accuracy as GPS-only. The use of Galileo system improves the performance of the GPS positioning giving mm level repeatability. The contribution of Galileo ameliorates the positioning accuracy around 30% in all directions (comparison GPS PPP-AR and Multi-GNSS PPP-AR).

This proved that the Galileo constellation together with GPS will give improved precise positioning with respect to the current GPS-only.

All these are indications that the Galileo system will contribute to precise positioning required by geoscience applications through a Multi-GNSS (GPS + Galileo) solution.

Key Words

GNSS, Galileo, GPS, Multi-GNSS, Ambiguity Resolution, Zero-difference, PPP, PPP-AR, IPPP, Precise Positioning

Résumé en Français

Les systèmes GNSS sont largement utilisés pour les applications de positionnement précis en géosciences, et en particulier en géodésie spatiale. Jusqu'à présent, les mesures du système GPS sont principalement utilisées seules pour des applications scientifiques. L'arrivée de la constellation européenne Galileo, rend possible les études sur ce nouveau système pour vérifier ses capacités et ses possibilités seul ou combiné avec GPS dans un traitement Multi-GNSS.

Le centre d'analyse CNES/CLS de l'IGS calcule de manière hebdomadaire les produits GNSS (GPS, GLONASS et Galileo) ; ces produits sont utilisés pour les applications scientifiques de positionnements précis. Un moyen d'obtenir la meilleure précision possible consiste à résoudre les ambiguïtés entières, inconnues, des mesures de phase. Jusqu'à présent, le centre d'analyse CNES/CLS effectue une résolution d'ambiguïté sur les observations GPS en utilisant la méthode zéro-différence et fournit les orbites et les horloges précises des satellites avec des ambiguïtés de phase fixées.

L'objectif de ce travail est d'implémenter et valider si la méthode zéro-différence peut également être appliquée au système Galileo. Celle-ci comprend deux étapes. La première est la résolution des ambiguïtés de la combinaison Wide-Lane ; il est prouvé que les biais des satellites Galileo Wide-Lane sont stables sur de longues périodes et homogènes pour les différents types de récepteurs. Ces résultats ont permis de résoudre les biais Wide-Lane avec un taux de réussite proche de 100%.

La deuxième étape de la méthode de zéro-différence est la résolution des ambiguïtés Narrow-Lane. Cette étape a été mise en œuvre pour le système Galileo dans un traitement de détermination précise de l'orbite multi-GNSS (avec les données GPS). Le pourcentage de succès de Galileo en matière de résolution des ambiguïtés atteint environ 93%, ce qui est similaire au système GPS. La propriété entière des horloges de phase Galileo permettant d'utiliser ces calculs au niveau utilisateur est démontrée. Les recouvrements d'orbite et « le Satellite Laser Ranging » utilisés pour valider les orbites obtenues ont montré une amélioration d'environ 50% des RMS3D (d'environ 7 cm à 3,5 cm) principalement dans les directions normales et tangentielles. Les résultats de ces travaux ont pu être appliqués aux produits du CA IGS CNES/CLS qui a commencé la livraison des produits « entiers » Galileo (orbites précises horloges et biais Wide-Lane satellites). D'autre part nous avons proposé une nouvelle méthode de comparaison des ambiguïtés.

Enfin, des traitements PPP et PPP-AR cinématiques sont réalisés en utilisant des mesures des constellations Galileo et GPS seules ou dans un traitement Multi-GNSS (GPS + Galileo). L'intérêt est de valider la précision de chaque système GNSS individuellement mais aussi de vérifier leur compatibilité et de mesurer l'intérêt de traitement combinés. Les résultats ont montré que la précision de positionnement du système Galileo utilisé seul est pratiquement du même niveau

que celle obtenue avec le système GPS. D'autre part l'utilisation conjoint des deux systèmes améliore les performances du positionnement GPS en offrant une répétabilité au niveau millimétrique et un gain de précision de positionnement d'environ 30% dans toutes les directions (comparaison GPS PPP-AR et Multi-GNSS PPP-AR).

Tout cela indique que le système Galileo peut contribuer de manière significative au positionnement précis requis par les applications de géoscience via une solution Multi-GNSS (GPS + Galileo).

Mots clés

GNSS, Galileo, GPS, Multi-GNSS, Résolution des ambiguïtés, zéro-différence, PPP, PPP-AR, IPPP, Positionnement précis

Acronyms

AC	Analysis Centers
ACC	Analysis Center Coordinator
ADEV	Allan Deviation
ANTEX	Antenna Exchange Format
APC	Antenna Phase Center
AR	Ambiguity Resolution
BDS	BeiDou Navigation Satellite System
CNES	Centre National d'Etudes Spatiales
CLS	Collecte Localisation Satellites
CODE	Center for Orbit Determination in Europe
COSPAS	Space System for Search of Distress Vessels
DoD	Department of Defense
DORIS	Doppler Orbitography and Radiopositioning Integrated by Satellite
DOY	Day of Year
EC	European Commission
ESA	European Space Agency
FOC	Full Operational Capability
GGOS	Global Geodetic Observing System
GGTO	GPS to Galileo Time Offset
GIA	Glacial Isostatic Adjustment
GIOVE	Galileo In-Orbit Validation Element
GIS	Geographic Information Systems
GLONASS	Globalnaya Navigatsionnaya Sputnikovaya Sistema
GNSS	Global Navigation Satellite Systems
GPS	Global Positioning System
GRGS	Groupe de Recherche de Géodésie Spatiale (Space Geodesy Research Group)
GSA	European Global Navigation Satellites Systems Agency
GST	Galileo System Time
GTRF	Galileo Terrestrial Reference Frame
HAS	High Accuracy Service
IAG	International Association of Geodesy
IAU	International Astronomical Union
IERS	International Earth Rotation and Reference Systems Service
IGS	International GNSS Service
ILRS	International Laser Ranging Service
IOV	In-Orbit Validation
IPPP	Integer Precise Point Positioning
IRNSS	Indian Regional Navigation Satellite System

ISB	Inter-system Bias
ITRF	International Terrestrial Reference Frame
IVS	International VLBI Service for geodesy and astrometry
LEO	Low Earth Orbit
LOD	Length of Day
LSE	Least Squares Estimation
MEO	Medium Earth Orbit
MGEX	Multi-GNSS Experiment
NAGU	Notice Advisory to Galileo Users
NAVIC	Navigation Indian Constellation
NL	Narrow Lane
NRCan	Natural Resources Canada
OS	Open Service
PCO	Phase Center Offset
PCV	Phase Center Variation
PE-90	Parameters of the Earth 1990 (GLONASS geodetic datum)
PM	Polar Motion
POD	Precise Orbit Determination
PPP	Precise Point Positioning
PPP-AR	Precise Point Positioning with Ambiguity Resolution
PPS	Precise Positioning Service
PRS	Public Regulated Service
QZSS	Quasi-Zenith Satellite System
RMS	Root Mean Square
VLBI	Very-Long-Baseline Interferometry
SARSAT	Search and Rescue Satellite-Aided Tracking
SBAS	Space-based augmentation systems
SLR	Satellite Laser Ranging
SPS	Standard Positioning Service
TAI	International Atomic Time
WGS-84	World Geodetic System 1984
WL	Wide Lane
UN	United Nations
UN-GGIM	United Nations initiative on Global Geospatial Information Management
UTC	Universal Time Coordinated
VLBI	Very Long Baseline Interferometry

Table of Contents

1. Introduction

1.1 Introduction in English

Global Navigation Satellite Systems (GNSS) like the existing American GPS, the Russian GLONASS or the forthcoming European Galileo and Chinese Beidou are intensively used for precise scientific applications thanks to permanent progress of instruments, algorithms and software. The necessity of improving the quality of the realization of the reference systems (e.g. ITRF) is critical in numerous fields of geosciences (sea level rise surveying, tectonics, etc.) and has been the object of a UN resolution in 2015. Facing these challenges, GNSS's are and will remain a necessity. They bring an essential and more and more precise information as new constellations and new signals are integrated into the current processing.

The CNES/CLS International GNSS Service (IGS) Analysis Center (AC) is routinely processing data from a global network of GPS, GLONASS and Galileo receivers with the goal of reaching the highest accuracy. The corresponding products are precise satellite orbit and clock solutions, station coordinates, Earth orientation parameters as well as hardware biases needed by users. The recent Multi-GNSS experiment (MGEX) of the IGS allowed the development of a global network of stations using a new generation of receivers, able to track a large variety of signals including the new satellites constellations.

One of the main issues in order to access the highest positioning accuracy possible is fixing the unknown ambiguities of the GNSS phase measurements. This tricky exercise has deserved hundreds of publications in the past and two main approaches can be identified. The historical one is based on the double-differencing of raw observations between pairs of satellites and pairs of receivers. More recently, CNES/CLS AC have demonstrated the success of strategies based on undifferenced GPS observations, the so-called zero-difference or undifferenced ambiguity resolution method. Basically, this method consists of two steps: The Wide-Lane ambiguity fixing and the Narrow-Lane ambiguity fixing. This method has been used both for calculation of satellite orbits and for precise positioning.

The Multi-GNSS solution done from the CNES/CLS AC is based on the simultaneous processing of undifferenced GPS, GLONASS and Galileo observations. However, at the beginning of the present thesis, only GPS phase ambiguities were fixed to integer values.

This thesis is focused on the implementation of the undifferenced strategy of ambiguity resolution for the Galileo system within a Multi-GNSS processing. The study consists of two target goals. The first goal was to examine the applicability of the zero-difference method to the Galileo system. Efforts are then made in order to be able to achieve the best Galileo orbit and clock products possible within a Multi-GNSS Precise Orbit Determination (POD) processing. Products for Galileo precise satellite orbits and clocks are to be delivered to the users from the CNES/CLS AC.

Later the second goal is to use the Multi-GNSS precise satellite orbits and clocks to be able to perform precise positioning with the best accuracy possible. This may be done through the Precise Point Positioning (PPP) method. The performance capabilities of the PPP method are also checked using the zero-difference method for fixing the phase ambiguities. This is the so-called PPP-AR (PPP with ambiguity resolution) or IPPP (integer PPP). Combinations of Galileo, GPS are tested to validate their precise positioning capabilities.

The overall objective is to examine what will be the new possibilities that the new Galileo system will bring in terms of precise positioning and how it can benefit the scientific community and especially geo-sciences.

1.2 Introduction en Français

Les systèmes globaux de navigation par satellite (GNSS), tels que les actuels systèmes GPS (Américain) et GLONASS (Russe) ou les futurs systèmes Galileo (européen) et Beidou (Chinois), sont utilisés de manière intensives pour les applications scientifiques de positionnement précis grâce au progrès permanent des instruments, des algorithmes et des logiciels. La nécessité d'améliorer la qualité de la réalisation des systèmes de référence (ITRF, par exemple) est essentielle dans de nombreux domaines des sciences de la terre (mesure du niveau moyen des mers, tectonique, etc.) et a fait l'objet d'une résolution des Nations Unies en 2015. Pour relever ces défis, les GNSS sont et resteront une nécessité. Ils apportent une information essentielle et de plus en plus précise au fur et à mesure que des nouvelles constellations et de nouveaux signaux sont intégrés aux traitements.

Le Centre d'Analyse (CA) CNES/CLS du Service GNSS International (IGS) traite régulièrement les données d'un réseau global de récepteurs GPS, GLONASS et Galileo dans le but d'atteindre la plus grande précision. Les produits correspondants sont des solutions d'orbite précises et d'horloge de satellite, des coordonnées de stations, des paramètres d'orientation de la Terre ainsi que les biais utiles aux utilisateurs. La récente expérience Multi-GNSS (MGEX) de l'IGS a permis de développer un réseau mondial de stations utilisant une nouvelle génération de récepteurs, capables de suivre une grande variété de signaux, y compris les nouvelles constellations de satellites.

L’un des problèmes principaux pour obtenir la plus grande précision de positionnement possible est de résoudre les ambiguïtés inconnues des mesures de phase GNSS. Cet exercice délicat a déjà fait l’objet de centaines de publications et deux approches principales peuvent être identifiées. L’approche historique repose sur la double différenciation des observations brutes entre des paires de satellites et des paires de récepteurs. Plus récemment, le CA CNES/CLS a démontré le succès des stratégies basées sur des observations GPS non différenciées ; la méthode ‘undifferenced’ ou ‘zero-difference’. Cette méthode consiste essentiellement en deux étapes : la correction de l'ambiguïté Wide-Lane et la résolution de l'ambiguïté Narrow-Lane. Cette méthode a été utilisée pour le calcul des orbites de satellites mais aussi pour le positionnement précis.

La solution Multi-GNSS réalisée par le CA CNES/CLS repose sur le traitement simultané d’observations non différenciées de GPS, GLONASS et Galileo. Cependant, au début de la présente thèse, seules les ambiguïtés de phase GPS étaient fixées à des valeurs entières.

Cette thèse est axée sur la mise en œuvre de la stratégie non différenciée de résolution des ambiguïtés du système Galileo au sein d’un traitement Multi-GNSS. L’étude comprend deux objectifs. Le premier objectif était d'examiner l'applicabilité de la méthode ‘zero-difference’ pour le système Galileo. Des efforts sont ensuite déployés afin de pouvoir obtenir les meilleurs produits d’orbite et d’horloge Galileo possibles dans le cadre d’un traitement de détermination précise de l’orbite (POD) Multi-GNSS. Les produits pour les orbites et les horloges satellites précises de Galileo sont mis à la disposition des utilisateurs par le CA CNES / CLS.

Ensuite, le deuxième objectif consiste à utiliser les orbites et les horloges satellitaires précises du satellite Multi-GNSS afin de pouvoir effectuer un positionnement précis avec la meilleure précision possible. Cela peut être fait par la méthode de positionnement de point précis (PPP). Les performances de la méthode PPP sont également évaluées au travers du processus de résolution des ambiguïtés de phase. C'est ce que l’on appelle le PPP-AR (PPP with Ambiguity Resolution) ou IPPP (Integer PPP). Les combinaisons de Galileo et de GPS sont testées pour valider leurs capacités de positionnement précis.

L’objectif général est d’examiner les possibilités offertes par le nouveau système Galileo en termes de positionnement précis et les avantages que la communauté scientifique peut en retirer en particulier pour les géosciences.

Ces travaux seront poursuivis pour quantifier l’impact de Galileo d’une part, sur la réalisation des systèmes de référence terrestres et sur le mode PPP (Positionnement Ponctuel Précis) pour le suivi de mobiles scientifiques.

Les travaux ont montré la haute qualité de positionnement précis en utilisant le système Galileo seul - au niveau du mm- avec un post-traitement en mode cinématique. Ce mode PPP (Positionnement Ponctuel Précis) pourra être utilisé pour de nombreuses applications scientifiques.

1.3 Outline of the thesis dissertation

Chapter 2 - GNSS in science

A general introduction is given about Space Geodesy, the IAG association and the GGOS component. Later an overview is given about the GNSS systems and about how these systems can contribute to the goals of GGOS as an important space geodetic technique. Additionally, the IGS service is described together with a description of the activities of the CNES/CLS AC.

Chapter 3 - GNSS Measurements

The basic GNSS observations used for geodesy are described. It is presented the problem of carrier phase ambiguities and the zero-difference ambiguity resolution method. The two steps of this method are further analyzed: The WL ambiguity fixing and the Narrow-Lane ambiguity fixing.

Chapter 4 - Galileo Wide-Lane AR

In this chapter the potentiality to use the zero-difference method for the Galileo system is examined and verified. The Galileo Wide-Lane ambiguity resolution is realized and the first step of the method is completed.

Chapter 5 - Galileo Narrow-Lane AR

This chapter focuses on fixing the Galileo Narrow-Lane ambiguities together with GPS in a Multi-GNSS POD processing. Products for orbit and clocks are validated through several ways. It was seen an improvement in orbit and clock overlaps. The integer property of the clocks is also verified. Investigations were made about the inter-system biases between GPS and Galileo. In addition, a new method is introduced about how to perform overlaps of AR matrices.

Chapter 6 - Precise Point Positioning

Precise orbit, clock and satellite biases products are used to perform precise positioning. Solutions from Galileo-only, GPS-only and their combination in a Multi-GNSS processing are compared for kinematic post-processed PPP and PPP-AR positioning. Examples of few stations are shown more in detail and results from an overall global network are given.

Conclusions and Suggestions

Finally, the overall conclusions from all the chapters are gathered and some suggestions are given for further improvement of the precise positioning.

2. GNSS in science

2.1 Introduction

Since the very beginning of human existence, people started questioning and studying the world that revolved around them. This gave birth to science and its many diverse branches. Today's modern science can be divided mainly in the following big categories: natural sciences (e.g. physics, chemistry, Earth sciences, etc.), social sciences (e.g. psychology, sociology etc.), formal sciences (e.g. mathematics, computer science) and applied sciences (e.g. engineering) (Bunge, 1998). The category of Earth sciences comprises all scientific domains that study planet Earth. One of them is Geodesy that studies the shape, the size and the gravity of the Earth.

Space geodesy is the field of geodesy that is using space techniques (mainly artificial satellites) in order to study the Earth. So far, the space geodetic techniques (GNSS, DORIS, SLR, VLBI etc.) contribute to various space geodetic applications: i.e. definition and realization of the International Terrestrial Reference Frame (ITRF), terrestrial kinematics, study of the Earth's rotations etc.

In this chapter an introduction is given about the different study interests of Space Geodesy, the way they are formally organized through commissions, services and the GGOS component. After describing the goals of GGOS, an overview is given to the GNSS systems and to how these systems can contribute to these goals as an important space geodetic technique.

2.2 The science of Geodesy

Geodesy is the field of Earth science which studies and measures the shape and orientation of the Earth and their variations in time (NOAA, 2018). The term itself is coming from Ancient Greek: γῆ + δαίω which literally means 'to divide the Earth'.

The scientific organization of International Association of Geodesy (IAG), founded in 1862, defines geodesy as:

"the science concerned with the Shape, Size, and the Gravity Field of the Earth" (IAG, n.d.)

The following figure (Fig. 2.1) represents the three pillars of geodesy. In order to measure accurately the shape (referred in the figure as 'geokinematics'), the gravity field and Earth's orientation (i.e. 'Earth rotation') and how these all change in time it is essential to have an adequate reference frame. As shown in the figure each pillar is intersecting with the others on the grounds of common Earth processes.

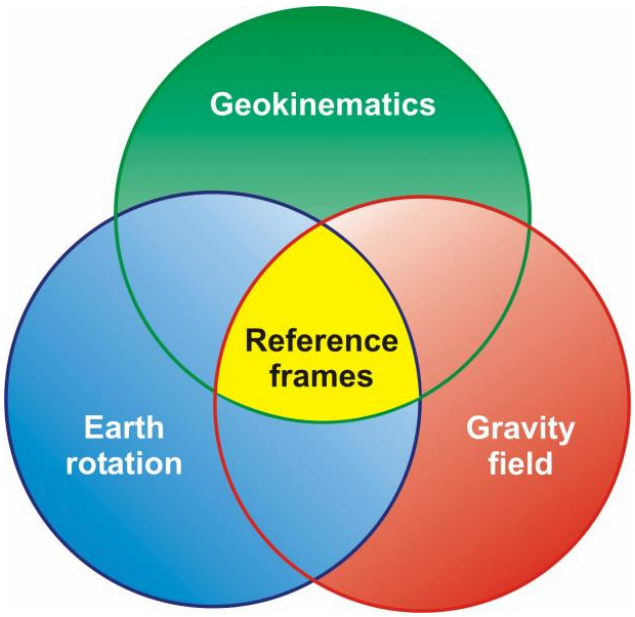

Fig. 2.1: The three pillars of Geodesy (GGOS, n.d.)

The IAG is an organization of scientists and researchers in the field of geodesy. Its mission is the advancement of geodesy and in general of understanding and representing better the shape, rotation and gravity field of the Earth and other planets.

To organize better its goals, the IAG has various components and actions. Some of these include:

- Commissions
- Services
- The Global Geodetic Observing System (GGOS)

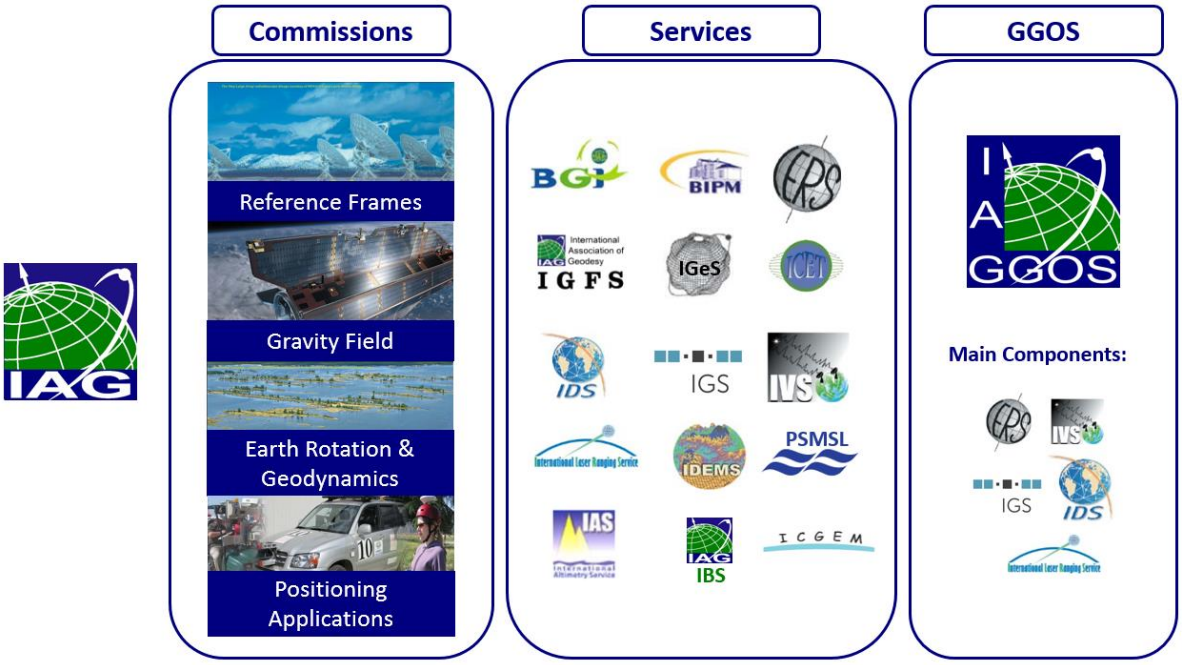

Fig. 2.2: The IAG and some of its main components: Commissions, Services, GGOS

The four commissions have as a goal to deal with several scientific topics. Commission 1 is interested in reference frames, both global and regional and its variations in time and their change due to tectonic plate motion, Earth's rotation axis and center of mass changes. Commission 2 is promoting research in the area of the Earth's gravity field as its change in time caused by several terrestrial and extraterrestrial reasons. Regarding the Earth as a 'living' planet, Commission 3 is studying the deformation of the Earth's crust and mass transports and the results these geodynamic effects have to the Earth's rotation and Length of Day (LOD). Finally, the last commission focuses on positioning and navigation applications. In this domain the GNSS system play an important role to support in surveying, engineering, precise navigation and Geographical Information Systems (GIS) (IAG, n.d.).

To achieve all these, the IAG is comprising various scientific services that specialize for every single domain of interest (e.g. Altimetry, Earth tides, Geoid etc.) and provides scientific products to the community. A few of these services that are cited extensively in the present thesis are: the International GNSS Service (IGS) and the International Earth Rotation and Reference Systems Service (IERS) (IAG, n.d.).

2.3 The Global Geodetic Observing System (GGOS)

The GGOS was initiated from the IAG in 2003, in order to encourage the use of geodetic applications and to provide measurements related to the Earth's shape, rotation and gravity field, with a view to observe the Earth's dynamic system changes. In order to do so, GGOS is

comprising several IAG services (i.e. IGS, IERS, International VLBI Service for Geodesy and Astrometry (IVS), International Laser Ranging Service (ILRS), International DORIS Service (IDS) etc.) that deliver products on a constant basis. The geodetic techniques used by the IAG services are namely space- and ground-based geodetic techniques such as: Very-Long-Baseline Interferometry (VLBI), Satellite Laser Ranging (SLR), Doppler Orbitography and Radiopositioning Integrates by Satellite (DORIS), GNSS, gravity satellite missions in Low Earth Orbits (LEO) orbits etc. (GGOS, 2016a) (IAG, n.d.). In Fig. 2.3 a graphic representation of the different space geodetic techniques is given.

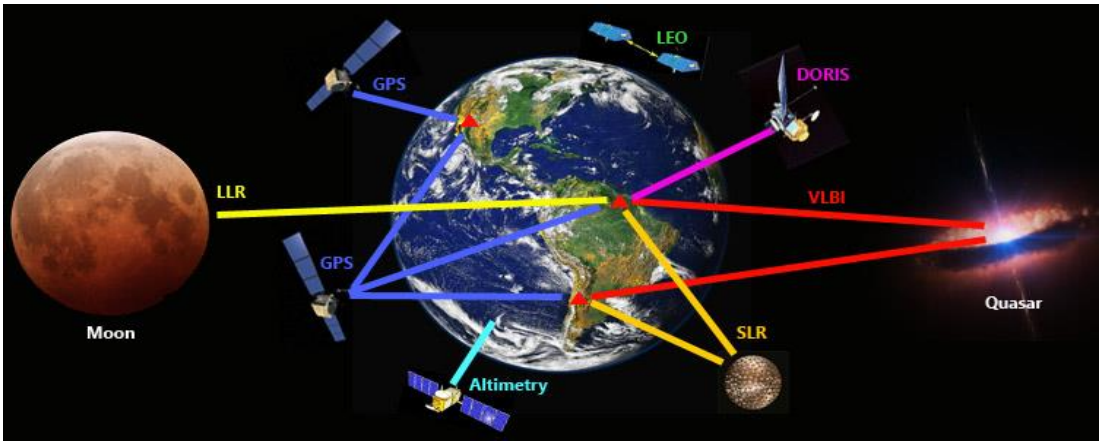

Fig. 2.3: Space and Ground- geodetic techniques used by the GGOS (IAG, n.d.)

The GGOS main vision is:

"to understand the dynamic Earth system by quantifying our planet's changes in space and time" (GGOS, 2016a)

The main points of interest of the GGOS comprise (GGOS, 2016a):

- To furnish any observations necessary for the study of the Earth's shape, rotation and mass distribution variations
- To provide the reference frame needed for any other scientific and societal purposes
- To benefit science and society by educating the importance of geodetic research benefits

All these goals are categorized and divided in four GGOS focus areas (GGOS, 2016b):

- Geohazards
- Sea Level change, Variability and Forecasting
- Unified Height System
- Geodetic Space Weather Research

2.4 The GNSS systems

The Global Navigation Satellite Systems (GNSS) are satellite-based systems that are generally used for positioning, navigation and precise time purposes. These systems are widely used also for various other applications (transportation, military, location-based services etc.) including scientific applications (ex. geodesy, surveying, precise time synchronization etc.) (ESPI, et al., 2017). As mentioned above they contribute also to the goals of GGOS as one of the space geodetic techniques.

Until now, there are two fully operational systems: the American Global Positioning System (GPS) and the Russian GLObalnaya NAvigatsionnaya Sputnikovaya Sistema (GLONASS). These two systems are widely used even from the 1980's. However, the global community has realized the importance of such systems: Another two systems are under development, the European Galileo and the Chinese Beidou (previously called COMPASS). Apart from those four global coverage systems there are also regional GNSS systems such as the Japanese Quasi-Zenith Satellite System (QZSS) and the Indian Regional Navigation Satellite System (IRNSS) (operational name: NAVigation with Indian Constellation (NAVIC)).

The GPS system

The GPS system is owned by the United States government and was initially developed for military purposes by the Department of Defense (DoD) in 1973. The civilian use started in the 80's and it paved the way for many geodetic uses. Until today many generations of satellites have passed (i.e. the newest being the Block I, nowadays the modernized GPS (GPS III) satellites belong to Block III –A or F) (US Department of Transportation, 2008). The GPS geodetic reference system is the World Geodetic System 1984 (WGS-84). With respect to time reference, the GPS time scale is related to the International Atomic Time (TAI) with a constant offset of 19sec. TAI and the Universal Time Coordinated (UTC) differ by a number of seconds. The GPS is providing two kinds of services: the Standard Positioning Service (SPS), used for civilian purposes, and the Precise Positioning Service (PPS), dedicated to authorized users (Hofmann-Wellenhof, et al., 2008).

The GLONASS system

In the decade of 70's the former Union of Soviet Socialist Republic (USSR) started the development of the GLONASS system. The completion of the system took place in 1996. It is operated by the Russian military forces and it is used mainly as a military system. In 2004, however, the Russian government decided to provide an open access for civilian purposes. Currently, GLONASS is under modernization program. The GLONASS geodetic reference frame is the PE-90 (also known in Russian as PZ-90). With respect to the time reference, the GLONASS

time is very closed to the UTC time with a constant offset of 3hr due to the difference between Moscow and Greenwich time (Hofmann-Wellenhof, et al., 2008).

The Galileo system

Galileo is the European GNSS system. It is developed by the European Commission (EC), the European Space Agency (ESA) and it is operated by the European GNSS Agency (GSA). The main purpose of this system is to be an open, global system of civilian use, compatible and interoperable with the GPS.

The first two satellites were the Galileo In-Orbit Validation Element (GIOVE) A and B that were test satellites (during the definition phase). In the In-Orbit Validation (IOV) phase, four experimental prototype satellites (that also carry the name IOV) where launched in orbit, in order to secure the frequency and to initially validate the system through tests (ESA, 2014). The completion of the constellation consists of the Full Operational Capability (FOC).

The European GNSS Agency declared initial services in 2016, moving from the test phase to the provision of services (GSA, 2018) (GSA, 2016). The next phase, the deployment phase, consists of launching the rest of the satellites and complete the ground segment. Full Operational Capability (FOC) is scheduled (at the time of this thesis publication) for 2020 with the launch of the last four satellites (ESA, 2019).

The geodetic reference frame of the Galileo system is called Galileo Terrestrial Reference Frame (GTRF) and is related to the International Reference Frame (ITRF). The Time reference is called Galileo System Time (GST) and has a constant offset to the TAI time. The difference of GPS time and GST, also called GPS to Galileo Time Offset (GGTO) is going to be distributed to the users.

As of 2019, the Galileo system will provide the following services to the users (GSA, 2018):

- Open Service (OS) that provides positioning and timing services freely to the users.
- High Accuracy Service (HAS) that is an extra service complementing the OS by delivering extra information
- Public Regulated Service (PRS) targeted to government-authorized users
- Search and Rescue Service (SAR) that is a service based on rescue alert system and it is the European participation to the COSPAS-SARSAT rescue system

The following Tab. 2.1 is showing some of the characteristics of the three GNSS systems that are studied in the present thesis (Hofmann-Wellenhof, et al., 2008).

GNSS System	GPS	GLONASS	Galileo
System's logo			
Origin	USA	Russia	Europe
Constellation	6 planes	Walker (24/3/1)	Walker (24/3/1)
Orbital Plane Separation	60°	120°	120°
Altitude	20180km	19130km	23222km
Revolutions / Sid. Days	2 / 1	17 / 8	17 / 10
Orbital Inclination	55°	65°	56°
Semimajor Axis	26560km	25508km	29601km
Revolution period	11h 58m	11h 16m	14h 04h
Main Frequencies	L1 / L2	G1 / G2	E1 / E5a
Time System	GPS time (UTC)	GLONASS time (UTC)	Galileo System time
Services	SPS, PPS	SPS, PPS	OS, HAS, PRS, SAR
Geodetic Reference	WGS-84	PE-90	GTRF
Number of satellites (Aug. '20)	32	27	24

Tab. 2.1: Some characteristics for GPS, GLONASS and Galileo

2.5 The GNSS systems as a geodetic technique

The GNSS systems apart from navigation and timing applications are an important space geodetic technique. The GPS system (as it was the first completed and operational GNSS system) gave rise to the use of GPS as a geodetic technique (Bock & Melgar, 2016). It was realized that when using GPS phase measurements (of L1 and L2 frequency bands) for relative positioning of a baseline of many km, it can give mm to cm level positioning accuracy (Bossler, et al., 1980) (Remondi, 1985). This started the development of worldwide baselines and finally a global network of GPS stations in the 1980s under civilian purposes. The advantage of using such a network was the amelioration of satellite orbit precision (Bock & Melgar, 2016). Nowadays, precise GNSS positioning is possible in the order of mm to cm levels in post-processed (Precise Point Positioning (PPP), Double Differenced (DD) Positioning) and real-time modes (Real Time Kinematic (RTK)).

Many scientific areas take advantage of this high precision positioning capability. To name a few, some of the numerous applications are:

- In the area of reference systems and frames: GNSS systems contribute to the ITRF construction together with other space-geodetic techniques. They help to provide geographic density because the GNSS network is denser with respect to the other techniques (See Fig. 2.4). They can also provide access to the ITRF (Altamimi, 2018).
- In the area of Earth rotation studies: The GNSS systems provide information to the IERS about Polar Motion (PM), Polar Motion Rates (PM rate) and Length-of-day (LOD).
- In the area of geohazards: by providing with the accurate positioning and timing information used to detect changes in motion or surfaces e.g. for studying earthquake faults, landslides and rock falls, volcano eruptions, that can as well be used by early warning systems (i.e. in case of Tsunami incidents) etc. (GGOS, 2016c) (GGOS, 2007).
- In the area of sea level studies by localizing (especially in vertical land movements) tide gauges that help gravity changes and sea level observations (GGOS, 2016d). They help to study tides, and any other seasonal and longer-term variations in water transport (Bock & Melgar, 2016).
- In the area of climate research: they give information about sea level rise, ice mass loss, changes in the cryosphere, ocean thermal expansion due to warming. They can contribute to the change of climate caused by anthropogenic sources: i.e. change of the land surface caused by the extraction of water, oil and minerals (Bock & Melgar, 2016).
- In the area of tectonic and volcano geodesy: Trough GNSS temporal series it is possible to study any crustal deformation of the solid Earth, earthquakes, glacial isostatic adjustment (GIA) due to long-term glacial retreat.
- In the interdisciplinary area of geodetic space weather research, they participate together with other geodetic techniques to provide information about the state of ionosphere and other atmospheric processes (GGOS, 2016e). The IGS is also delivering atmospheric products regarding the tropospheric Zenith Path Delay (ZPD) and ionospheric Total Electron Content (TEC) grid.

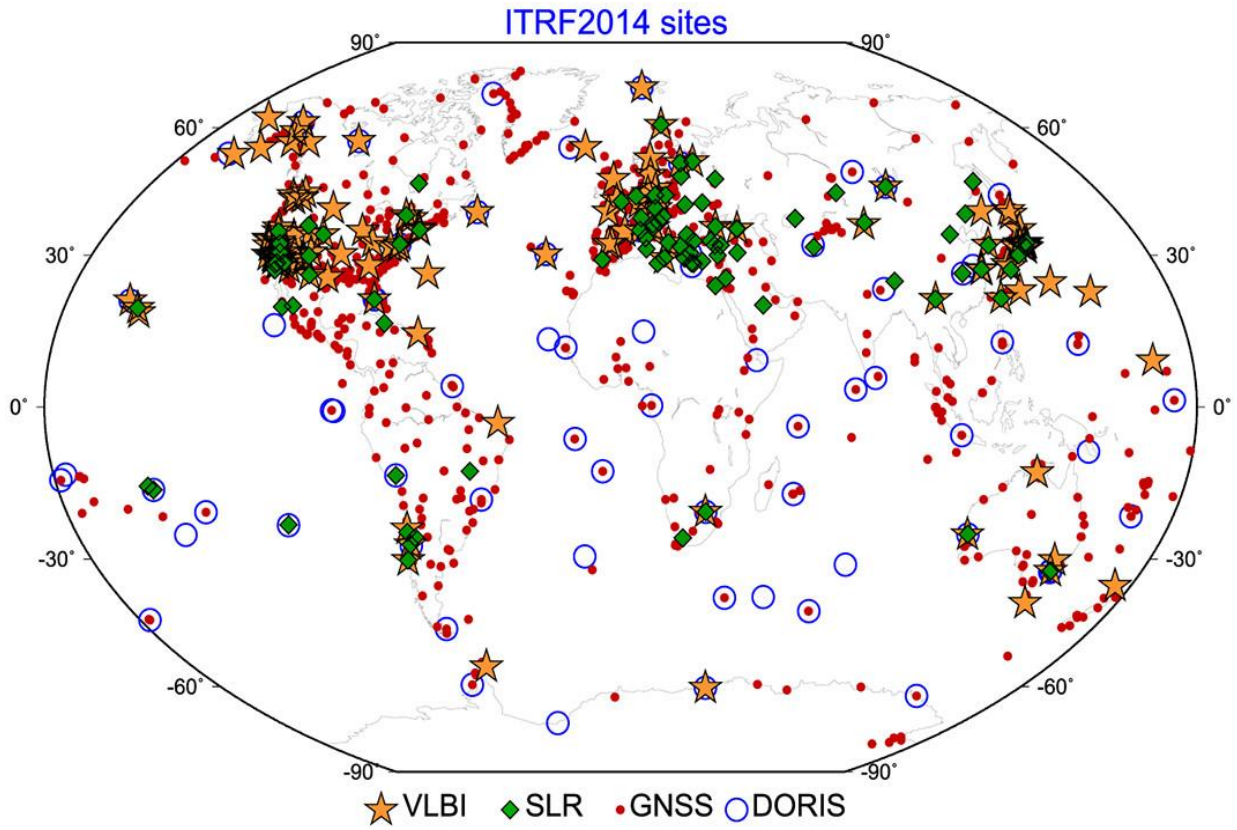

Fig. 2.4: ITRF2014 network highlighting VLBI, SLR, and DORIS sites co-located with GNSS (Altamimi, et al., 2016)

The importance of the GNSS systems has led to the creation of the United Nations (UN) initiative on Global Geospatial Information Management (UN-GGIM). The goal of this initiative is the development of global geospatial information. One of the working areas include the creation of a global geodetic reference frame (UN, 2019). Apart from this initiative the UN office for outer space affairs have their program on space applications that include goals for the GNSS systems in order to improve the overall GNSS service provision to benefit people around the world. The office supports projects related to the establishment of regional reference frame networks that will enhance applications in fields such as geodesy, mapping, surveying, geo-information, natural hazards mitigation, and earth sciences (UN, 2012). Furthermore, the role of Earth Observation (EO) and geolocation as provided from the GNSS systems is acknowledged from the UN to achieve the Sustainable Development Goals (SDGs) as defined in the 2030 Agenda for Sustainable Development (UN, 2018) (UN, n.d.).

2.6 The IGS Service and the MGEX

IGS

The International GNSS Service (IGS) was founded in 1994 as an IAG service (IAG, n.d.) with the goal of providing high-quality of GNSS data, products and services worldwide with open access (IGS Central Bureau, 2013). It consists of more than 220 agencies, universities and research institutions all over the world that provide their products using a global network (Fig. 2.5 & Fig. 2.6) of over 400 active monitoring stations (as of 2019) (IGS, 2010) (Kouba, 2009). It also provides an archive of measurements and analyses of previous years. These permanent monitoring stations are continuously operating providing data of different GNSS systems.

The IGS is consisting of around 12 Analysis Centers (AC), an Analysis Center Coordinator (ACC) (IGS, 2017) several Geodetic networks, several Working groups and two pilot projects (IGS, 2017b).

MGEX

With the emergence of new GNSS systems in the last decade, we are brought to the Multi-GNSS era. Ergo, it became important to start using the data of all systems together for the various benefits that the hybridization of GNSS systems can bring: capabilities for more precise positioning, better coverage, end of the dependency of military systems etc. (IGS, 2011) (IGS Central Bureau, 2013).

The Multi-GNSS Experiment (MGEX) is one of the pilot projects of the IGS (IGS, 2011). It has as purpose to provide and analyze all types of GNSS signal data coming from all GNSS systems including Galileo, BeiDou, QZSS and NAVIC and the modernized GPS and GLONASS as well as SBAS systems. Several AC are participating in the MGEX project by processing and providing orbit and clock and bias products from various new GNSS systems (in addition to the initial GPS and GLONASS) on a weekly basis.

MGEX activities are currently continued as a part of the Multi-GNSS Working Group (WG) (Montenbruck, et al., 2017). The principal goals of the Multi-GNSS WG are (IGS, 2018):

- Transfer information essential to the IGS about the advancements of the GNSS systems
- To help improve the Multi-GNSS network by enabling to track the new signals from the new GNSS systems, by advising the receiver and antenna providers
- To gain experience about the tracking of the new signals, and analyzing them for producing Multi-GNSS products

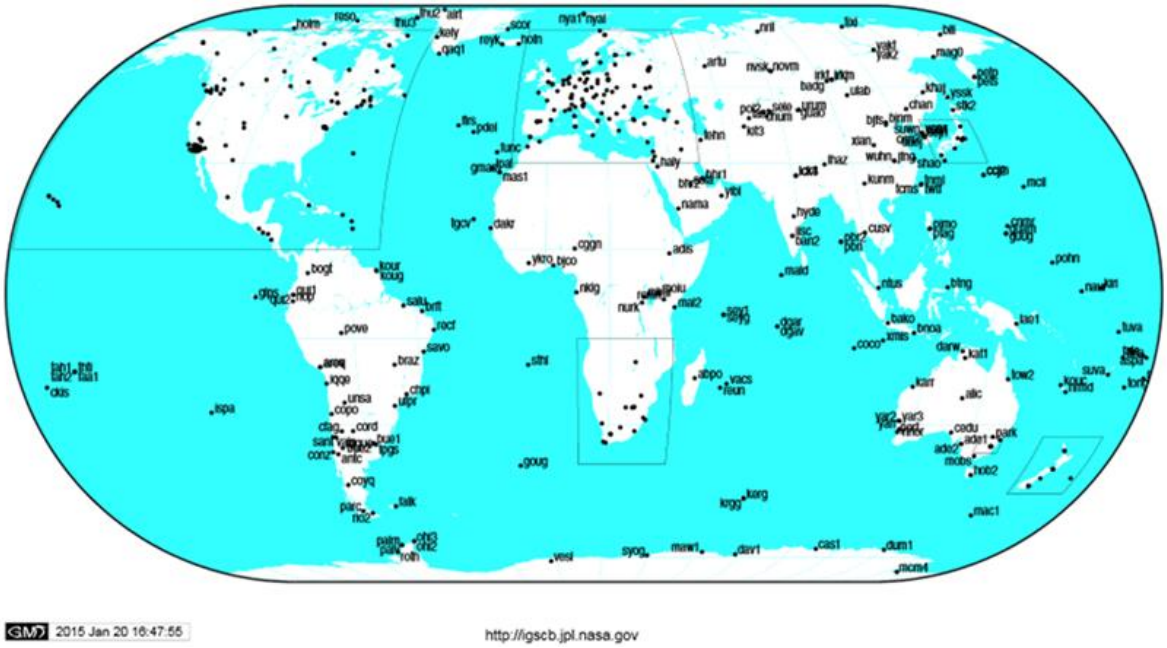

Fig. 2.5: World map of IGS stations (IGS, 2010)

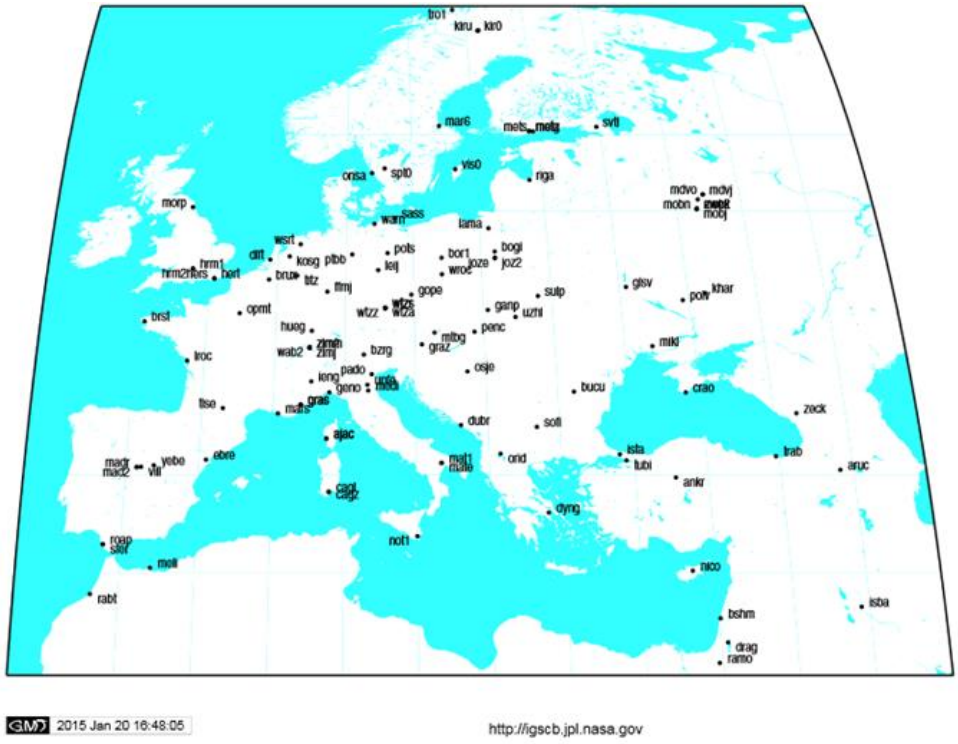

Fig. 2.6: IGS stations in the European region (IGS, 2010)

The CNES/CLS Analysis Center

Since 2010, the Centre National d' Etudes Spatiales (CNES) and Collecte Localisation Satellites (CLS) are an IGS AC. They participated in the past in MGEX and they are currently joining the Multi-GNSS WG. In addition, they participate in the orbit WG and in the ambiguity WG of the IGS. For these purposes, the AC provides precise GNSS orbits, clock and biases products, station coordinates and Earth orientation parameters (CNES/CLS, 2017). The Multi-GNSS products provided are including GPS, GLONASS and Galileo systems. The software used is the GINS software (Marty, 2013). It is a multi-technique (i.e. DORIS, GPS, VLBI, SLR etc.) software used for various space geodesy applications.

The team is a contribution of scientists and engineers from the space geodesy research group GRGS (Groupe de Recherche de Géodésie Spatiale) of France (GRGS, n.d.). The CLS group is a subsidiary company of CNES that contributes in localizing and collecting the satellite data. Furthermore, the CLS team is contributing to the processing of the space data for the domain of orbitography, terrestrial kinematics, space geodesy, space weather, etc.

2.7 Conclusions

Geodesy, one of the oldest branches of science, is an important contribution to understanding the Earth's size, shape and gravity field. Space geodesy is using space-based techniques in order to contribute to this understanding. Several space geodetic methods are widely used from the geo-scientists. One of them -a quite important one- is the GNSS systems, that are used in various geodetic applications that require precise positioning and timing.

With the arrival of the new European GNSS system, it became necessary to study and check the new possibilities that such new system will bring to space geodesy: not only as a separate system under civilian use but also within a Multi-GNSS formation together with the existing GPS system (already widely used for scientific applications today).

In the following chapter we will study the GNSS types of measurements used for this study and we will explain the zero-difference ambiguity resolution method.

3. GNSS Measurements

3.1 Introduction

In Chapter 2 it is described the importance of the Precise GNSS positioning to geodetic and scientific applications. As a consequence, there is a great scientific interest of the CNES/CLS IGS AC to examine the future positioning capabilities of the European GNSS system. However, the Galileo constellation is yet to be complete. In the beginning of the present thesis (November 2016) the Galileo constellation was comprising of 7 operational satellites and 2 satellites in elliptical orbits and by the end (October 2019) it was only 4 satellites away to the full constellation (i.e. 22 operational satellites and 2 satellites in elliptical orbit)(See Fig. 3.1). This made it questionable whether the uncompleted Galileo constellation alone at that time was sufficient to provide mm level positioning accuracy. One necessary and important step was to calculate precise Galileo Orbits within a Multi-GNSS formation together with GPS. The reason for adding the GPS constellation was decided so that Galileo can take advantage of the precise GPS orbits; having more common satellite passes per station, better connectivity, solving for common station errors and parameters (i.e. tropospheric delay, receiver clock delay etc.). It is clear that the more precise the satellite orbits are (as reference), the better positioning accuracy it can be achieved.

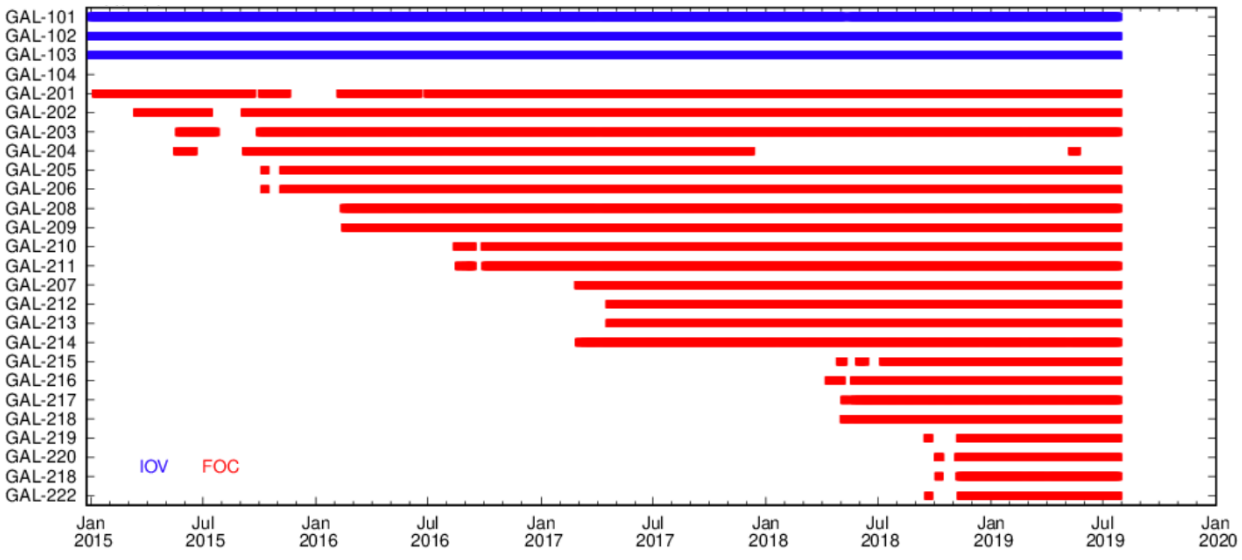

Fig. 3.1: Galileo operational satellites from 01/01/2015 to 01/07/2019 (IGS/MGEX, 2019)

In this chapter they are described the basic GNSS observations used for geodesy. It is presented the problem of carrier phase ambiguities and the method used already from CNES/CLS AC for resolving the GPS phase ambiguities. This method is currently applied from the AC both for Precise Orbit Determination (POD) and Precise Point Positioning (PPP) for the GPS system.

3.2 GNSS observations used for Geodesy

The GNSS observations used for geodesy are mainly of two types: the pseudorange (or code or range) measurement and the carrier phase (or phase) measurement[1] (Hofmann-Wellenhof, et al., 2008). The equation model bellow is given for the pseudorange (code) and carrier phase measurements for two frequencies i and j:

$$P_{r,i}^s = \rho_r^s + c\Delta t + T_r^s + I_r^s + b_i^s + b_{r,i} + E_{r,i}^s \quad (3.1)$$

$$P_{r,j}^s = \rho_r^s + c\Delta t + T_r^s + \frac{f_i^2}{f_j^2} I_r^s + b_j^s + b_{r,j} + E_{r,j}^s \quad (3.2)$$

$$L_{r,i}^s = \lambda_i \varphi_{r,i}^s = \rho_r^s + c\Delta t + T_r^s - I_r^s + \lambda_i N_{r,i}^s + \lambda_i W_r^s + \beta_i^s + \beta_{r,i} + \varepsilon_{r,i}^s \quad (3.3)$$

$$L_{r,j}^s = \lambda_j \varphi_{r,j}^s = \rho_r^s + c\Delta t + T_r^s - \frac{f_i^2}{f_j^2} I_r^s + \lambda_j N_{r,j}^s + \lambda_j W_r^s + \beta_j^s + \beta_{r,j} + \varepsilon_{r,j}^s \quad (3.4)$$

with:

$P_{r,i}^s$, $P_{r,j}^s$: code measurements at receiver r from satellite s on frequency i or j [m]

$L_{r,i}^s$, $L_{r,j}^s$: phase measurements at receiver r from satellite s on frequency i or j [m]

ρ_r^s : geometric distance between receiver r and satellite s [m] (Phase Center Offset (PCO) included). $\rho_r^s = \sqrt{(x_r - x^s)^2 + (y_r - y^s)^2 + (z_r - z^s)^2}$

Δt : clock corrections of the satellite (δt^s) and the receiver (δt_r) with respect to the synchronization to the GNSS time [s]. $\Delta t = \delta t_r - \delta t^s$

[1] The zero-difference ambiguity fixing method is based originally on the Laurichesse-Mercier model of equations for code (P_i and P_j) and carrier phase (L_i and L_j) (Laurichesse, et al., 2009). This model of equations is written in such a way that stochastic parameters (ionosphere-free phase and pseudorange clocks) are separated from the clock parameters, that are affected by long-term variations. Furthermore, the term for the geometric propagation distance is including the tropospheric delay and relativistic effects (Laurichesse, et al., 2009). In the present thesis, it was chosen to use another more generalized and simple measurement model notation for the equations.

T_r^s : tropospheric signal delay [m] that depends on the temperature, pressure, and humidity along the signal path through the troposphere

I_r^s : ionospheric signal delay [m] caused by change in the propagation speed of the GNSS signal when passing through the ionospheric layer[2]

$E_{r,i}^s$, $E_{r,j}^s$: code measurement noise at receiver r from satellite s on frequency i or j [m] ~ $\mathbb{O}$ (1m). This term is including all sources of code errors: e.g. multipath

f_i , f_j : carrier frequency i or j [Hz]

c : speed of light in vacuum [m/s]

λ_i , λ_j : nominal wavelength of the carrier frequency i or j [m]

$\varphi_{r,i}^s$, $\varphi_{r,j}^s$: carrier phase measurement at receiver r from satellite s on frequency i or j [cycles]

$N_{r,i}^s$, $N_{r,j}^s$: integer carrier phase ambiguity at receiver r from satellite s on frequency i or j

W_r^s : carrier phase wind up effect [cycles]

b^s , b_r : code phase biases of satellite and receiver [m]

β^s , β_r : carrier phase biases of satellite and receiver [m]

$\varepsilon_{r,i}^s$, $\varepsilon_{r,j}^s$: carrier phase measurement noise at receiver r from satellite s on frequency i or j [m] ~ $\mathbb{O}$ (1mm). This term is including all sources of code errors: multipath, etc.

The difference of these two types of GNSS measurements are extensively discussed in numerous publications ((Hofmann-Wellenhof, et al., 2008), (ESA, et al., 2013), (Verhagen, 2005) etc.). It is important to note, however, that the pseudorange measurement is accurate but not precise whereas the carrier phase measurement is precise but not accurate; this is because of the integer ambiguity term that is unknown. The ambiguity term is introducing a bias that needs to be determined. This bias can be determined either as a real number or an integer number. The process of calculating the bias an as integer number is called integer ambiguity resolution and it has been a major research topic over the past decades.

[2] The ionosphere speeds up the propagation of the carrier phase beyond the speed of light, while it slows down the code by the same amount. Note the different signs in the Eq. for code and carrier phase.

3.3 Integer Ambiguity Resolution

When using the carrier phase measurements, there is a bias that is related to the integer number of the past cycles (ambiguous term). There are many methods published worldwide over many years that deal to estimate this integer number (Verhagen, 2005). After the resolution of the integer ambiguity bias, the phase measurement can be used as a both precise and accurate GNSS measurement.

Fixing GNSS phase ambiguities to their integer values is known to be the key to access the highest accuracy. It is an essential step that is used both when doing satellite POD, positioning or any other precise positioning application. The general procedure requires basically three steps. Firstly, an estimation of the so-called float solution is calculated, when the ambiguity is estimated as a real ($\mathbb{R}$) number. Secondly, a type of transformation from $\mathbb{R}$ to integer ($\mathbb{N}$) is applied. There are multiple methods for this step (i.e. nearest integer rounding, integer bootstrapping, integer least-squares etc.) (Verhagen, 2005). At the end, after the ambiguity resolution procedure, phase measurements are corrected and the estimation of the remaining parameters of interest is done again.

This complicated problem has generally two main approaches. The historical one is based on the double-differencing of raw observations between pairs of satellites and pairs of receivers. In the last decade, various authors have demonstrated the success of strategies based on the zero-difference (or undifferenced) GPS observations (Mercier & Laurichesse, 2007) (Ge, et al., 2008) (Banville, et al., 2008).

The following graph (Fig. 3.2) is showing an example of the improvement of the CNES/CLS AC final GPS orbit product (GRG) when the ambiguity resolution (AR) started to be applied (starting at GPS week 1555). The graph is showing the smoothed weighted RMS of all IGS ACs GPS final orbit solutions compared to the IGS final orbits between GPS week 700 (07/06/1993) and GPS week 2050 (26/04/2019). After applying ambiguity resolution, the weighted RMS dropped from 35 mm to 20 mm.

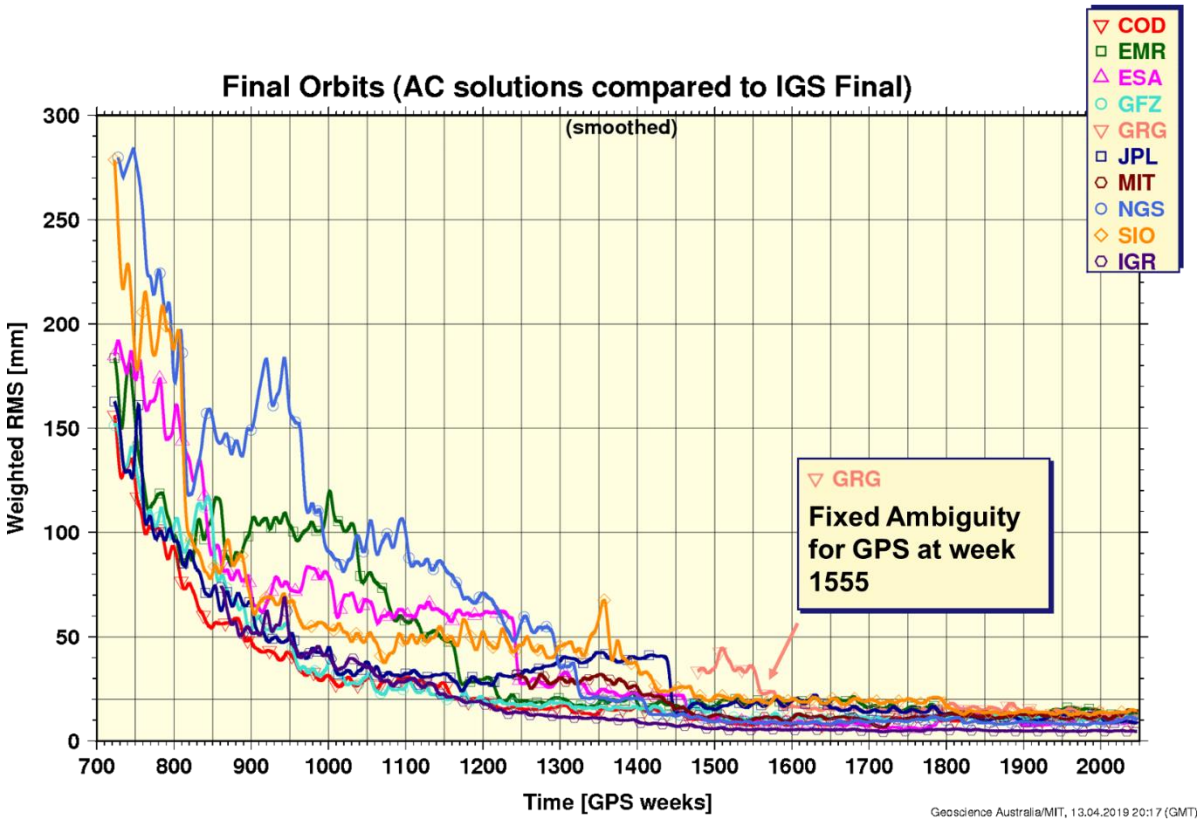

Fig. 3.2: The benefit of the ambiguity fixing for the GPS final orbits from the GRG AC (IGS, 2019).

In the beginning of the present thesis the CNES/CLS AC was already delivering Galileo float orbit products (i.e. without ambiguity resolution). The quality of Galileo float orbit modelling at that time resembled the quality of GPS float orbits before the start of the ambiguity fixing algorithm application; around 10-20 cm RMS from orbit overlaps. This gave the idea that efforts should be made to perform Galileo ambiguity resolution respectively. After the successful ambiguity resolution, Galileo orbits would be more precise.

Up until recently, there are some efforts of Galileo ambiguity fixing using the double-difference method. The German Aerospace Center (Deutsches Zentrum für Luft- und Raumfahrt e.V - DRL) has tested the success rate of ambiguity resolution for the Galileo constellation until 2016. It has been found that the percentage of ambiguity resolution depends on the number of available satellites and it can reach above 90% (Steigenberger & Montenbruck, 2016). The Helmholtz Centre Potsdam GFZ German Research Centre for Geosciences (GFZ) has studied Galileo ambiguity fixing for the IOV satellites using a combined GPS/Galileo method of Ge, et al. (2005) showing a percentage of about 85% success rate for Galileo ambiguity fixing (Uhlemann, et al., 2016). Nevertheless, it is a new topic to apply the zero-difference ambiguity resolution method to the Galileo system.

3.4 Zero-difference Ambiguity Resolution Method

In the following subchapter it is described the zero-difference ambiguity resolution method that is already used from the CNES/CLS AC for the GPS system. Basically, this method is divided in two steps:

- The Wide-Lane ambiguity fixing
- The Narrow-Lane ambiguity fixing

With the definition of the wide-lane combination, it is meant that the combined wavelength is larger than the largest individual wavelength in the combination. In the same way, the narrow-lane combination, which have a shorter wavelength than the individual signal with the shortest wavelength in the combination (Teunissen & Montenbruck, 2017).

Wide-Lane ambiguity fixing

From the Eq.3.1 to 3.4, the Wide-Lane (WL) linear combinations for code (PW_r^s) and carrier phase (LW_r^s) and the Narrow-Lane (NL) linear combinations for code (PN_r^s) and carrier phase (LN_r^s) are defined as:

$$PW_r^s = \frac{f_i}{f_i - f_j} P_{r,i}^s - \frac{f_j}{f_i - f_j} P_{r,j}^s \tag{3.5}$$

$$LW_r^s = \frac{f_i}{f_i - f_j} L_{r,i}^s - \frac{f_j}{f_i - f_j} L_{r,j}^s \tag{3.6}$$

$$PN_r^s = \frac{f_i}{f_i + f_j} P_{r,i}^s + \frac{f_j}{f_i + f_j} P_{r,j}^s \tag{3.7}$$

$$LN_r^s = \frac{f_i}{f_i + f_j} L_{r,i}^s + \frac{f_j}{f_i + f_j} L_{r,j}^s \tag{3.8}$$

With the corresponding WL wavelength (λ_{wl}) and NL wavelength (λ_{nl}) as:

$$\lambda_{wl} = c/(f_i - f_j) = \lambda_i \lambda_j / (\lambda_j - \lambda_i) \tag{3.9}$$

$$\lambda_{nl} = c/(f_i + f_j) = \lambda_i \lambda_j / (\lambda_i + \lambda_j) \tag{3.10}$$

The following table Tab. 3.1 gives the wide-lane and the narrow-lane wavelengths for GPS and Galileo for some combinations of their basic frequencies:

GNSS Frequency	λ_{wl} [m]	λ_{nl} [cm]
GPS ($L1$, $L2$)	0.862	10.7
GPS ($L1$, $L5$)	0.751	10.9
GPS ($L2$, $L5$)	5.861	12.5
Galileo ($E1$, $E5a$)	0.751	10.9
Galileo ($E1$, $E5b$)	0.814	10.8
Galileo ($E5a$, $E5b$)	9.768	12.6

Tab. 3.1: Table of values for wide-lane and narrow-lane wavelength for GPS and Galileo

The noise amplification factors[3] for the wide-lane (σ_{wl}) and the narrow-lane (σ_{nl}) become (Teunissen & Montenbruck, 2017):

$$\sigma_{Pwl} = \sqrt{\frac{{f_i}^2}{(f_i - f_j)^2}\sigma_{Pi}^2 + \frac{{f_j}^2}{(f_i - f_j)^2}\sigma_{Pj}^2} \tag{3.11}$$

$$\sigma_{Pnl} = \sqrt{\frac{{f_i}^2}{(f_i + f_j)^2}\sigma_{Pi}^2 + \frac{{f_j}^2}{(f_i + f_j)^2}\sigma_{Pj}^2} \tag{3.12}$$

$$\sigma_{Lwl} = \sqrt{\frac{{f_i}^2}{(f_i - f_j)^2}\sigma_{Li}^2 + \frac{{f_j}^2}{(f_i - f_j)^2}\sigma_{Lj}^2} \tag{3.13}$$

$$\sigma_{Lnl} = \sqrt{\frac{{f_i}^2}{(f_i + f_j)^2}\sigma_{Li}^2 + \frac{{f_j}^2}{(f_i + f_j)^2}\sigma_{Lj}^2} \tag{3.14}$$

were:

σ_{Pwl} , σ_{Lwl} : wide-lane noise for code and carrier [m]

σ_{Pnl} , σ_{Lnl} : narrow-lane noise for code and carrier [m]

σ_{Pi} , σ_{Pj} : code noise for frequency i or j [m]

σ_{Li} , σ_{Lj} : carrier noise for frequency i or j [m]

Assuming that the noise is identical regardless of the frequency, the terms are substituted for the code noise (σ_P) and the carrier noise (σ_L):

[3] For the general equations of noise propagation when performing linear combinations please refer to Appendix II

$$\sigma_{Pwl} = \sqrt{\frac{f_i^{\,2} + f_j^{\,2}}{(f_i - f_j)^2}}\,\sigma_P \tag{3.15}$$

$$\sigma_{Pnl} = \sqrt{\frac{f_i^{\,2} + f_j^{\,2}}{(f_i + f_j)^2}}\,\sigma_P \tag{3.16}$$

$$\sigma_{Lwl} = \sqrt{\frac{f_i^{\,2} + f_j^{\,2}}{(f_i - f_j)^2}}\,\sigma_L \tag{3.17}$$

$$\sigma_{Lnl} = \sqrt{\frac{f_i^{\,2} + f_j^{\,2}}{(f_i + f_j)^2}}\,\sigma_L \tag{3.18}$$

From these expressions it is possible to calculate the amplification factor for noise of the wide-lane and the narrow-lane combinations. The results are given in the following table Tab. 3.2. It is worth noticing that the amplification factor for the narrow-lane combinations is similar for any combination of frequencies.

GNSS Frequency	A_{wl}	A_{nl}
GPS $(L1, L2)$	5.74	0.71
GPS $(L1, L5)$	4.93	0.71
GPS $(L2, L5)$	33.24	0.71
Galileo $(E1, E5a)$	4.93	0.71
Galileo $(E1, E5b)$	5.39	0.71
Galileo $(E5a, E5b)$	54.92	0.71

Tab. 3.2: Table of values for wide-lane and narrow-lane noise amplification factors

From the Eq. 3.6 and 3.7 it is possible to form a Melbourne-Wübbena (MW) linear combination that is the difference of wide-lane carrier combination and narrow-lane code combination. It has the identity to cancel out any geometric, first-order ionospheric effects, clock and phase wind up terms (Melbourne, 1985) (Wübbena, 1985). It is a useful combination to detect cycle slips. For periods with no cycle slips this combination shows a constant value:

$$\begin{aligned} MW_r^s = \lambda_{wl}\varphi_r^s = LW_r^s - PN_r^s = \\ = \left(\frac{f_i}{f_i - f_j}L_{r,i}^s - \frac{f_j}{f_i - f_j}L_{r,j}^s\right) - \left(\frac{f_i}{f_i + f_j}P_{r,i}^s + \frac{f_j}{f_i + f_j}P_{r,j}^s\right) \end{aligned} \tag{3.19}$$

Which can further be written:

$$\begin{aligned} MW_r^s = \lambda_{wl}\varphi_r^s &= \lambda_{wl}(N_{r,i}^s - N_{r,j}^s) + MW(b^s, \beta^s) + MW(b_r, \beta_r) \\ &\approx \lambda_{wl}(N_{r,i}^s - N_{r,j}^s - \mu^s(t) + \mu_r(t)) \\ &\approx \lambda_{wl}(N_{wl,r}^s - \mu^s(t) + \mu_r(t)) \end{aligned} \quad (3.20)$$

where:

MW_r^s : Melbourne-Wübbena linear combination at receiver r from satellite s [m]

λ_{wl} : WL wavelength [m]

$N_{wl,r}^s$: WL ambiguity between receiver r and satellite s. $N_{wl,r}^s = N_{r,i}^s - N_{r,j}^s$

$\mu^s(t)$: delay coming from the satellite (also known in the bibliography as WL satellite bias - WSB). This bias is the result of other biases combined from Eq. 3.1 to 3.4.

$\mu_r(t)$: delay coming from the receiver (also known in the bibliography as WL receiver bias - WRB). This bias is the result of other biases combined from Eq. 3.1 to 3.4

The combined noise from the MW linear combination can be formulated as:

$$\sigma_{MW} = \sqrt{\frac{{f_i}^2 + {f_j}^2}{(f_i - f_j)^2}}\sigma_L + \sqrt{\frac{{f_i}^2 + {f_j}^2}{(f_i + f_j)^2}}\sigma_P \quad (3.21)$$

By inserting some exemplary values for code (e.g. 0.5m) and carrier phase noise (e.g. 3mm) the following magnitude of MW noise is given in table Tab. 3.3:

GNSS Frequency	MW noise [m]
GPS ($L1, L2$)	0.37
GPS ($L1, L5$)	0.37
GPS ($L2, L5$)	0.45
Galileo ($E1, E5a$)	0.37
Galileo ($E1, E5b$)	0.37
Galileo ($E5a, E5b$)	0.52

Tab. 3.3: Exemplary noise of MW combinations

It is noticed that the noise magnitude of the MW is nearly half of a wide-line wavelength (Refer to both Tab. 3.1 and Tab. 3.3). This means that it is possible to resolve the wide-lane ambiguities. This is also the reason why the MW linear combination is extensively used for carrier phase AR. The trade-off however, is a large noise that is given by the code noise.

As it is clearly seen from the Eq. 3.20, the terms $N_{wl,r}^{s}$, $\mu^{s}(t)$ and $\mu_r(t)$ are totally correlated. It has been observed that for the GPS system the $\mu^{s}(t)$ biases are stable and can be considered as constant during at least one day (Mercier & Laurichesse, 2007). Therefore, they are considered not time dependent in this formulation. This identity made possible the decorrelation of the μ^{s} from the others. Normally for the GPS system, the μ^{s} is known from the previous day value (i.e. is calculated and provided from the CNES/CLS AC to the users) (See Fig. 3.3).

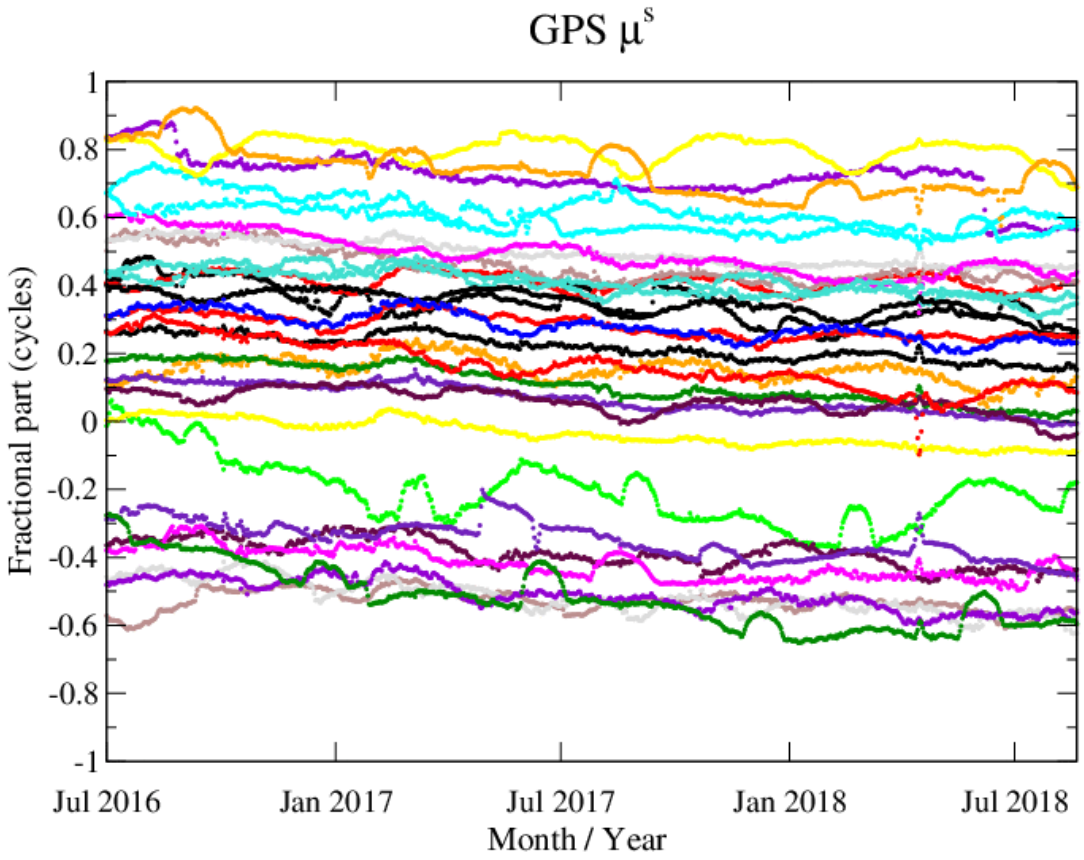

Fig. 3.3: GPS μ^{s} values from July 2016 until July 2018

In order to be able to separate the $\mu_r(t)$ from the $N_{wl,r}^{s}$ and thus solve for the WL ambiguity, an estimation has to be done. The knowns parameters are the MW observations and the estimated parameters are the $N_{wl,r}^{s}$ and $\mu_r(t)$.

The above processing is done for each station individually. The result is the WL ambiguities resolution.

Narrow-Lane ambiguity fixing

Once the $N^s_{wl,r}$ is known, the following step is to form an ionosphere-free (IF) linear combination. These combinations use the equations in the two frequencies where they apply to them a coefficient: α_i to the frequency i and α_j to the frequency j respectively. This type of linear combination contains geometry, clock corrections, troposphere corrections and, for carrier phase IF, the phase ambiguities.

$$\alpha_i = \frac{f_i^2}{f_i^2 - f_j^2} \tag{3.22}$$

$$\alpha_j = \frac{-f_j^2}{f_i^2 - f_j^2} \tag{3.23}$$

where the following are valid:

$$\alpha_i + \alpha_j = 1 \tag{3.24}$$

$$\alpha_i + \alpha_j \frac{f_i^2}{f_j^2} = 0 \tag{3.25}$$

Using the above coefficients, the ionosphere-free linear combinations for code and carrier phase become:

$$P^s_{r,IF} = \alpha_i P^s_{r,i} + \alpha_j P^s_{r,j} = \rho^s_r + c\Delta t + T^s_r + E^s_{r,IF} \tag{3.26}$$

$$\begin{aligned} L^s_{r,IF} &= \alpha_i L^s_{r,i} + \alpha_j L^s_{r,j} = \\ &= \rho^s_r + c\Delta t + T^s_r + \frac{c}{f_i^2 - f_j^2}\left(f_i N^s_{r,i} - f_j N^s_{r,j}\right) + \frac{c}{f_i^2 - f_j^2}\left(f_i W^s_r - f_j W^s_r\right) + \varepsilon^s_{r,IF} = \\ &= \rho^s_r + c\Delta t + T^s_r + \lambda_{nl} N^s_{r,i} + \frac{\lambda_{nl}\lambda_{wl}}{\lambda_j} N^s_{wl,r} + \lambda_{nl} W^s_r + \varepsilon^s_{r,IF} \end{aligned} \tag{3.27}$$

with:

$P^s_{r,IF}$: ionosphere-free code measurement at receiver r from satellite s [m]

$E^s_{r,IF}$: ionosphere-free code measurement noise at receiver r from satellite s [m]

$L^s_{r,IF}$: ionosphere-free carrier measurement at receiver r from satellite s [m]

$\varepsilon^s_{r,IF}$: ionosphere-free carrier measurement noise at receiver r from satellite s [m]

λ_{nl} : narrow-lane (NL) wavelength [m]

$N_{r,i}^{s}$: Ambiguity between receiver r and satellite s for the frequency i. It is equal to the NL ambiguity $N_{nl,r}^{s} = N_{r,i}^{s}$

The combined noise from the IF linear combination for code and carrier phase can be formulated as:

$$\sigma_{IF\_P} = \frac{{f_i}^4 + {f_j}^4}{f_i^2 - f_j^2}\sigma_P \tag{3.28}$$

$$\sigma_{IF\_L} = \frac{{f_i}^4 + {f_j}^4}{f_i^2 - f_j^2}\sigma_L \tag{3.29}$$

The amplification factor for noise of the IF linear combinations are given in table Tab. 3.4. It is worth noticing that the amplification factor for the narrow-lane combinations is similar for any combination of frequencies.

GNSS Frequency	A_{IF}
GPS ($L1$, $L2$)	2.98
GPS ($L1$, $L5$)	2.59
GPS ($L2$, $L5$)	16.64
Galileo ($E1$, $E5a$)	2.59
Galileo ($E1$, $E5b$)	2.81
Galileo ($E5a$, $E5b$)	27.47

Tab. 3.4: Table of values for the Ionosphere-free noise amplification factors

By inserting again, the same exemplary values for code (e.g. 0.5 m) and carrier phase noise (e.g. 3 mm) the following magnitude of IF noise is given in table:

GNSS Frequency	IF code noise [m]	IF carrier noise [mm]
GPS ($L1$, $L2$)	1.49	9
GPS ($L1$, $L5$)	1.29	8
GPS ($L2$, $L5$)	8.32	50
Galileo ($E1$, $E5a$)	1.29	8
Galileo ($E1$, $E5b$)	1.40	8
Galileo ($E5a$, $E5b$)	13.74	82

Tab. 3.5: Exemplary noise of IF code and IF carrier combinations

It is noticed that the noise magnitude of the IF carrier combination is well smaller that the narrow lane wavelength. That is not the case for the IF code noise. This is showing that a combination of IF code and carrier phase measurements must be processed together. Since the IF code noise is much bigger, more importance must be given to the IF carrier observations. This can be done by applying different weighting to the IF measurements.

Nevertheless, as the IF combination is geometry dependent, the geometrical distance must be more precise to at least half a narrow-lane cycle (i.e. less than 5cm). Primarily this can be achieved by using good satellite orbits, precise station positions etc.

As a final step, all equations are gathered and estimated together simultaneously for all stations and all the satellites. The term for the wind up effect W_r^s is calculated and applied to each individual observation (Kouba, 2009). Other models are used for the calculation of other terms e.g. geometry, troposphere etc. Further discussion will be given in later[4].

At this point the solution gives the $N_{r,i}^s$ values in $\mathbb{R}$. This is the so-called float (or unfixed) solution. The process that is used by the CNES/CLS AC to fix ambiguities is the so-called sequential integer rounding, also named as integer bootstrapping method (Verhagen, 2005).

After the successful ambiguity fixing to integer values, phase observations are corrected and a last processing is repeated.

The following Fig. 3.4 gives an overview of the entire process.

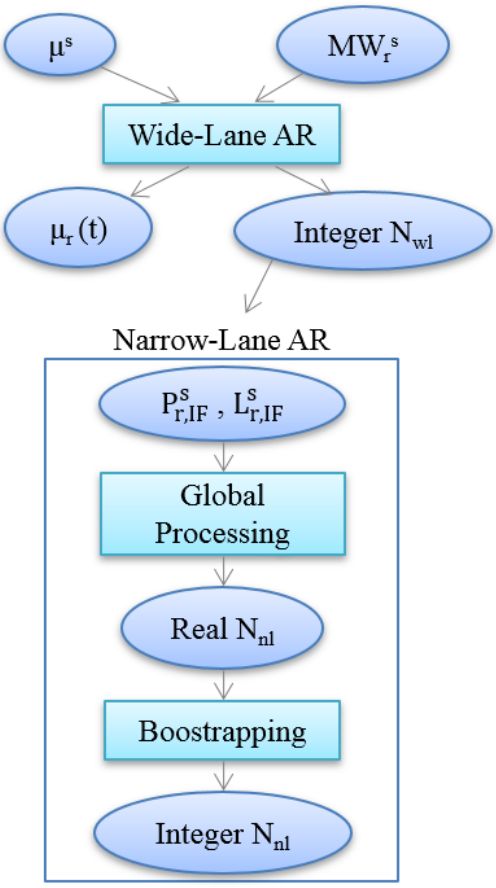

Fig. 3.4: The zero-difference method formed in two steps as done for the GPS system in L1/L2

[4] Models used are shown later in table Tab. 5.1

3.5 Conclusions

A key to achieving precise GNSS obits and high precision positioning is using very precise carrier phase GNSS measurements. Nevertheless, these very precise GNSS observations are not accurate. There are biased by an ambiguous number of integer cycles (i.e. ambiguities). Solving for the carrier phase ambiguities allows for the acquisition of a very precise and accurate measurement. In the past, many efforts have been made to solve this issue by proposing numerous different ambiguity resolution algorithms. One of these methods used and developed by the CNES/CLS AC is the so-called zero-difference AR. This method is already applied successfully to the GPS system for the frequencies L1 and L2.

In the following two chapters we will study the potentiality to use and apply this method to the Galileo system. Several questions and difficulties of this method will be addressed and discussed for each of the two steps of this method individually.

4. Galileo Wide-Lane AR

4.1 Introduction

Ambiguity fixing to integer numbers of the phase measurements has been proven to ameliorate the accuracy of GNSS data processing. The method of zero-difference AR is a two-step procedure. In the first step, the wide-lane ambiguity resolution is required. As explained in Chapter 3, the successful WL AR demands the decorrelation of three terms; the WL ambiguity, the WL satellite biases and the WL receiver bias. In the past, that necessity was successfully reached for the GPS system; it was realized that the GPS WL satellite biases are stable during a day. This made possible the decorrelation of these terms and the WL AR.

This chapter addresses the following questions:

- Can the zero-difference method used already for GPS be applied to Galileo? And if yes, are there any differences between the two systems?
- Do $\mu^s(t)$ biases show enough stability to achieve good WL fixing?
- What is $\mu^s(t)$ behavior? Is it different for IOV and FOC satellites?
- How can the terms $N_{wl,r}^s$, $\mu^s(t)$ and $\mu_r(t)$ be de-correlated and estimated?
- What is the success rate of WL Galileo fixing?

For the following processing and graphs were made by creating MATLAB scripts.

4.2 Galileo Wide-Lane satellite biases

The network that is used for the experimentation is a collection of 96 IGS stations (See Fig. 4.1). These were previously deployed in the frame of the MGEX experiment and provide both GPS and Galileo measurements. A duration of 50 days from 01/01/2017 (Day of year (DOY): 001) until 19/02/2017 (DOY: 050) is used. At that time frame 13 Galileo satellites were operational (See Fig. 3.1). For the experiment, measurements from the frequencies E1/E5a for Galileo and

L1/L2 for GPS were used. The preference of E5a frequency over E5b for Galileo is made because more IGS stations track that signal[5].

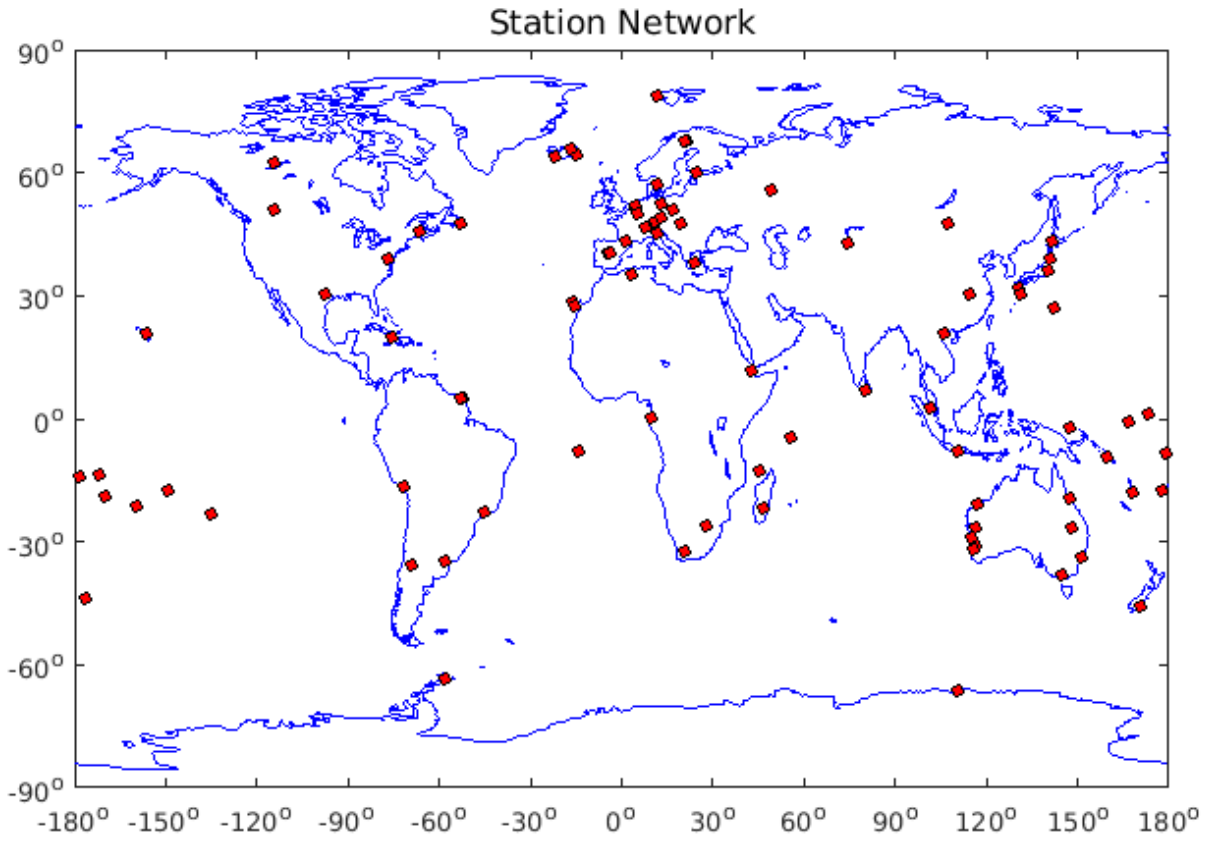

Fig. 4.1: Station network used for the experiments, that provides GPS and Galileo measurements (as of 01/01/2017)

The first stage is to form the Melbourne-Wübbena linear combinations (Eq. 3.20) for each epoch, for each day and each station individually for the 50-day period. Fig. 4.2 to Fig. 4.4 show some examples for 1 day for all Galileo satellite passes (one color per satellite pass). In Fig. 4.2 it is clearly seen that the values of the combinations for each satellite pass are very stable over time. It is therefore deduced that the summation of the terms $(N_{wl,r}^{s} - \mu^{s}(t) + \mu_{r}(t))$ from Eq. 3.20 results to stable values. This enables the calculation of an average value for every pass. All stations that were processed show similar behavior like this.

Nevertheless, there were some cases like GOP7 station in Fig. 4.3 where some hourly gaps of the observations were seen. It was assumed that there might be a problem on the receiver side. In such cases for each 'real' satellite pass it was considered as multiple separate sub-passes. The calculation of an average value for every sub-pass was still done. It was noticed that when

[5] Statistics used from the CNES/CLS AC in DOY 001/2017: Total number of stations was 147, out of which 143 stations (97%) tracked E5a frequency and 113 stations (77%) tacked E5b frequency. Similar statistics for DOY 250/2019: Total number of stations was 178, out of which 176 stations (99%) tracked E5a frequency and 153 stations (86%) tracked E5b frequency.

the gaps are present, the sub-passes were noisier especially at the edges; e.g. small sub-pass of E22 around 13 hours. The noise appears in the two ends of the MW curve due to the multipath effect appearing when the satellite is in low elevation.

Other cases that were observed are shown in Fig. 4.4. Sometimes there were seen very short passes (e.g. pass of E12 around 14 hours) or sparse observations that do not show stability (e.g. pass of E19 around 19 hours). It was decided that these types of passes had to be removed because they were noisier or because they do not show stability over time. As a consequence, it was also decided to keep passes of more than 100 epochs (i.e. 50 min).

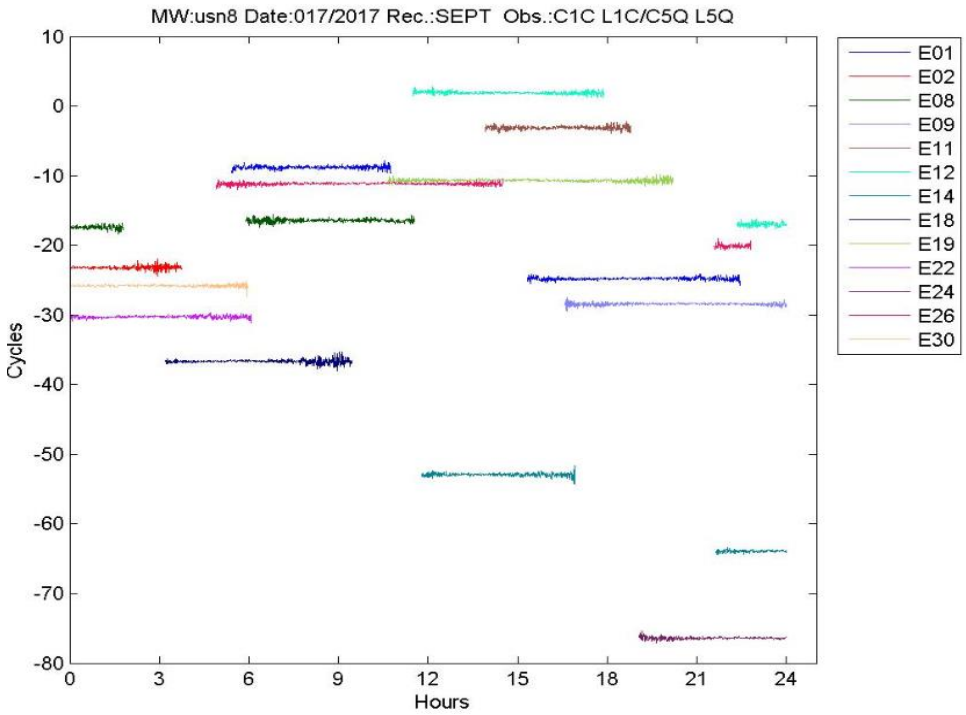

Fig. 4.2: Melbourne-Wübbena linear combination example for station USN8 for DOY: 017/2017 in wide-lane cycles

The fractional values of the MW and their standard deviation per pass for all stations for all days are saved as the linear combination is defined modulo one wide-lane cycle. That means that the fractional part is considered to represent the $(-\mu^s(t) + \mu_r(t))$ terms (they will later be called as WL biases). The integer part that is removed, is considered to represent the $N_{wl,r}^s$ term.

In Fig. 4.5 and Fig. 4.6 there are two examples of the fractional part of WL biases (in cycles) over the 50-day period, for the stations USN8 and ZIM3. The main objective is to check the stability over satellite passes. It can be observed that the fractional parts for all satellites remains stable, with small fluctuations that do not exceed 0.1 cycles.

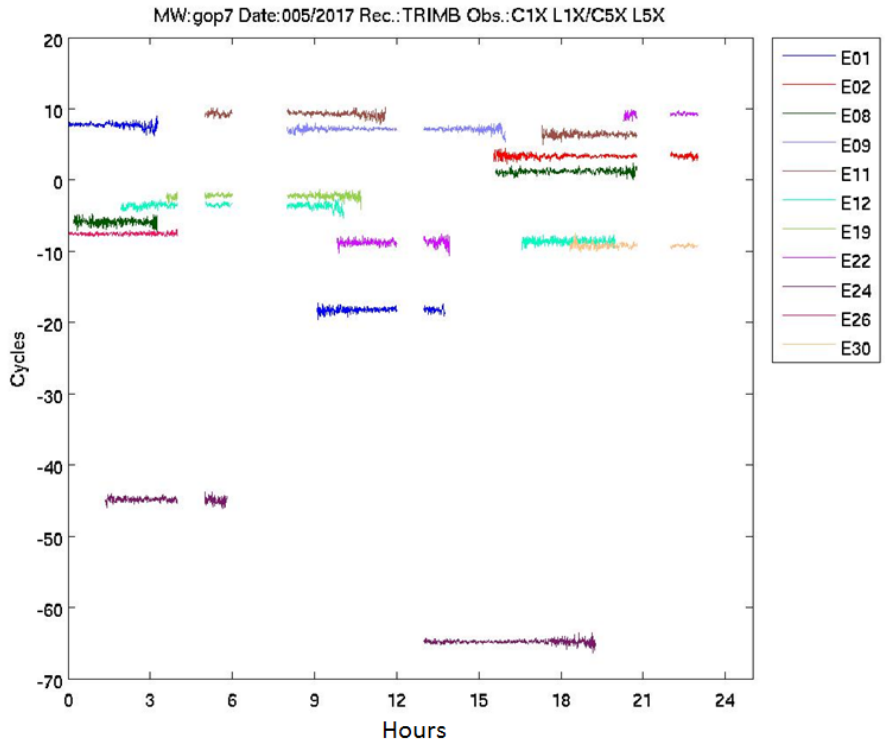

Fig. 4.3: Melbourne-Wübbena linear combination example for station GOP7 for DOY: 005/2017 in wide-lane cycles

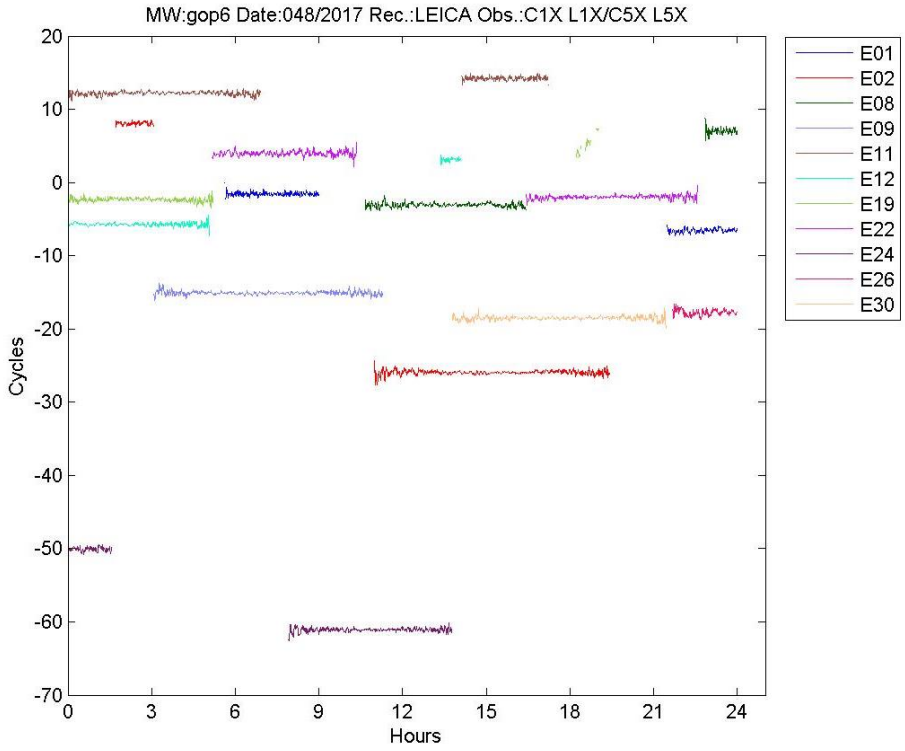

Fig. 4.4: Melbourne-Wübbena linear combination example for station GOP6 for DOY: 048/2017 in wide-lane cycles

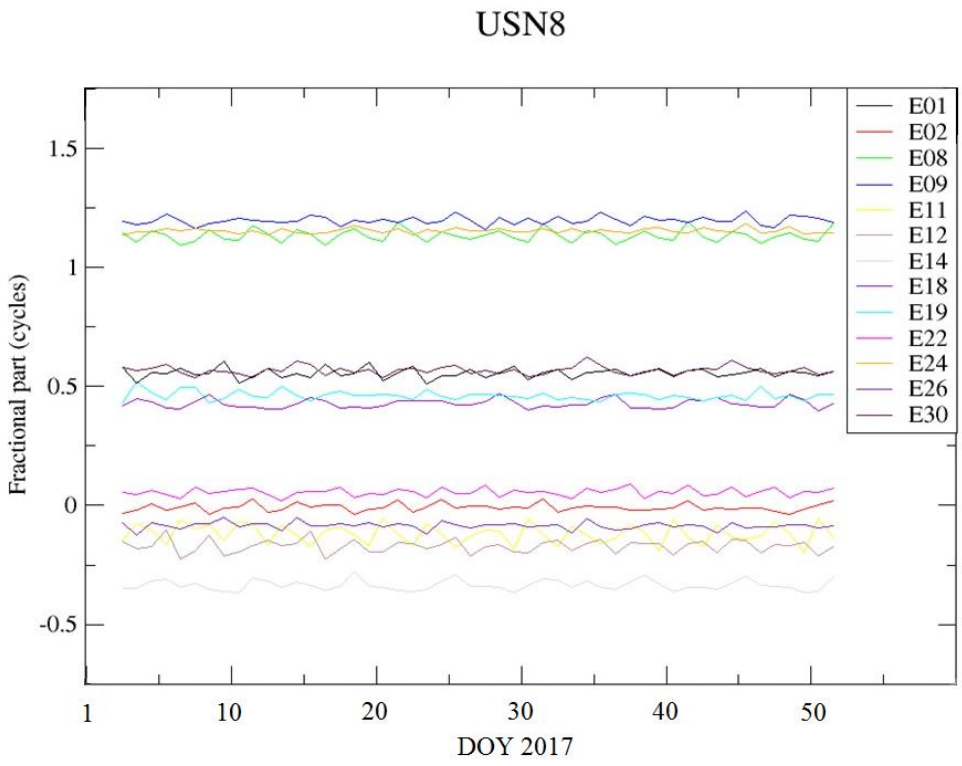

Fig. 4.5: The fractional part of Galileo satellite phase biases for the station USN8

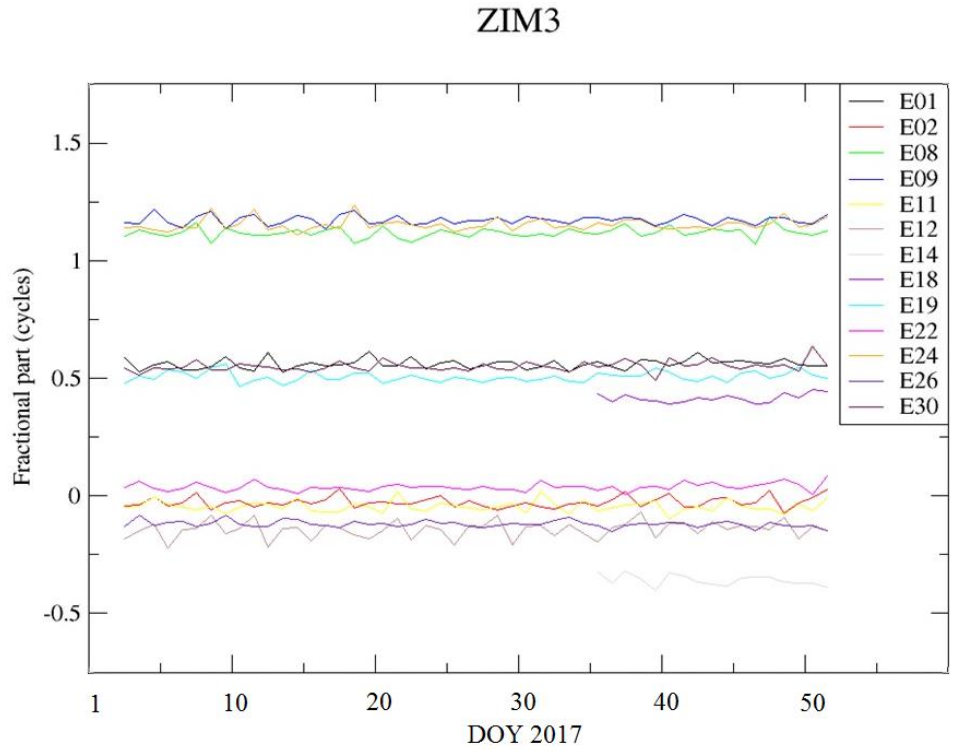

Fig. 4.6: The fractional part of Galileo satellite phase biases for the station ZIM3

These small fluctuations show periodic variations different for each station. Fig. 4.7 is displaying that these fluctuations of the fractional parts of the MW biases are repeated for every 10 days. On the y-axis every unit from one Galileo PRN to the next represents one wide-lane cycle.

Arbitrary values of wide-lane cycles are added in order to be able to separate the satellites. Each 10-day box shows a pattern of the small fluctuations of the WL biases. It has been realized that these patterns are similar for every 10-day periods and for satellites orbiting to the same orbital plane. It is also interesting that these patterns are similar for satellites belonging to the same orbital plane. The reason is probably due to the geometry (and/or phase multipath errors) that reoccur due to repeatability of the Galileo constellation (i.e. every 10 days with 17 orbits, therefore 14 hours and 21.6 minutes per day). However, these fluctuations are considered to be very small (around 0.1 WL cycle) and therefore they do not affect the processing of WL AR in the following steps.

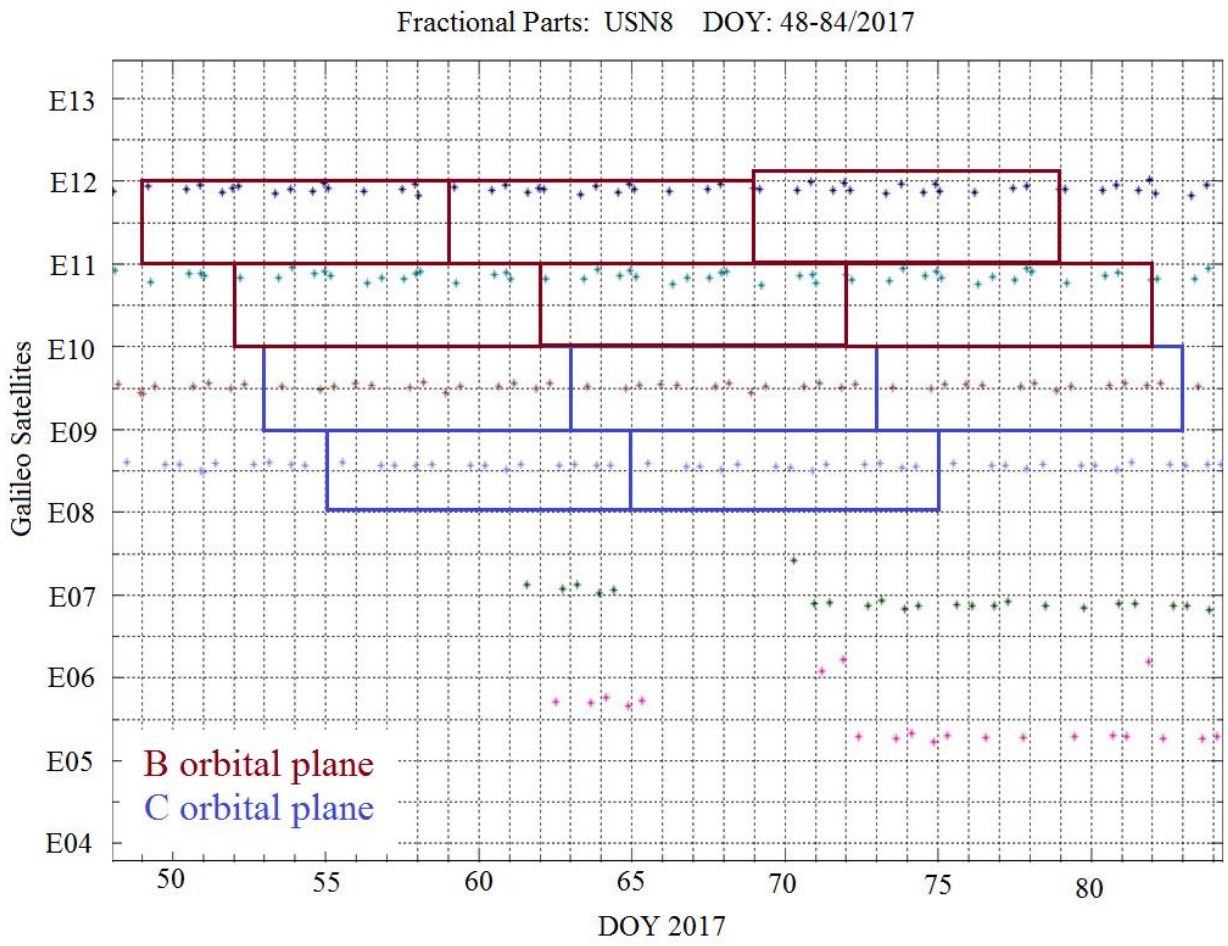

Fig. 4.7: The fractional part of Galileo WL biases for the station USN8 for DOY: 048-84/2017.

In Fig. 4.8 there is an example about the standard deviation and the fractional part of the WL biases with respect to the length of the passes for USN8 station for the period of DOY: 1-84/2017. Each point represents a satellite pass (like as in Fig. 4.2). Each color represents a Galileo satellite. It is deduced that the WL biases are stable also regardless of the length of the passes during the whole period studied. Furthermore, the values of standard deviation are smaller than half a WL cycle for all passes (i.e. less than 0.45 WL cycles). This is a good indication that the MW noise is small and therefore the WL ambiguities can be fixed to integer WL cycles.

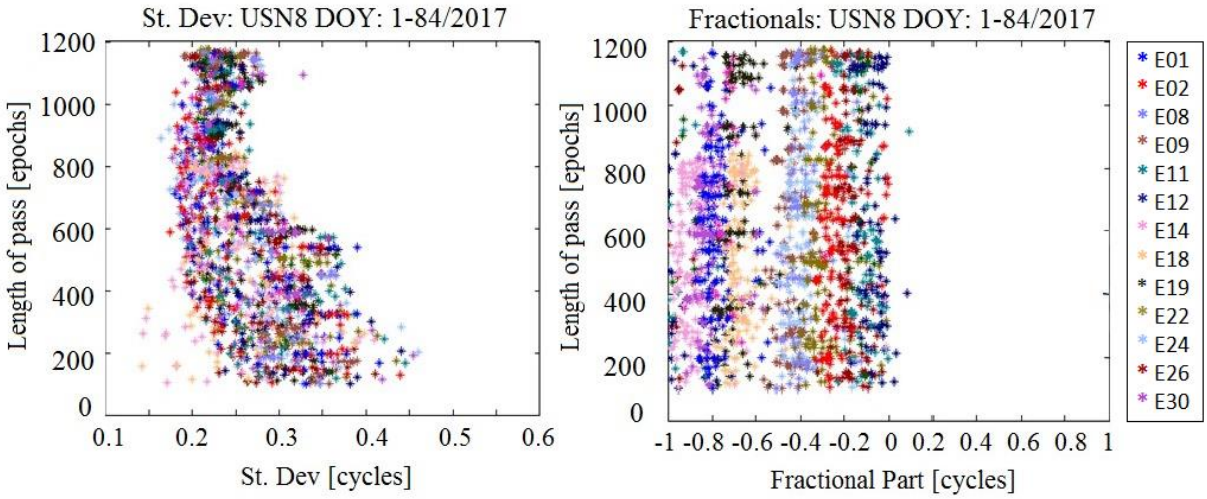

Fig. 4.8: Standard Deviation and Fractional part of Galileo MW of station USN8 for DOY: 001-84/2017.

The previous results gave rise to another query whether the behavior of the fractional parts is different for IOV and FOC batch of satellites. The following WL biases normal histograms (Fig. 4.9) for IOV and FOC satellites are obtained over the 50-day period. They both look symmetric, single peaked and bell-shaped. There is a difference between the histograms of IOV satellites that are more spread with respect to FOC. The IOV histograms expand over nearly 0.5 WL cycles whereas for FOC they expand over nearly 0.25 WL cycles. A possible explanation for this is the fact that IOV and FOC satellites are constructed by different companies and they have different design causing different hardware delay behaviors. This makes the identification of the peak easier for FOC but still remains satisfactory for IOV satellites. In addition, the WL biases (peak values) were kept and were used for further processing as a-priori values.

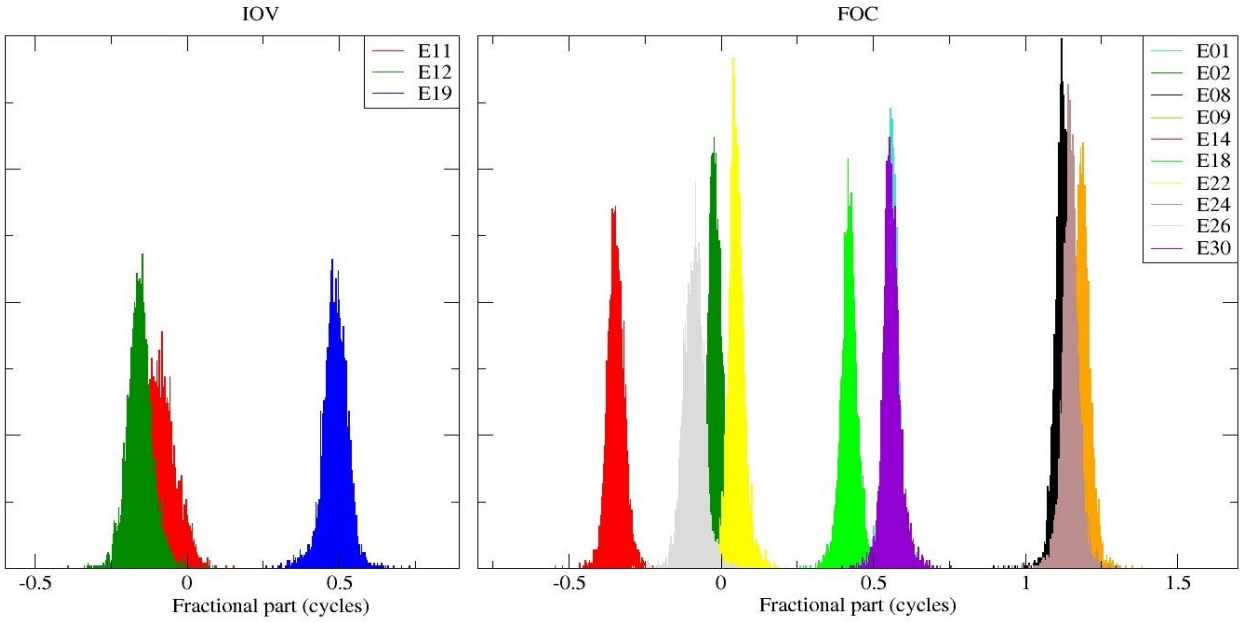

Fig. 4.9: The normalized histograms of μ^s values for IOV and FOC satellites using data from all stations and all days processed.

All the above results indicate that the fractional parts are stable during the days but slightly different for each station (refer to Fig. 4.5 and Fig. 4.6). In order to investigate whether there are any dependencies between different receiver manufacturers, the WL biases series observed during the total period from each receiver has been compared to all the others. In Fig. 4.10 there is an example of the difference of the fractional values shown previously in Fig. 4.5 and Fig. 4.6. Each color represents the difference for each Galileo satellite for the entire period of study. The thick turquoise line is the mean value of all the differences for each epoch. It is seen that the differences expand between -0.15 and 0.1 WL cycles. From the mean value of all the satellite differences (thick turquoise line) a mean value is calculated for the entire period (i.e. 0.04 for this station pair).

All possible combinations of station pairs were calculated in the same way. Later they were categorized and sorted by:

- the type of observations: i.e. 1C/5Q and 1X/5X as indicated in the header of the RINEX files (See Fig. 4.11)
- their receiver manufacturers and models (See Fig. 4.12)

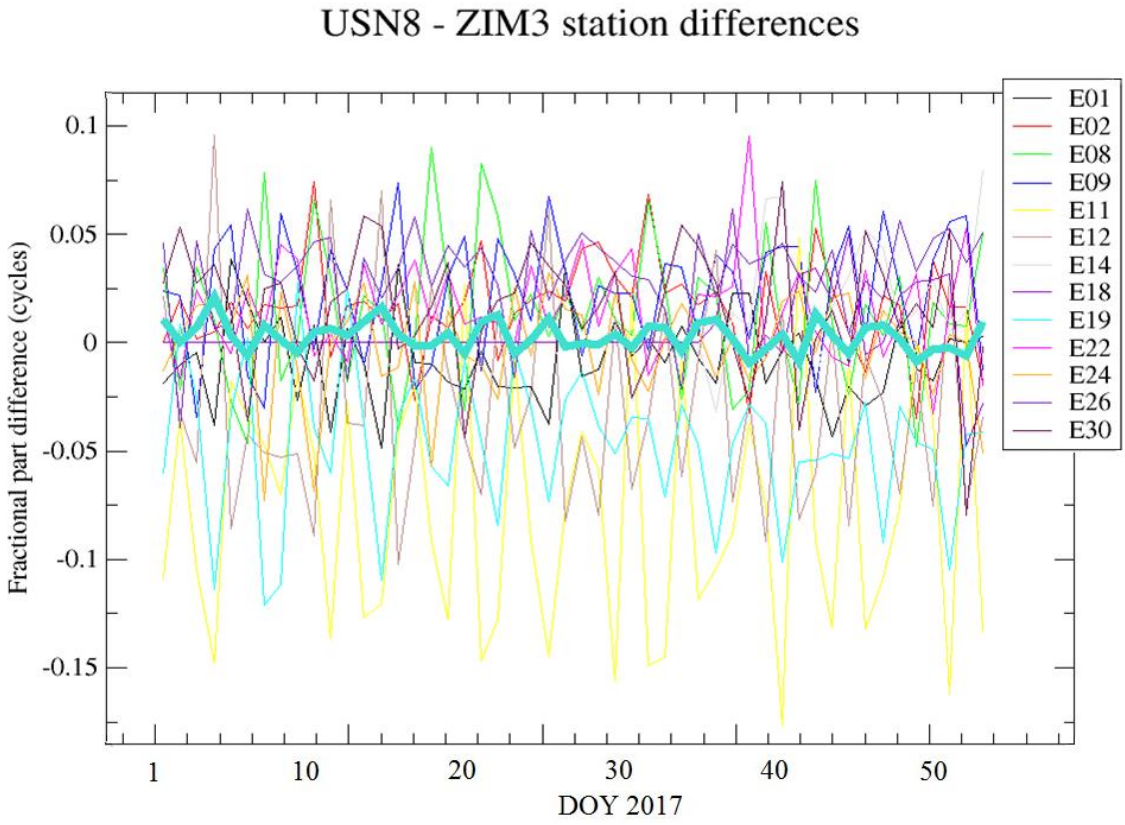

Fig. 4.10 : The differences of the WL fractional part between stations USN8 and ZIM3.

In Fig. 4.11 each value (pixel) is the result of the RMS differences among two stations (in WL cycles). Each value (pixel) is the result of the RMS differences among two stations (in WL cycles). The values of the differences expand from 0 to 0.09 WL cycles. These differences are considered negligible for the WL AR problem. It is not seen any disagreement or systematic pattern among the different types of observations.

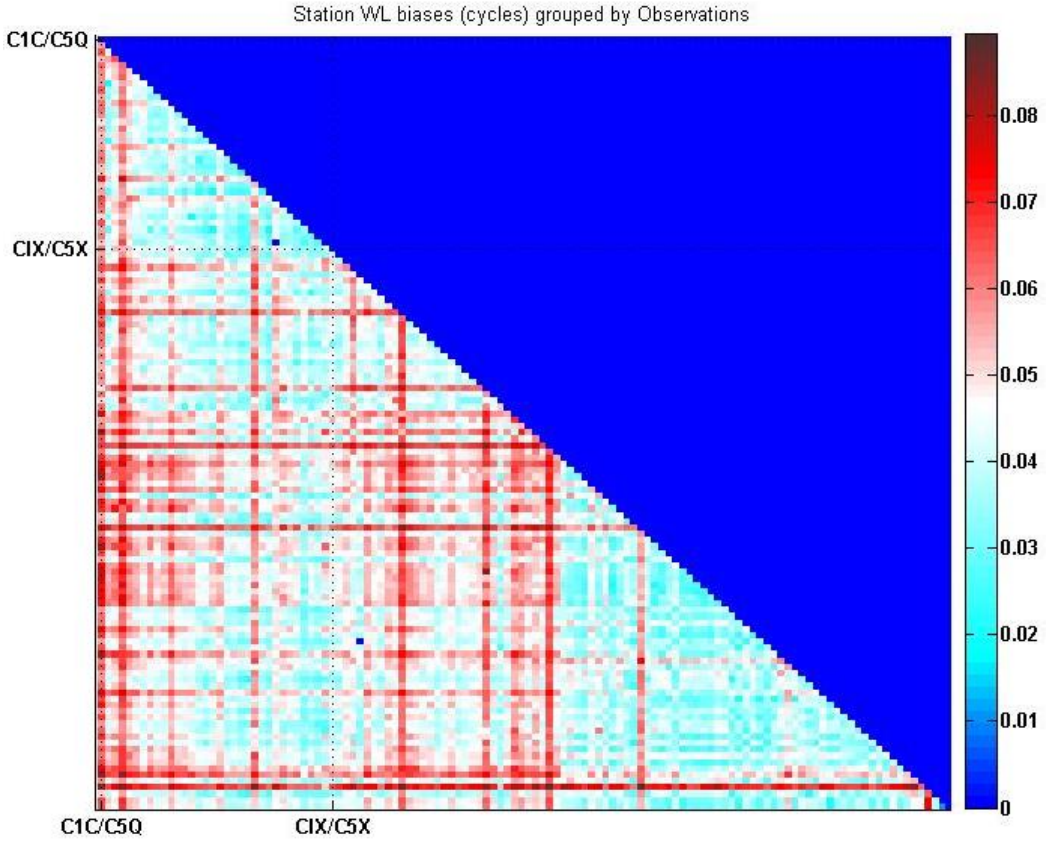

Fig. 4.11: Comparison of different types of Galileo observations among themselves.

The following Fig. 4.12 shows a similar comparison as in Fig. 4.11 except that the stations are ordered by receiver providers. In addition, results are shown for both Galileo and GPS. For the Galileo system, differences are of course again below 0.08 cycles and do not show any specific pattern associated with a given manufacturer brand. This means that all receivers measure consistent values of WL fractional parts.

For GPS it is seen a little larger inconsistency up to 0.15 cycles. There has been no clear explanation for the noticeable differences between receiver families of different providers or between the same provider (e.g. Trimble). A possible reason might be different hardware solutions to overcome the anti-spoofing degradation for GPS P2 code. Nevertheless, it has been tested that a level of inconsistency of 0.15 cycles is not impacting the GPS WL fixing (Loyer, et al., 2012).

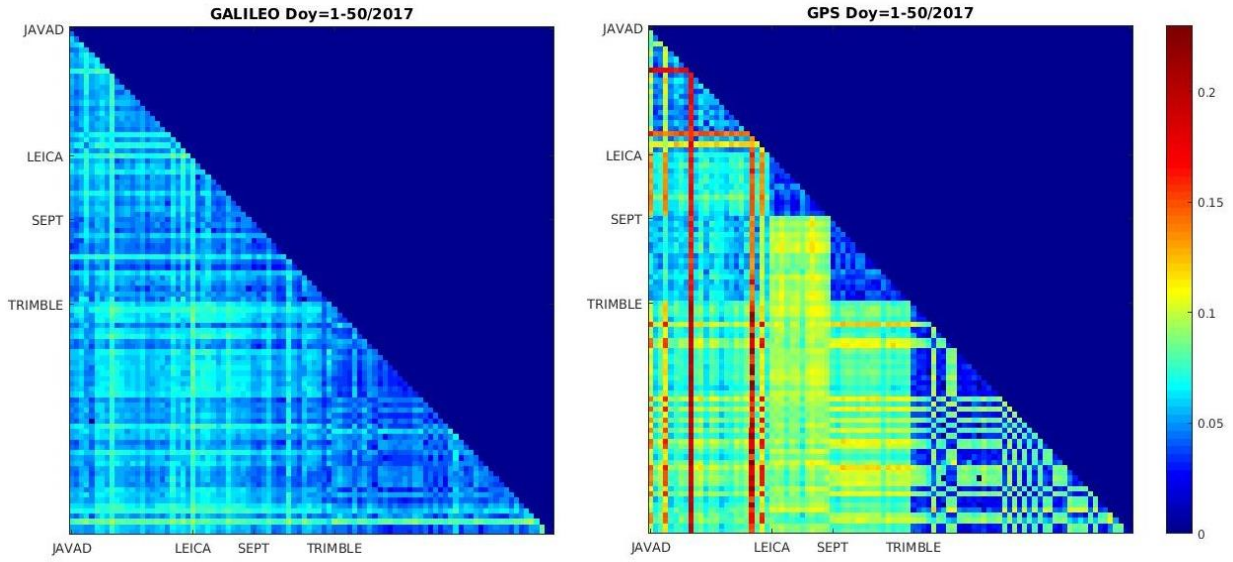

Fig. 4.12: The WL biases organized by receiver manufacturers and models for GPS and Galileo. Each point corresponds to the RMS computed between two receivers over a 50-day time series (in WL cycles).

Since the summation of the terms $(-\mu^s(t) + \mu_r(t))$ proved to be a stable quantity, it can be assumed that the $\mu^s(t)$ and the $\mu_r(t)$ individually show stability. If the $\mu_r(t)$ were not stable, a behavior (or pattern) would be seen commonly for all satellites. This is not the case as seen in Fig. 4.2 to Fig. 4.4.

In addition, it is seen in Fig. 4.12 that differences among receivers are negligible. On the other hand, if the $\mu^s(t)$ values were not stable, the histograms in Fig. 4.12 would not have sharp peaks. From Fig. 4.7 and Fig. 4.8 it is seen that the fractional parts per pass are stable within a day.

All the above results and graphs indicate that the Galileo μ^s are very stable, can be considered as constant over time ($\mu^s(t) = \mu^s$) and be taken from averaging the individual values. These μ^s values were extracted from the peak fractional part values from Fig. 4.9. They will later be used as input values of μ^s for the WL AR.

All the above results are strong indicators that the method used by the CNES/CLS IGS AC on a routine basis for GPS WL ambiguity fixing can as well be used for the Galileo system. The calculation of the fractional part of the μ^s can facilitate the task of $N^s_{wl,r}$, μ^s and $\mu_r(t)$ decorrelation.

4.3 Galileo Wide-Lane Ambiguity Resolution

In the previous sub-chapter, it was proved that the fractional parts Galileo μ^s values are measurable and constant quantities. Then the task is the separation between $N_{wl,r}^s$ and $\mu_r(t)$. It is done by removing the input a-priori μ^s values and by solving a least squares system. All equations (Eq. 3.20) are gathered and solved for all the 50 days and all satellites.

The software PRAIRIE developed from the CNES/CLS AC in 2007 was used for the processing. It is a software of pre-processing GNSS measurements for the zero-difference WL AR. In general, it is using RINEX files and μ^s values as inputs, forms the MW combinations and solves for the $N_{wl,r}^s$ and $\mu_r(t)$ using a bootstrap method (CLS, 2018).

By using PRAIRIE, the system of equations is solved for $\mu_r(t)$ and $N_{wl,r}^s$. The knowns parameters are the MW observations and the estimated parameters are the $N_{wl,r}^s$ and $\mu_r(t)$. In this way the WL ambiguities are fixed. The percentage of Galileo WL AR for that period and for all the stations was satisfactory: around 100%.

The following Fig. 4.13 is showing the μ^s a-posteriori values and their behavior in time. It is seen that μ^s values are constant for much longer periods than one day. In such case, it is decided to maintain the same values as a-priori except for cases when a change has been seen. The changes are investigated: Either, they coincide with the publication of a Notice Advisory to Galileo Users (NAGU) incidents published by the GSA (GSA, n.d.) or, they appear due to the beginning of signal transmission of newly added satellites.

In contrast to Galileo, the μ^s values for the GPS satellites are varying each day (as shown in Fig. 3.3). This is forcing to have as a-priori μ^s values the ones from the previous day of processing.

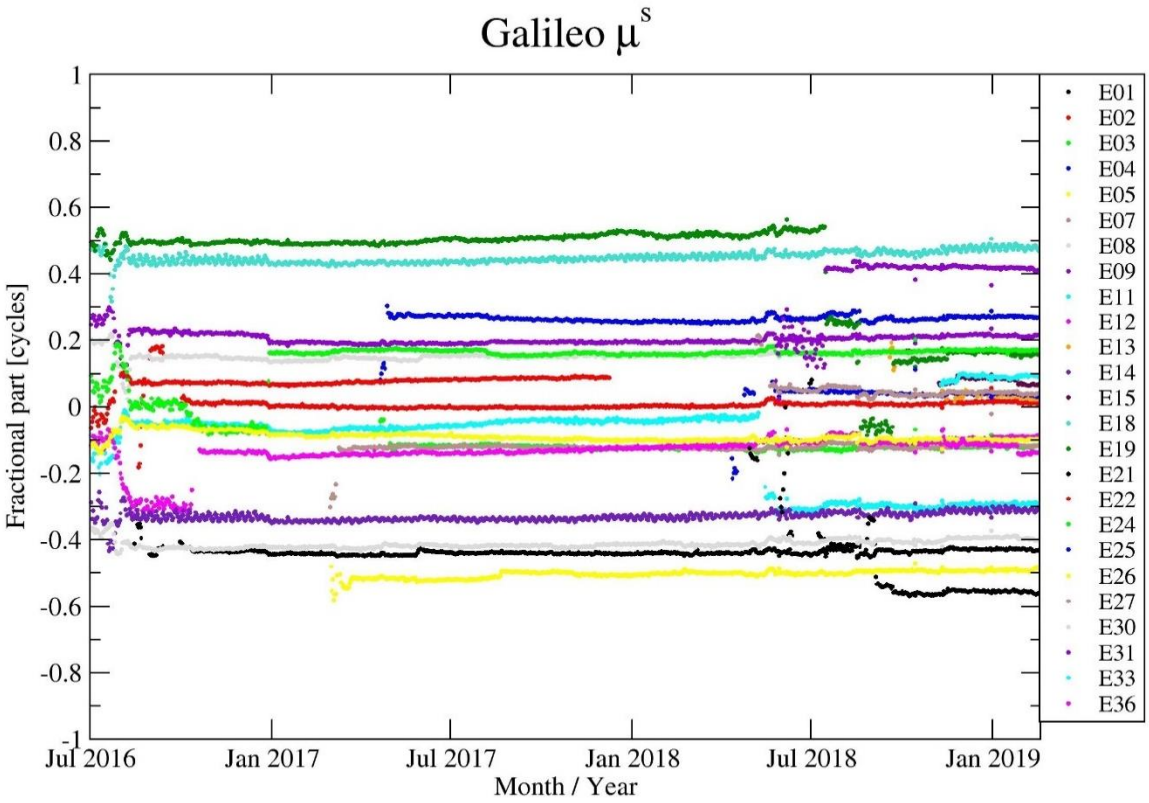

Fig. 4.13: Galileo μ^s values from July 2016 until February 2019

The following Tab. 4.1 is giving the μ^s fractional part values for all Galileo satellites processed at GPS week 2041 (17-23/02/2019).

Galileo	E01	E02	E03	E04	E05	E07	E08	E09	E11	E12	E13	E14
μ^s	-0.44	0.0	-0.09	0.29	-0.49	-0.08	0.12	0.19	-0.29	-0.14	0.0	-0.34
Galileo	E15	E18	E19	E21	E24	E25	E26	E27	E30	E31	E33	E36
μ^s	0.09	0.43	0.15	-0.5	0.16	0.05	-0.8	0.05	-0.42	0.45	0.07	-0.12

Tab. 4.1: Galileo μ^s fractional part values for individual satellites (in WL cycles)

In the Fig 4.14 below it is given the only example found of WL AR for the FTNA station where the $\mu_r(t)$ showed instability. Nevertheless these $\mu_r(t)$ instabilities do not pose a problem for WL fixation because they are already been calculated and taken into account from PRAIRIE software.

The Fig 4.14 is showing the processing in steps done by PRAIRIE: Initially the MW linear combination is formed (a). Secondly, the values for the μ^s fractional part as calculated above are added respectively for each satellite's pass (b). From this graph it is seen that there is a common behavior for all satellites (e.g. a falling curve around 2 to 7 hours and a rising curve around 20 to 24 hours). This common pattern can be isolated as it is a behavior of the station receiver and not of the satellites (c). The result is the WL receiver bias values over time ($\mu_r(t)$). Correcting the MW also from this receiver patterns results in the graph like in (d). At this point it is apparent that each pass is around a sole integer WL number. The WL AR is accomplished.

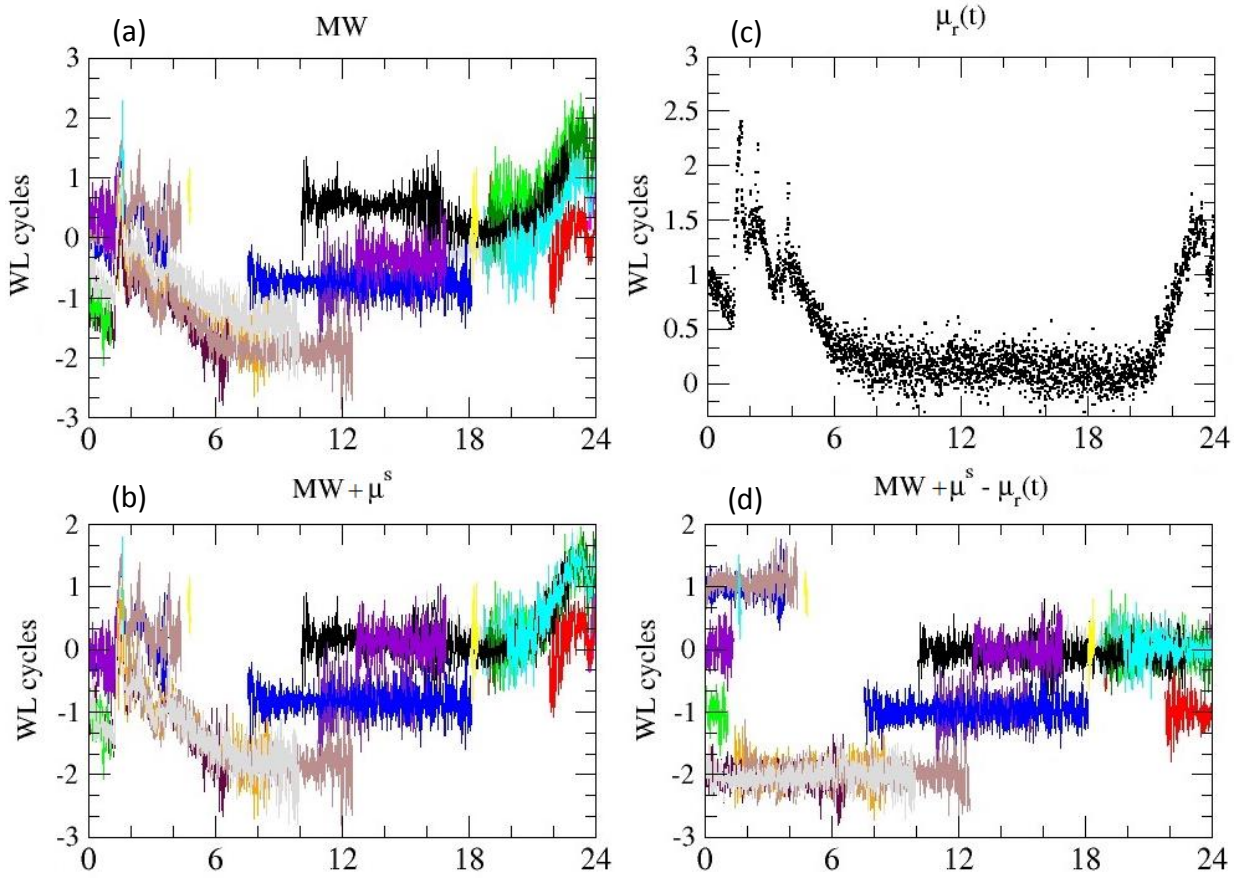

Fig. 4.14: An Example of Galileo WL fixing for FTNA station (DOY: 200/2018) expressed in WL cycles for 24 Hours: (a): the MW linear combination, (b): the MW corrected by the μ^s a-priori values, (c): the FTNA $\mu_r(t)$, (d): the MW corrected by the μ^s and the $\mu_r(t)$

4.4 Conclusions

In this chapter the Galileo fractional μ^s values are extensively studied and the Galileo WL ambiguities are blocked. From the results it is seen that:

- The WL phase biases are stable over time and the satellite delays μ^s can be estimated with the accuracy of approx. 0.1 WL cycles
- Any observed fluctuations in the order of 0.1 WL cycles of the satellite delays are repeated every 10 days due to the repeatability of the Galileo constellation
- The distribution of the IOV satellites is more spread than the FOC satellites
- There exists better homogeneity among receiver families and observation types for Galileo than for GPS

- The WL fractional μ^s values for the Galileo system are stable over long periods of time whereas for the GPS system they are stable only daily. This fact inspired the CNES/CLS AC to use a different simpler way for determining the Galileo WL satellite biases. They use the same initial values for much longer periods than one day.

The first step of the zero-difference method is achieved for the Galileo system. In the following Chapter 4 we will include efforts for fixing the Galileo NL ambiguities, i.e. solve the $N_{r,i}^s$ and $N_{r,j}^s$.

The results and conclusions of this Chapter have been published in 2017 at the 6th International Colloquium of Scientific and Fundamental Aspects of GNSS/Galileo in Valencia, Spain under the title: *"Galileo E1/E5a phase measurements Wide-Lane ambiguity fixing at the undifferenced level using the IGS network"*

5. Galileo Narrow-Lane AR

5.1 Introduction

After the successful WL AR for the Galileo system, the next step would be to fix the NL ambiguities. This task was done within a Galileo POD processing to obtain precise Galileo satellite orbits and clocks.

This chapter addresses the following questions:

- How can the Galileo Narrow-Lane ambiguity be resolved? How can Galileo be combined with GPS in a Multi-GNSS processing?
- What are the success rates of Narrow-Lane AR?
- Is there any improvement for the orbit and clock products after AR? And if yes, at what level?

The AR was validated through numerous ways: ambiguity fixing success rates, orbit overlaps, clock overlaps, SLR residuals etc. In addition, a new way was developed to evaluate the correctness of AR.

5.2 Multi-GNSS Narrow-Lane Ambiguity Resolution

Due to the fact that the constellation of Galileo is still incomplete, it was decided to combine Galileo and GPS observations in order to better estimate common parameters (e.g. station clocks) in a Multi-GNSS processing. The inputs were station measurements and the outputs would be satellite precise orbits and clocks. The general procedure for performing POD with the zero-difference method is shown in Fig. 5.1.

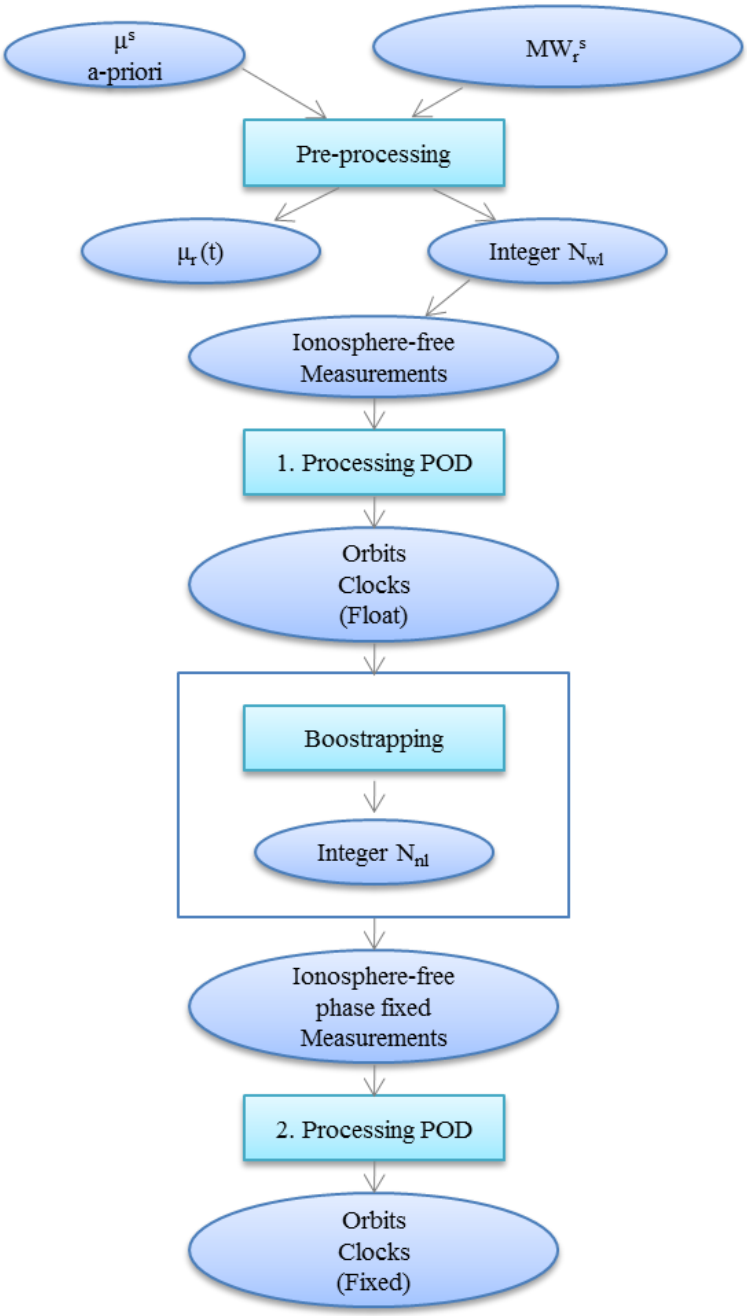

Fig. 5.1: Procedure applied to compute phase fixed GNSS products (satellite orbits and clocks)

For processing both GPS and Galileo in a Multi-GNSS formation the following scenarios were considered shown in Fig. 5.2. The first scenario consists of two steps: In the first step the procedure for GPS-only AR is done. This step is already implemented and validated from the CNES/CLS AC since 2010 and no changes are needed to adapt it to the Multi-GNSS processing. In the second step the GPS fixed measurements are combined with the Galileo float ones to form a Multi-GNSS processing. This procedure is done in order to resolve the Galileo ambiguities. The advantage of this scenario is the easy implementation to the routine used already for GPS.

The second scenario considered, consists also of two separate individual steps. The first step is the same as the first step in Scenario 1. The second step is using Galileo-only measurements to resolve the ambiguities. In this case each system is processed individually and separately. The disadvantage of this scenario, however is that in the two solutions the receiver clocks and the tropospheric parameters are different and hard to combine.

The third scenario is the processing of GPS and Galileo measurements together in one step. The output is fixed GPS and fixed Galileo ambiguities. Even though this is a much simpler processing than the others, it is very different from the current CNES/CLS processing of GPS and therefore much effort is required relatively to the previous processings.

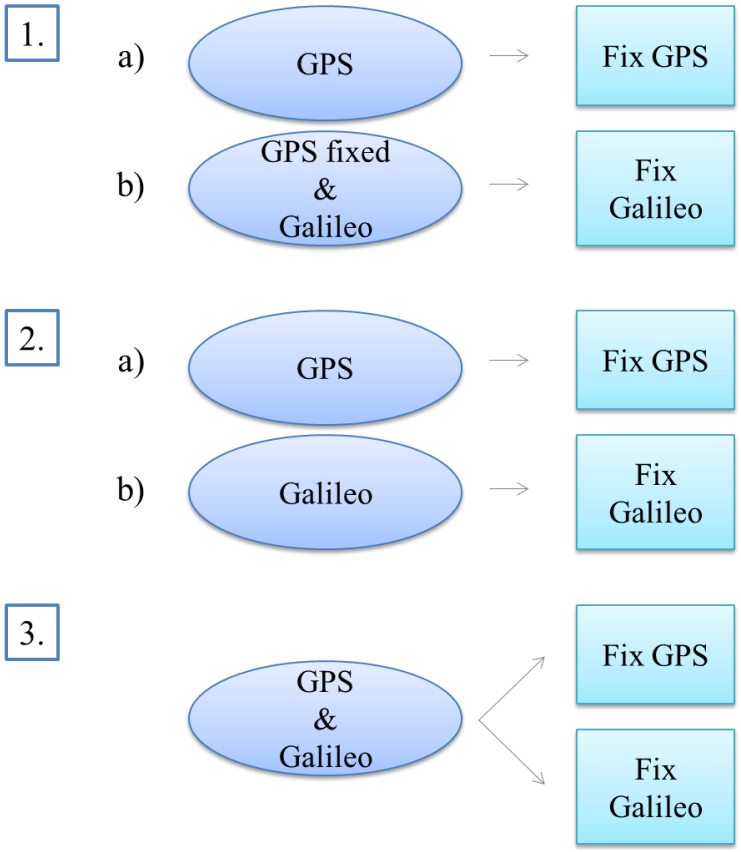

Fig. 5.2: The three possible scenarios for Multi-GNSS AR that were considered

Since the GPS AR method and processing had already been proven to be successful from previous studies of the CNES/CLS AC, it was decided to combine GPS fixed with Galileo float products as shown in Scenario 1[6].

The Multi-GNSS processing, including the POD computations, is described in more details in Fig. 5.3. In the first step, GPS measurements (both code and phase) are used as input to compute a GPS constellation solution and fix phase ambiguity measurements. Then for the second step, a

[6] The AR for Galileo was applied and tested for the CNES/CLS products (GRM products). Scenario 1 was first tested but the processing of GPS and Galileo systems together for phase ambiguities resolution according to Scenario 3 was finally adopted after modification of the GINS and DYNAMO software.

combination of GPS phase fixed and Galileo code and float phase measurements are used to calculate a multi-constellation solution. Galileo phase ambiguities are then fixed. As a last step, fixed phase only measurements from both systems are processed to estimate satellite orbits and clocks.

For the POD processing, the GINS and DYNAMO software (Marty, 2013) were used developed by GRGS. The GINS software is a multi-technique space geodesy processing software that has been also used to process GNSS signals. It is the software that is currently used from the CNES/CLS AC on a weekly basis to compute orbit, clock and Earth rotation products for the IGS. The measurements and the model parameters are processed by least squares adjustment of the linearized observation equations (Loyer, et al., 2012). As an output, GINS is providing normal equation matrices that are later used as input matrices to the DYNAMO software. The DYNAMO software is a matrix processing software of normal equations (summation, reduction, and linear system resolution).

For the Multi-GNSS processing of the chosen Scenario 1, parts of GINS and DYNAMO software had to be modified by the CNES/CLS AC to be capable to process the Galileo data as wanted.

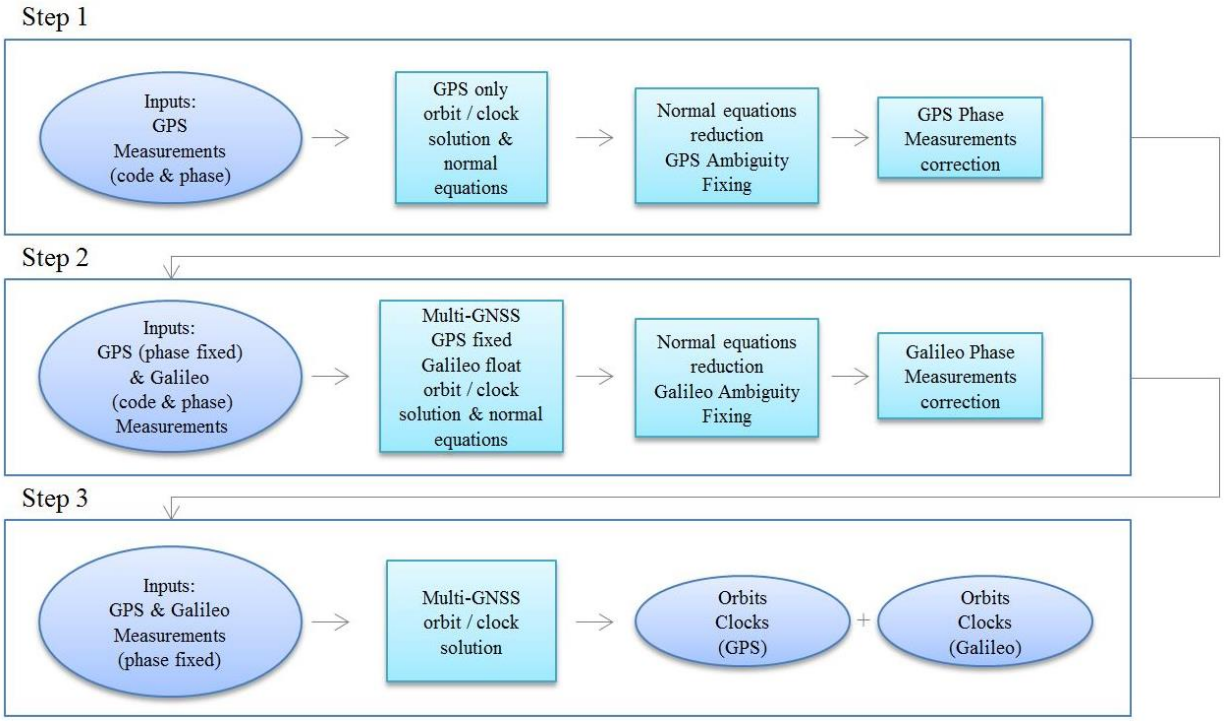

Fig. 5.3: The Multi-GNSS processing in a three-step procedure

5.3 Multi-GNSS POD Models

The following models and parameters given in the Tab. 5.1 are applied. Because of the GPS/Galileo combination, the inter-system biases (ISB) (See Section 5.4) had to be taken into account (Håkansson, et al., 2017). One parameter of inter-system phase bias is taken into account for every station per day applying the constraint that the mean of all ISBs relative to one satellite are equal to zero for every processed day.

	GPS	Galileo
Processing strategy		
Number of satellites	31	13-24 (incl. E14, E18)
Number of stations	~ 100-120	~ 60-80
Arc duration	6h + 24 h + 6 h (to allow overlaps)	
Observation sampling	300 sec	
Elevation mask	8°	
Measurement weights	Code: 0.35m Phase: 0.0035m	
GNSS system weights	GPS=Galileo	
Models		
Antenna phase center corrections	ANTEX14	
Troposphere model	VMF + GPT2 (Böhm, et al., 2014)	
Ionosphere model	Ionosphere-free combination & second order corrections (Hernández-Pajares, et al., 2007)	
Reference frame	ITRF 2014 (Altamimi, et al., 2016)	
Attitude model	(Kouba, 2008)	(GSA, 2017)
Solid earth tides, polar tides, ocean loading effects	Oceanic tide: FES2012	
	Oceanic pole tide: (Desai, 2002)	
Ocean loading effects	FES2012 (Carrère, et al., 2012)	
Earth orientation modelling	IERS Conventions 2010	
Earth orientation parameters	EOP C04	
Phase windup	(Kouba, 2008)	
Estimated Parameters		
Solar radiation pressure, empirical forces	ECOM2 (Arnold, et al., 2015)	
Troposphere	1 ZTD / 2h	
	1 pair of gradients (E, N) / day	
Inter-system biases (phase obs.)	1 / station (zero mean condition)	
Satellite state vector	Position, Velocity	
Ambiguities	1 / pass (float solution)	
Satellite and receiver clocks	1 / epoch	

Tab. 5.1: Models applied during the Multi-GNSS processing

For NL ambiguity fixing, Eq. 3.26 and 3.27 which are geometry dependent, are used. Therefore, it is crucial to use highly accurate models (including station coordinates, satellite orbits and clocks, troposphere, receiver clocks, measurement biases, wind up effect etc.). The combined resulting error should not exceed half a NL cycle (i.e. around 5 cm in the measurement direction) in order to successfully fix the ambiguities. As a consequence, in case of a badly modelled orbit (e.g. inconsistencies in satellite attitude) the fixing procedure can fail.

Galileo satellites E14 and E18 are placed on elliptical orbits. Those satellites were initially excluded from the processing. Later they were added as the Galileo constellation augmented.

Since autumn 2017, the latest release of the Galileo IOV and FOC satellite metadata (box & wing and attitude law) from GSA is used (GSA, 2017) for better modelling the satellite attitude and the geometrical properties of the satellites.

The NL AR was done sequentially for one pass at a time within a bootstrap method (Verhagen, 2005). For the AR some constraints were applied. Passes with the following characteristics were not fixed to an integer value:

- passes that have high co-variance: higher than 0.038 NL cycles
- float passes with difference higher than 0.2 cycles from the nearest integer
- short passes (i.e. 600 sec)

The IGS is compiling a consistent set of absolute Antenna Phase Centre (APC) corrections for both receivers' network and satellites, which are provided in so-called the Antenna Exchange Format (ANTEX) files. These corrections are very important for the calculation of the geometrical distance between satellite and receiver. For the APC corrections, it was decided to use the ANTEX14 file from the IGS. During the present thesis ANTEX14 file was including the APC values of the receivers for GPS L1/L2 frequencies, but not of Galileo E1/E5a frequencies. Delivery of the respective receiver APC values for the Galileo E1/E5a frequencies was underway from the IGS Antenna WG.

5.4 Validation of the results

This section has two main objectives: firstly, to quantify and validate the Galileo NL ambiguity fixing and secondly to evaluate its impact on orbit and clock quality using overlaps and Satellite Laser Ranging (SLR) observations.

The following ways are used for GNSS processing validation (Steigenberger, et al., 2014). These ways show that the Galileo NL AR was done successfully giving satisfactory results. Positive impact of correct AR is seen at orbit overlaps, clock overlaps and SLR residuals.

The Multi-GNSS processing was successfully performed for the period from 2017 until 2019 for the same network of IGS stations shown in Fig. 4.1.

Ambiguity Fixing

The success rates of ambiguity fixing (number of fixed passes / total number of passes) for both GPS and Galileo can be found in the following Fig. 5.4 for the period DOY:41/2019-89/2019 (i.e. 10/02/2019 – 30/03/2019). The average success of 96% for GPS is consistent with the today's processing of the CNES/CLS AC. For Galileo, the success rate is about 92% for the period shown in the example. The overall Galileo AR percentage may be lower than the one of GPS, but it is anticipated that future completion of the constellation and model improvements will increase this number and its stability.

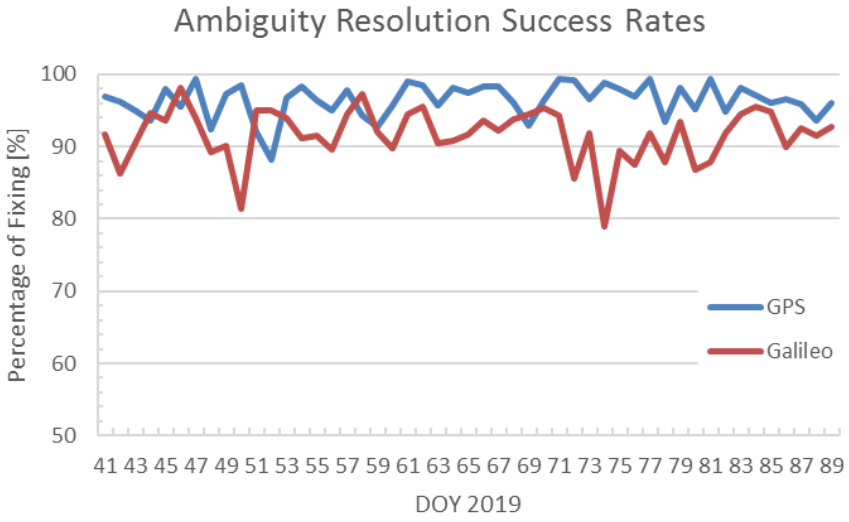

Fig. 5.4: Ambiguity fixing success percentages (Period: GPS weeks 2040 - 2046)

Integer Recovery Clocks Overlaps

Another way of validation consists of arc overlap comparisons. An arc is considered as the data interval between the beginning and the end of each processing. Every IGS AC has its own strategy as to how long these overlapping arcs should be. For the CNES/CLS AC each arc starts 6 hours before and ends 6 hours after the central day. Hence there is a 12-hour overlapping period between two successive arcs (Fig. 5.5). Ideally, when comparing the results for the same 12-hour period from two different consecutive solutions, the difference should be negligible.

The term of Integer Recovery Clocks (IRCs) first appeared with the publication of the zero-difference method (Laurichesse & Mercier, 2007). The aim of the IRCs approach is to keep the "integer" nature of the phase clock solutions. As a consequence, consecutive clock products must differ by an integer number of narrow-lane wavelengths (Loyer, et al., 2012). Fig. 5.6 shows a representative example of the overlap difference expressed in NL cycles between two sequential GPS and Galileo clock solutions. The "integer" property of the phase clock solution is verified. It is seen that the clock overlap difference curves are distant from each other within

±n NL cycles for both GPS and Galileo. This confirms the correct ambiguity fixing and the proper IRC products. It is worth noticing that in this figure the GPS curves are centered to integer values whereas the Galileo ones are not. There is a bias between the GPS and the Galileo overlaps that is a reflection of the ISB differences that are correlated with the clock estimates. That is to say (refer to Eq. 3.27): for the GPS graph the curves represent the terms ($c\delta t^{s,GPS} \pm \lambda_{nl,GPS} N_{r,i}^{s,GPS}$) whereas for the Galileo graph they represent the terms ($c\delta t^{s,GAL} \pm \lambda_{nl,GAL} N_{r,i}^{s,GAL} + \delta ISB$).

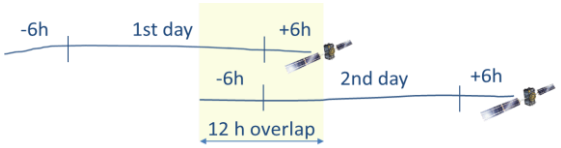

Fig. 5.5: Representation of arc duration (6h + 24h +6h)

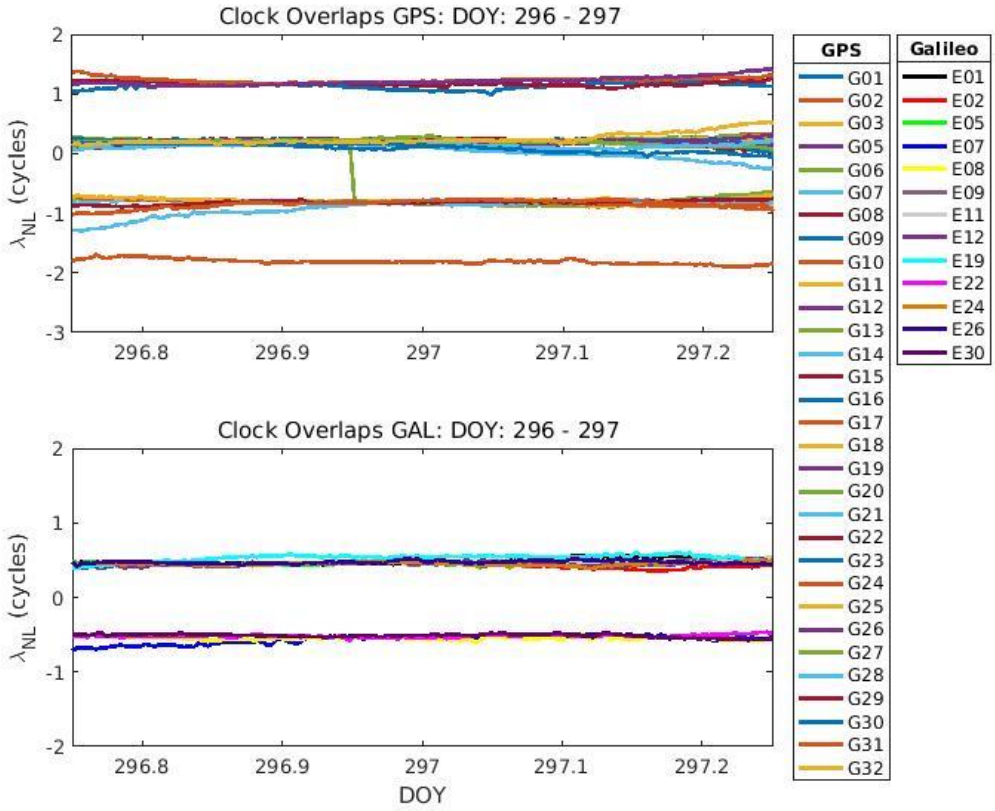

Fig. 5.6: Clock overlaps example of GPS and Galileo satellites (DOY: 296 - 297/2017)

Orbit Overlaps

In a similar way to clock overlaps, orbit products can also be compared for each 12-hour overlapping period. In Fig. 5.7 an example is given of the orbit overlap between DOY 297 and 298/2017 for the Galileo orbits with float and fixed ambiguities respectively. The orbits overlaps are noticeably lower in the fixed case with the most significant improvements in the along and normal directions.

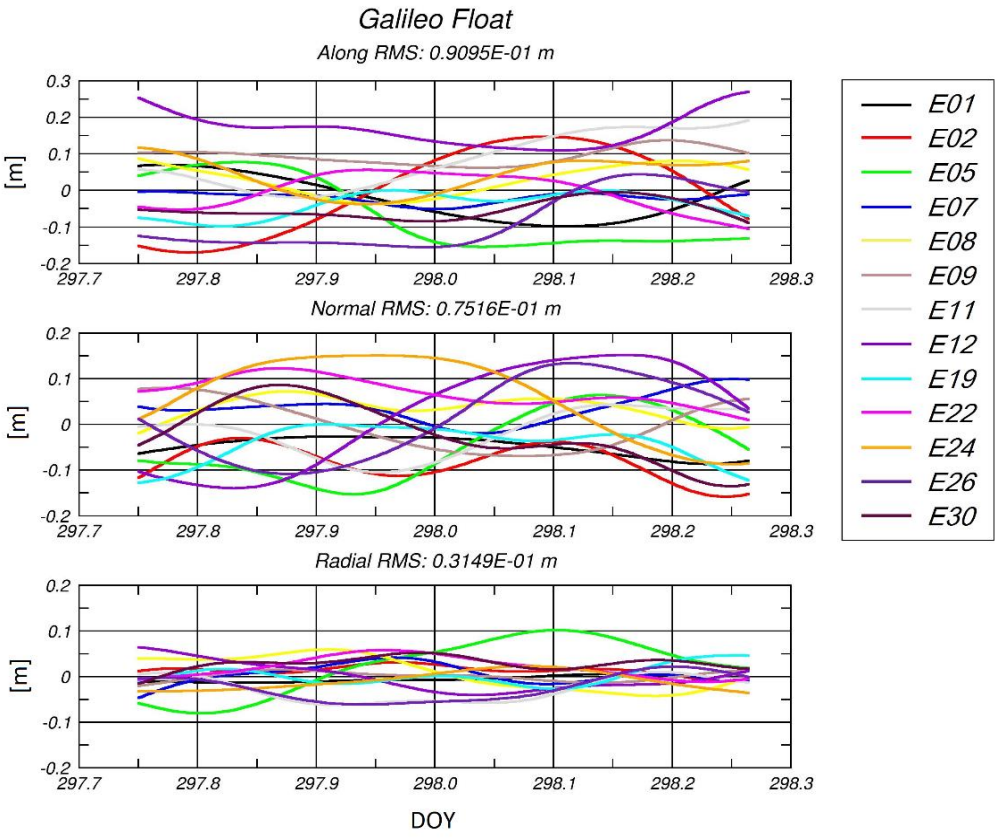

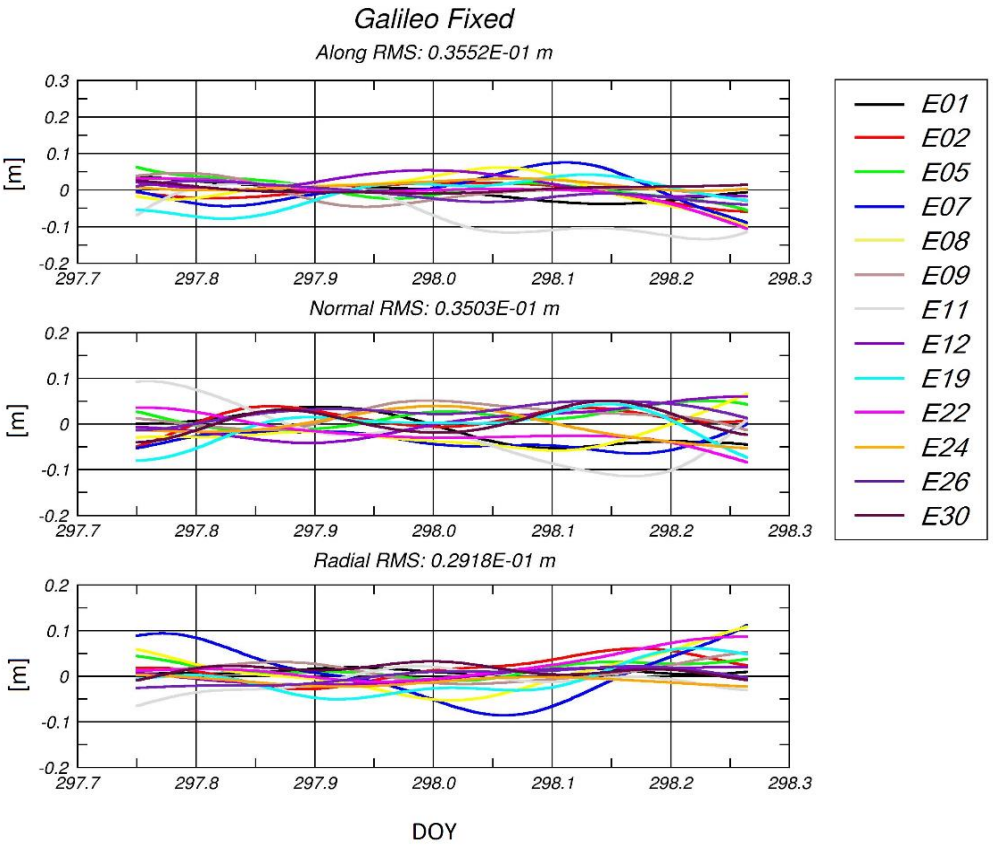

Fig. 5.7: Orbit overlaps for Galileo float and fixed solutions for along, normal and radial directions (DOY: 297 – 298/2017)

Such orbit overlaps were computed for 07/10/2017 (DOY: 280) until 06/11/2017 (DOY: 310) and their RMS values were gathered. The histograms of Fig. 5.8 compare the Galileo orbit overlaps using float and fixed ambiguities. The peacks of the histograms for the normal and the along component are significantly shifted towards smaller values indicating an orbit improvement. The corresponding mean numbers are given in Tab. 5.2. Hence, fixing the ambiguities is beneficial. Overall the 3D RMS orbit overlap improved by nearly 2 cm. However, this is not the case for the radial component where ambiguity fixing does not seem to change significantly the results.

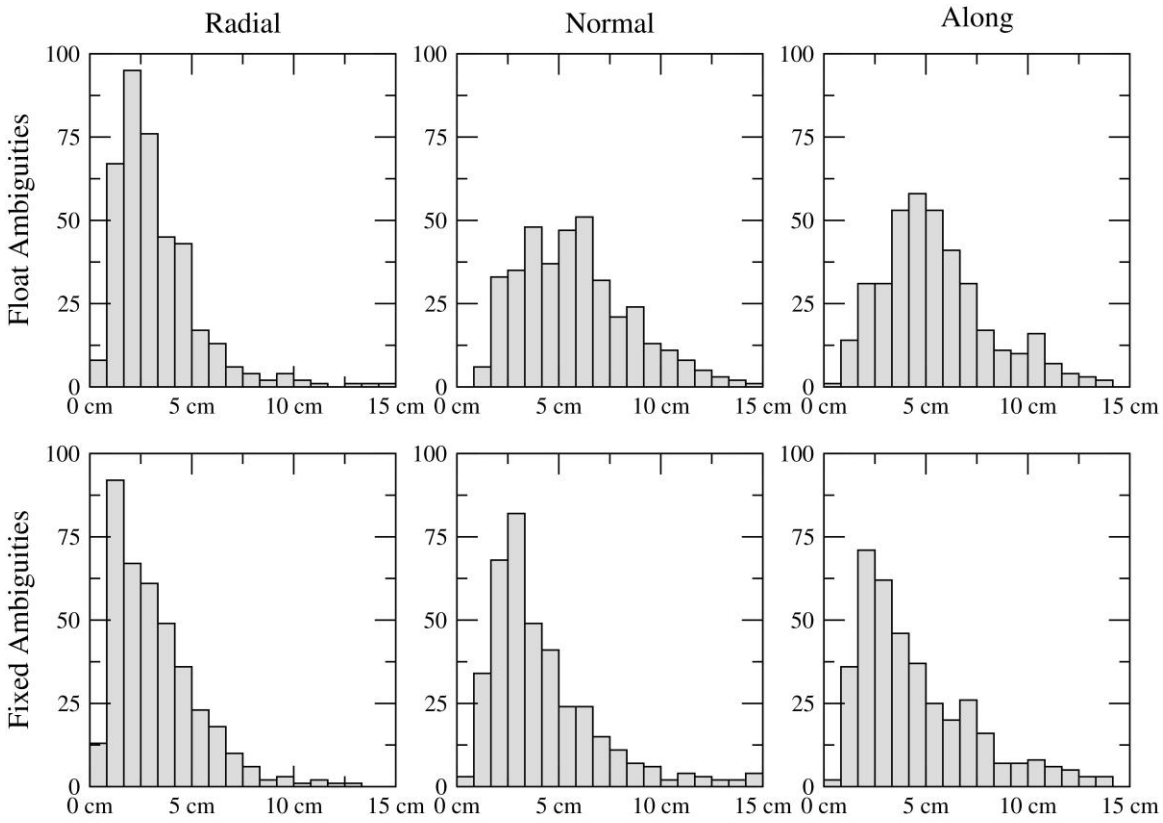

Fig. 5.8: Histograms for radial, normal and along components for the Galileo system in float and fixed orbit overlaps.

	Float (cm)	Fixed (cm)
Radial	3.2	3.2
Normal	5.4	4.4
Along	5.6	4.1
3D	7.8	6.1

Tab. 5.2: Orbit overlaps for Galileo satellites for along, normal and radial directions and three-dimensional in Fixed and Float solutions (mean values).

Another example of a more recent period (June 2019) is shown in figures Fig. 5.9 to Fig. 5.12. For every day of the shown period and for all the satellites the 3D overlaps RMS number is calculated and represented by a color. It is clearly seen the improvement for both systems from float to fixed orbit overlaps.

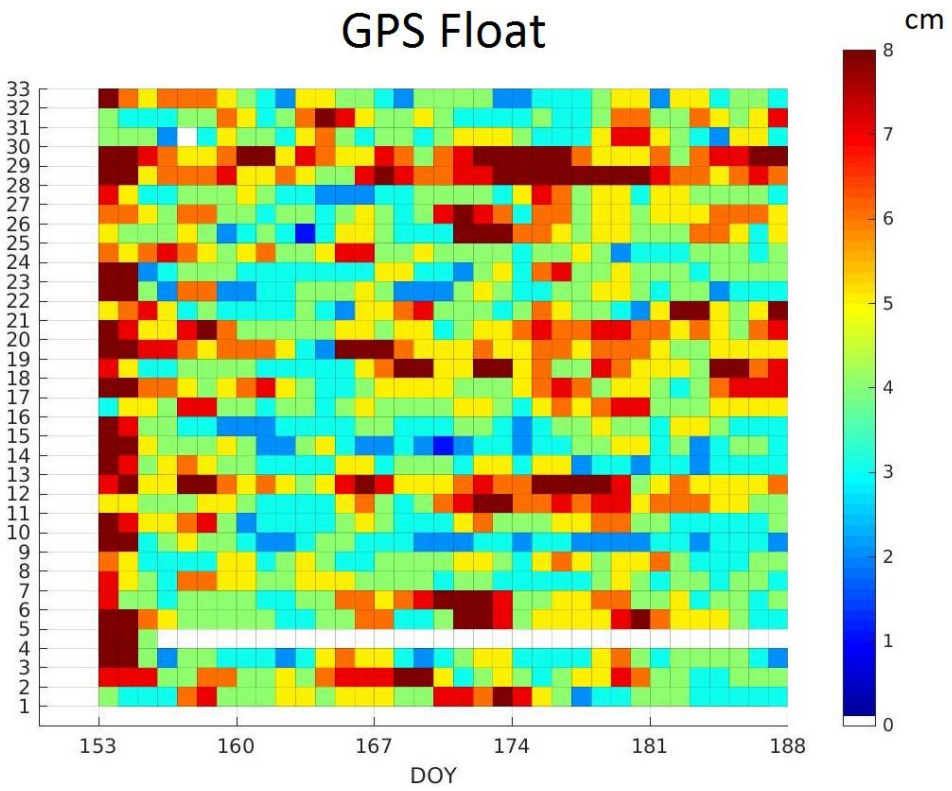

Fig. 5.9: 3D RMS of float orbit overlaps for the GPS system for the period: DOY 153-188/2019. The global 3D RMS for this period is around 5.2 cm.

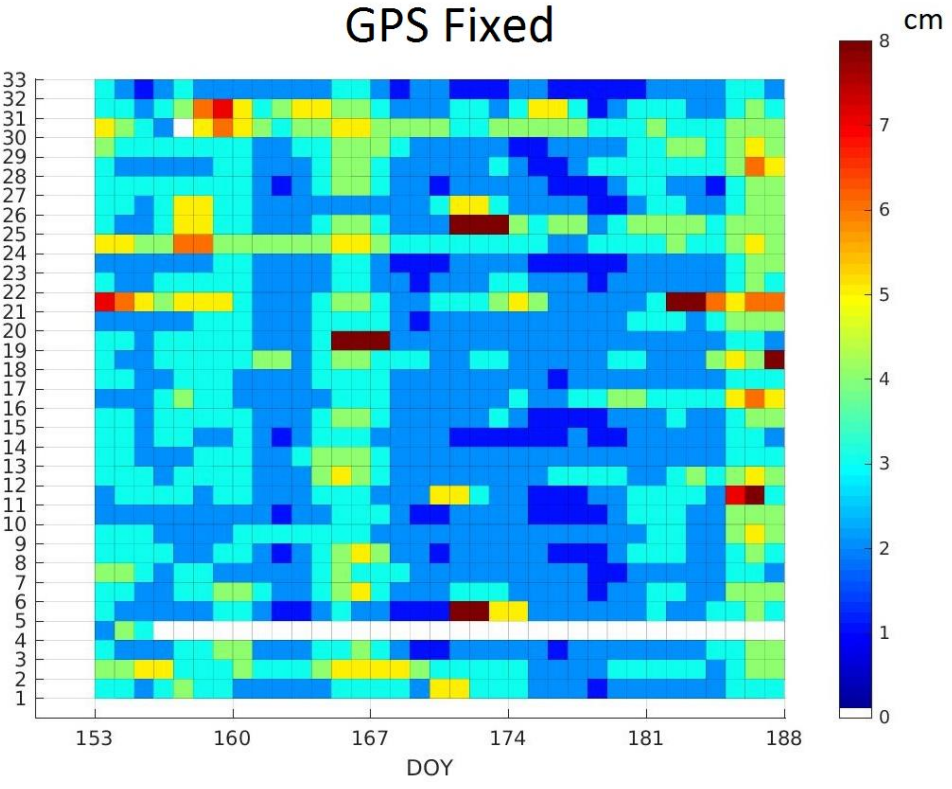

Fig. 5.10: 3D RMS of fixed orbit overlaps for GPS for the period: DOY 153-188/2019. The global 3D RMS for this period is around 2.7 cm.

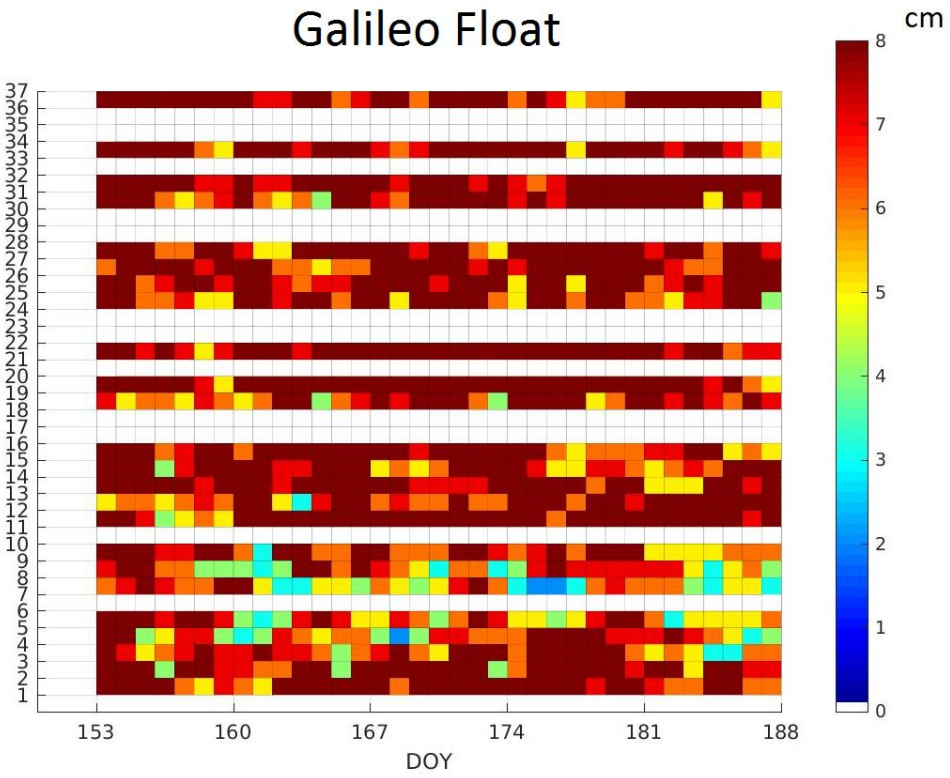

Fig. 5.11: 3D RMS of float orbit overlaps for GPS for the period: DOY 153-188/2019. The global 3D RMS for this period is around 7.1 cm.

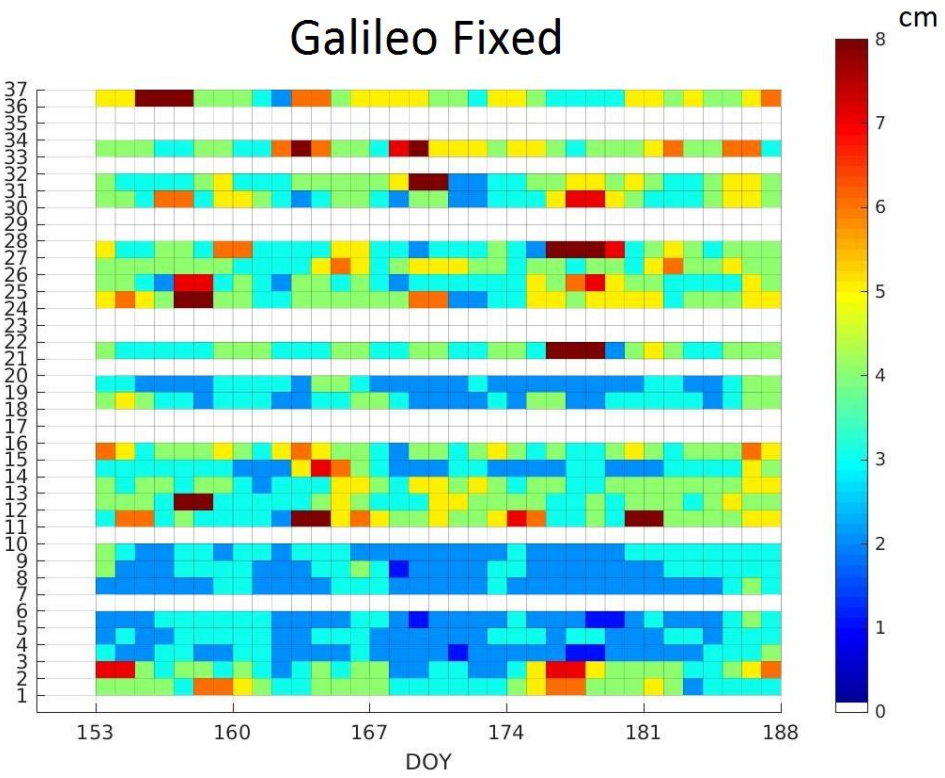

Fig. 5.12: 3D RMS of fixed orbit overlaps for Galileo for the period: DOY 153-188/2019. The global 3D RMS for this period is around 3.6 cm.

SLR Residuals

Satellite Laser Ranging (SLR) is an optical technique that determines the ranges between ground stations and satellites (Sośnica, et al., 2017). These observations are commonly used for orbit validation. Both IOV and FOC Galileo satellites are equipped with laser retro-reflector arrays (LRAs) (ESA, 2017). SLR data are widely used for examining the precision and accuracy of the MGEX orbit products (Steigenberger, et al., 2014). SLR observations are mostly sensitive to the radial orbit direction, because the maximum incident angle of a laser beam for Galileo is 15° (Zajdel, et al., 2017).

In March 2017 an online service was initiated by the Associated Analysis Center of the International Laser Ranging Service at the Wrocław University of Environmental and Life sciences (IGG ILRS ACC) called Multi-GNSS Orbit Validation Visualizer Using SLR (GOVUS), allowing for GNSS orbit validation using SLR measurements in near-real time mode (Zajdel, et al., 2017).

This online service is used to examine the SLR residuals of the Galileo float and fixed ambiguity orbits. In Fig. 5.13 is shown the average values and standard deviations of the SLR residuals for each satellite separately for the whole period of study. The statistics were computed taking into account only SLR residuals whose absolute value did not exceed 250 mm. Greater values are considered as outliers and are removed. All SLR stations are included. An increase of standard deviation of SLR residuals during an eclipsing period (approximately when $|\beta \text{ angle}| < 8°$)[7] is generally expected because of unmodeled attitude switch on the satellite. The satellites E05/E07/E08/E09/E19 were approaching that range thus that may be the reason for slightly increased values of standard deviation of SLR residuals for these satellites.

Overall, the standard deviation for the solution with fixed ambiguities is lower than for the solution with floating ambiguities at the level of 5mm (15%). The only exceptions are satellites E01 and E07; the number of observations for these satellites are observed to be about 30 % lower than the average. On the other hand, the offset of SLR residuals is lower in the solution with floating ambiguities for the satellites on the plane C and for IOV satellites (E11, E12, E19). The rest of the offset in SLR residuals may come from the unmodeled impact of antenna thrust or albedo. Considering that fixing ambiguities has a limited impact on the radial direction, even a small reduction of SLR residuals can be considered as an improvement of the orbit.

[7] As β angle is defined the smaller angle between the Sun vector and the satellite orbital plane.

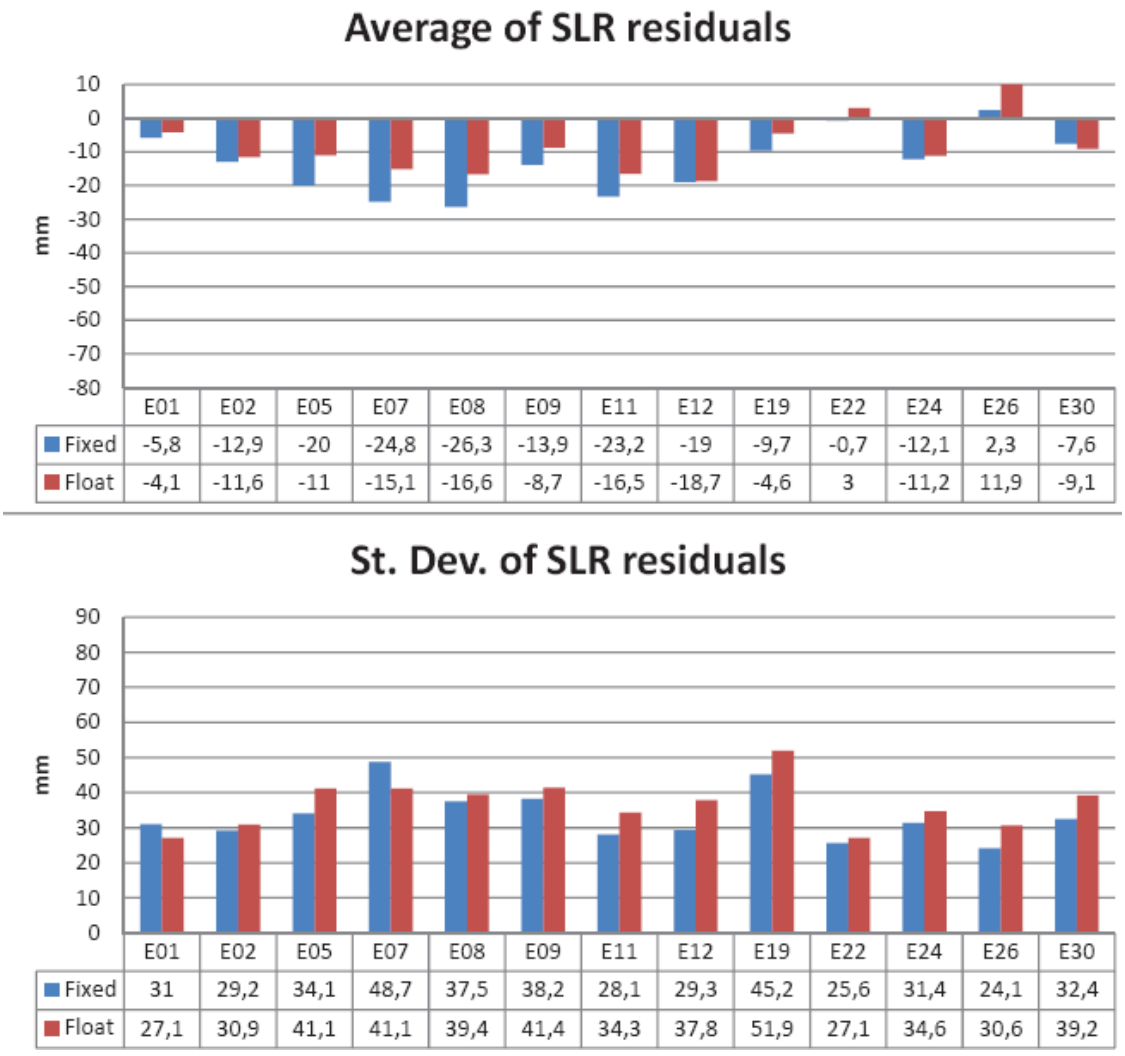

	E01	E02	E05	E07	E08	E09	E11	E12	E19	E22	E24	E26	E30
Fixed	-5,8	-12,9	-20	-24,8	-26,3	-13,9	-23,2	-19	-9,7	-0,7	-12,1	2,3	-7,6
Float	-4,1	-11,6	-11	-15,1	-16,6	-8,7	-16,5	-18,7	-4,6	3	-11,2	11,9	-9,1

	E01	E02	E05	E07	E08	E09	E11	E12	E19	E22	E24	E26	E30
Fixed	31	29,2	34,1	48,7	37,5	38,2	28,1	29,3	45,2	25,6	31,4	24,1	32,4
Float	27,1	30,9	41,1	41,1	39,4	41,4	34,3	37,8	51,9	27,1	34,6	30,6	39,2

Fig. 5.13: Average values and standard deviations of the SLR residuals for each Galileo satellite for phase float ambiguities and phase fixed ambiguities orbits.

Inter System Biases

When combining two (or more) GNSS systems, one must take into account the difference of these systems with respect to timescales, coordinate systems and hardware delays of the receiver (Montenbruck, et al., 2011) (Odijk, et al., 2012). These differences are expressed as a bias, the so-called intersystem bias (ISB). Early studies of the ISBs between GPS and Galileo were done for several GNSS products providers (including the CNES/CLS AC) and showed the ISBs are receiver dependent and stable in time and may be estimated as one parameter per session (Paziewski & Wielgosz, 2015).

In the CNES/CLS AC processing the GPS-Galileo ISBs are considered stable for each day. The ISB terms are added to the equations for the Galileo system. One ISB bias is estimated per station and per day under the condition that the mean of all ISBs refereing to the same satellite equals to zero.

A small investigation was made to confirm this hypothesis. POD processings were done for Galileo-only and Multi-GNSS processings. One week of data was used from 14/01/2018 (DOY: 014) until 20/01/2018 (DOY: 020). The station's clocks of the network used (See Fig. 4.1) were compared for the two processings. The following equations from the Iono-free phase fixed measurements are describing the hypothesis:

$$c\delta t_{r,GAL} = c\delta t_r + \varepsilon_{r,GAL} \tag{5.1}$$

$$c\delta t_{r,MULTI} = c\delta t_r + ISB + \varepsilon_{r,MULTI} \tag{5.2}$$

$$D = c\delta t_{r,MULTI} - c\delta t_{r,GAL} = ISB + \varepsilon_D \tag{5.3}$$

were:

$c\delta t_{r,GAL}$, $c\delta t_{r,MULTI}$: clock corrections of the station ($c\delta t_r$) calculated from Galileo-only ($c\delta t_{r,GAL}$) and Multi-GNSS processing ($\delta t_{r,MULTI}$) [s]

ISB : Inter-System bias [s]

$\varepsilon_{r,GAL}$, $\varepsilon_{r,MULTI}$, ε_D : remaining receiver noise [m]

Following the hypothesis that the ISBs are stable for each session, then the difference (D) of station clocks between Galileo-only and Multi-GNSS processing must also be stable. Generally, in most cases that were checked, it is confirmed that the hypothesis of stable ISBs is valid. The following Fig. 5.14 is showing the result of the difference of Galileo-only and Multi-GNSS receiver clock estimates expressed in units of distance. Each colored line represents another station. In this figure all stations checked are shown. It is confirmed that the ISBs are stable during one day and their mean value is around zero.

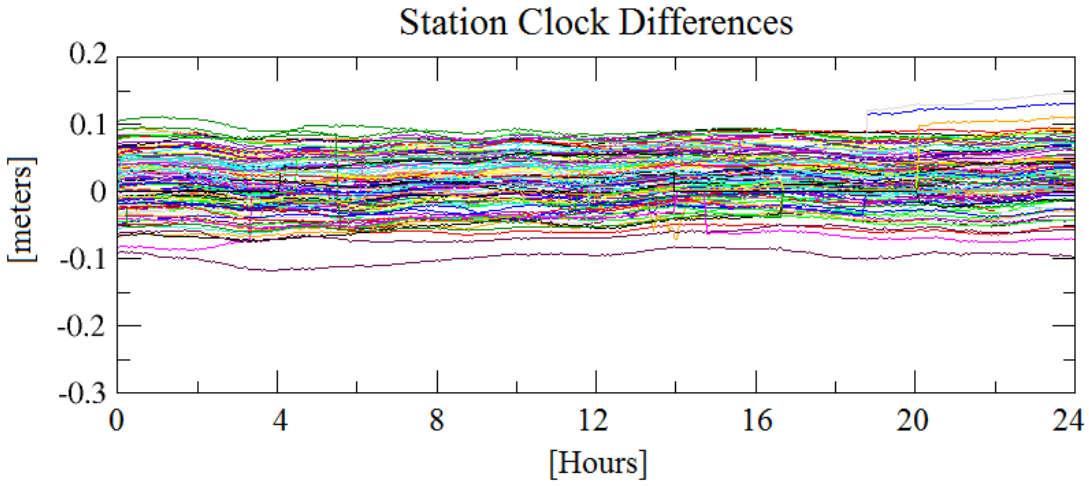

Fig. 5.14: Station clock differences between Galileo-only and Multi-GNSS for DOY: 018

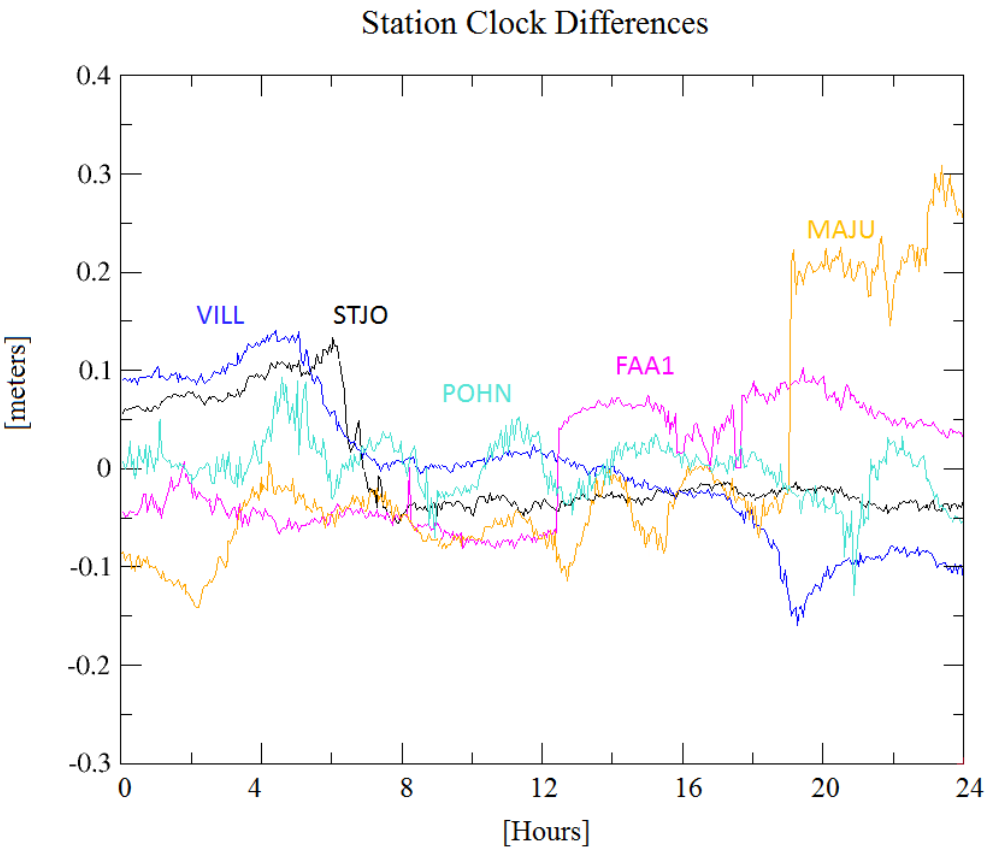

Fig. 5.15: Few clock differences between Galileo-only and Multi-GNSS for DOY: 014

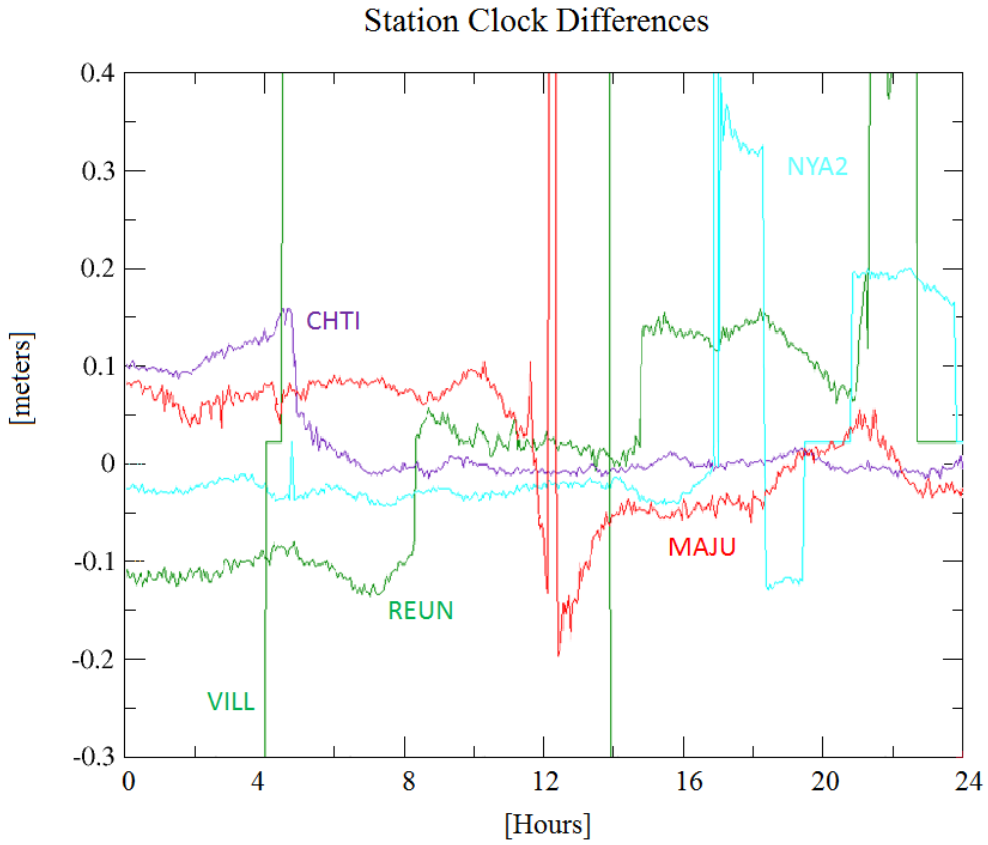

Fig. 5.16: Few clock differences between Galileo-only and Multi-GNSS for DOY: 017

Nevertheless, it was observed that few stations (out of around 60 stations) show 'jumps' and irregular lines. As shown in the examples of Fig. 5.15 and Fig. 5.16 for the days DOY 014 and DOY 017. The following Tab. 5.3 is a summary of the few stations that were identified for the week studied. The reason for this behavior or common characteristics of these stations could not be found.

DOY	Stations
014	VILL, STJO, POHN, FAA1, MAJU
015	FAA1, VOIM, TOW2
016	VILL, MATG, POHN, MAJU, NRMD, REUN, METG, TOW2, STJO
017	CHTI, VILL, REUN, MAJU, NYA2
018	REYN, WIND, MAJU
019	VOIM, MAJU, FAA1, TOW2
020	TOW2, FAA1, VILL, CHPG, KRGG, PIE1, CHTI, REUN, CNB3

Tab. 5.3: Stations that show unstable clock differences for the period of study

This indicates that the hypothesis used might not be adequate for all stations. Perhaps another way of ISB estimation must be introduced and tested: e.g. calculation of ISBs per epoch or per satellite pass.

5.5 Method for AR solution comparison

So far, there are no direct tools that permit to compare and validate the ambiguity fixing solutions. The indirect tools used until today comprise: the percentages of ambiguity fixing, the overall improvement of orbit and clock overlaps, the overall quality of PPP-AR solution etc. It is hard to know so far where and when an erroneous ambiguity fixing may occur. All the above are indications that a tool is needed to compare and check ambiguity fixing solutions:

- in case of changing models, measurement weighting, processing strategies etc.
- in case of overlapping arcs between successive days

The basic idea is to be able to compare integer ambiguity resolution solutions with common satellite passes either from successive days, or from the same day but using different solution strategies (Fig. 5.17). Without restrictions, the AR solutions (i.e. the common ambiguity fixed passes) can be organized to simple integer value matrices where e.g. in the rows there are the stations and in the columns are the satellites organized.

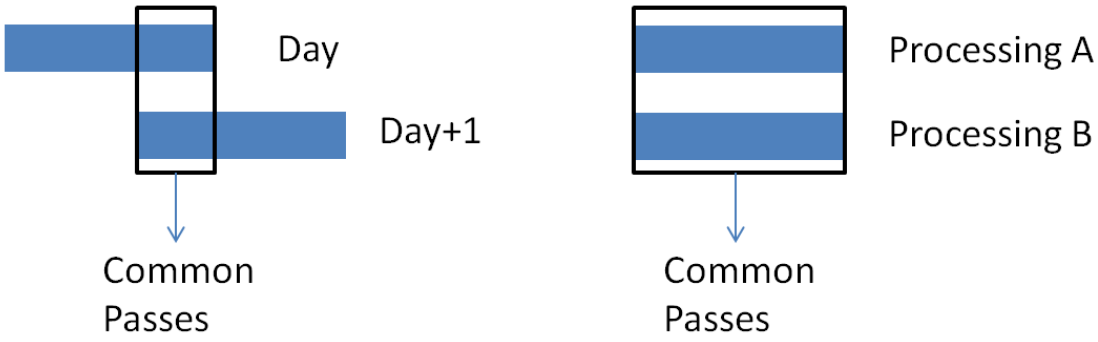

Fig. 5.17: The two ways to compare integer ambiguity matrices: successive days, different processing strategies

The difficulty is that different AR solutions do not have equal AR matrices for the same processing. From Eq. 3.27 it is noticed that the terms $c\delta t^s$, $c\delta t_r$ and $\lambda_{nl}N_{r,i}^s$ are totally correlated. This means that arbitrary integer numbers can be added or subtracted to these terms resulting to the same solution. For this reason, it is not possible to solve for the absolute values of the integer ambiguities. In contrast it is feasible and important to compute their relative values (or relative differences) among themselves.

The AR processing takes into account all measurements (i.e. from all satellites and all stations) simultaneously and conjointly. Globally, the relative relations among integer ambiguity values must be also kept for every single station or satellite. In Fig. 5.18 there are two examples that explain the relative relation of the integer ambiguities for a satellite (a) and a station (b). The (a) example is showing one satellite visible by three stations. It is possible to have any arbitrary integer number $+n$ to all the integer ambiguities of the three measurements shown. This addition is not changing the relative value relation of the stations in view. Likewise, in the example (b) a station is tracking three satellites. In the same way it is possible to have another arbitrary integer number $+m$ that is common to all measurements for the three visible satellites.

As a consequence, when comparing two AR matrices (e.g. matrices A and B) they may be unequal even for the exact same processing. They can have different integer values added for each row and each column (i.e. each satellite and each station). That is to say, there are unknown arbitrary integer numbers added to entire columns and rows. The following Fig. 5.19 is showing an example for two matrices A and B. For two different solutions these matrices are not equal. The values of matrix B can have arbitrary integer values ($+n$, $+m$) added to any entire column(s) and/or row(s).

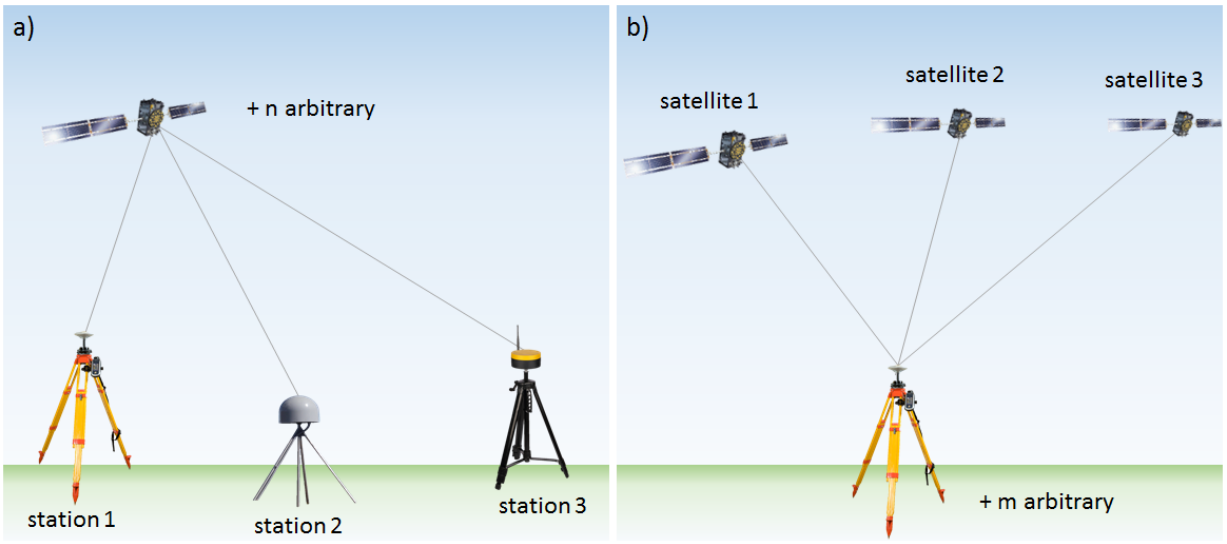

Fig. 5.18: Illustration example of relative ambiguity values relation: (a) for a satellite (b) for a station

These arbitrary integer numbers depend on the initialization during the bootstrapping process during AR. The bootstrapping procedure starts by defining an initial pass that is resolved first to the nearest integer number. As a result, the other passes are resolved with respect to the integer number of the initial pass. Assigning different initial passes gives different AR matrices (like in the example in Fig. 5.19).

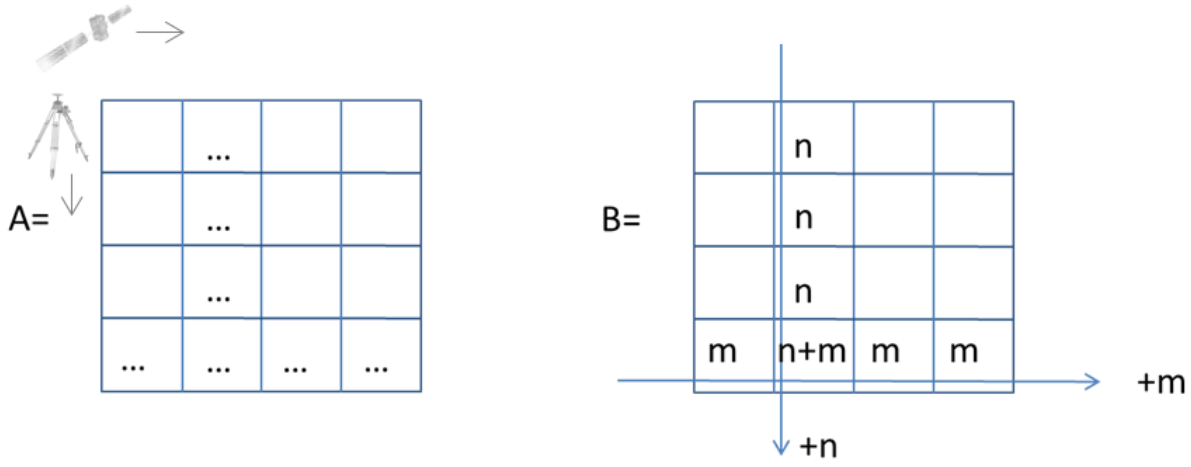

Fig. 5.19: Two unequal AR solution matrices A and B with the same relative relation of integer ambiguities

Another difficulty is that it may be possible to have data gaps for some stations and some satellites (e.g. due to cycle slips, loss of signal). In these cases, the gaps force the consideration of multiple passes and multiple initializations (an example of this case is illustrated Fig. 4.3). These multiple passes may not have the same integer ambiguity number in common for all the multiple passes.

A way to deal with this issue is to organize and sort (with respect to time) the passes considering the starting and the ending epoch of the pass. The passes must be sorted for every station and every satellite, e.g. using the Bubble Sorting method (Cormen, et al., 2001) to detect the gaps. Then, wherever a gap is detected, it must be considered as two (or more) separate cases. The following Fig. 5.20 shows an example with data gaps, for OUS2 station. In this example, station OUS2 was considered to be four separate independent stations (e.g. OUS21, OUS22, OUS23 and OUS24) and in the AR matrix there are four independent lines representing each one. In the same way in Fig. 5.21, there is an example showing a gap for the G21 satellite. In this case two satellites were considered (e.g. G211 and G212) and in the AR matrix there were two columns.

The two matrices A and B are not equal as explained above. Nevertheless, their relative integer values relation between the passes must agree. Without restrictions we may define a third matrix C=A-B. The matrix C is not equal to a zero matrix but it must agree to a zero matrix (i.e. be equal) after performing a transformation. The hypothesis used is that if the C matrix is equal to a zero matrix after applying an adequate transformation then the relative integer relation between A and B agrees.

The transformation made and used is shown in Fig. 5.22. From the two solution files A and B only the common passes to these solutions are used. The matrices A and B are subtracted to formulate the matrix C. If matrix C is a zero matrix, then the solutions were exactly identical from the beginning and therefore their integer relative relation is confirmed. In most cases however, the matrix C is not a zero matrix initially. Then, the following transformation has to be applied. For every line (or column) of the matrix iteratively: the most common value is found and subtracted to all the elements of the entire line (or column in case of columns). In case there are more than one most common values a decision must be made (e.g. the value closer to zero). When all the lines and columns are processed, the resulted C matrix is compared to the initial one. If there are differences among those two, then the loop is continued until the C matrix remains unmodified. After the loop is terminated, all non-zero elements are gathered and used in statistic values accordingly. The non-zero values reflect the difference in integers for a particular cell (i.e. showing the satellite-station pair) among solutions A and B. For further details, two examples of this transformation are presented in Appendix I section.

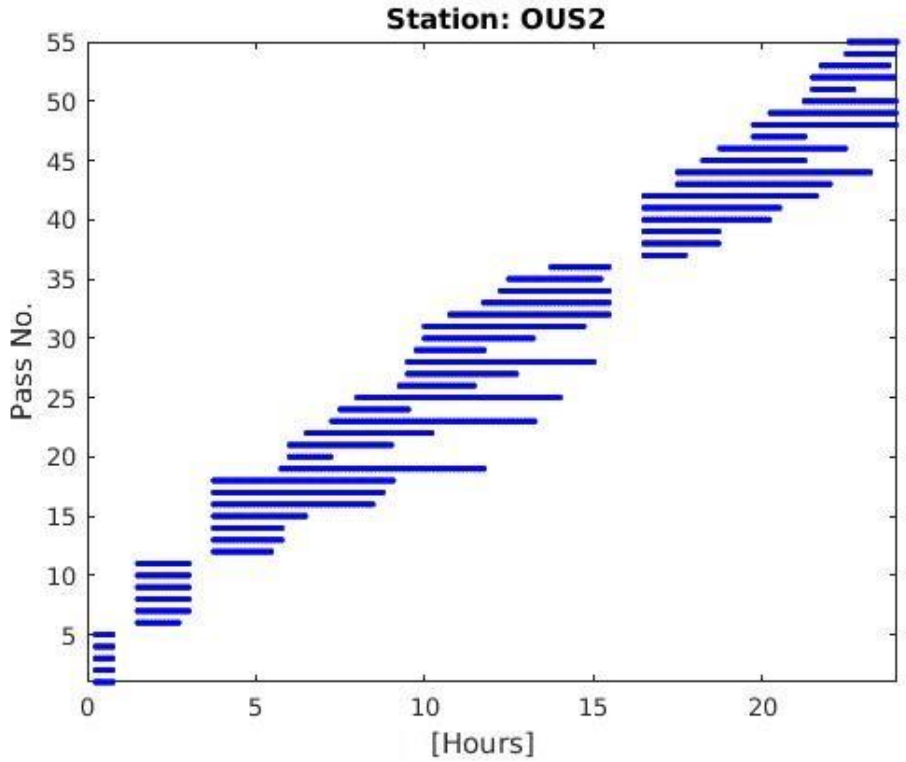

Fig. 5.20: Example of OUS2 station with gaps of data during one day (DOY: 080/2018)

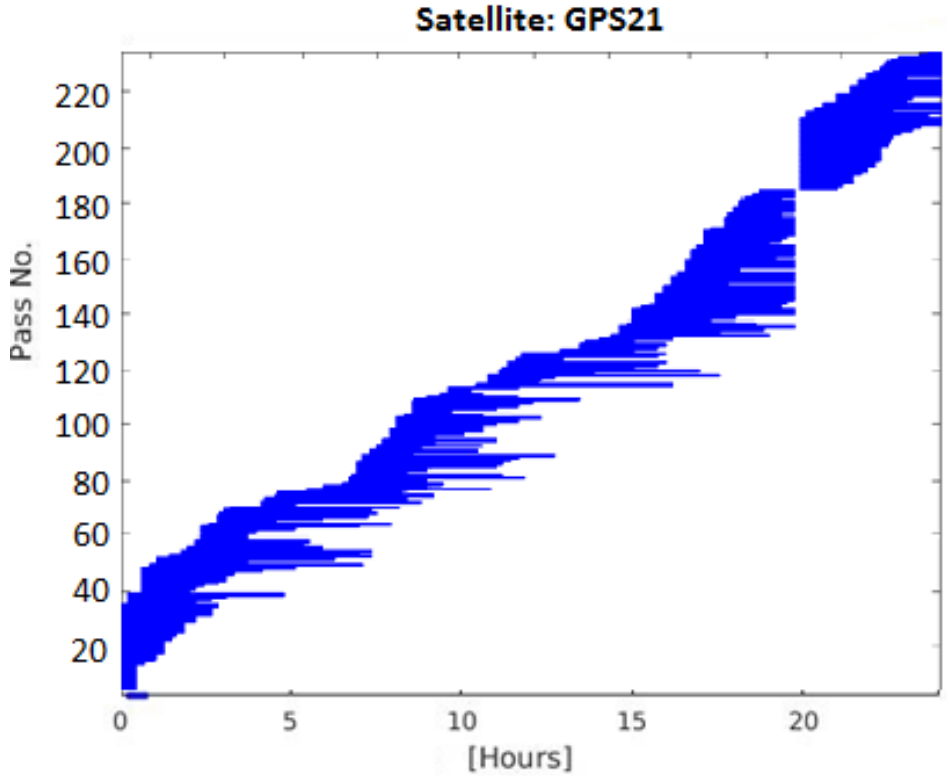

Fig. 5.21: Example of GPS 21 satellite with one gap of data during one day (DOY: 080/2018)

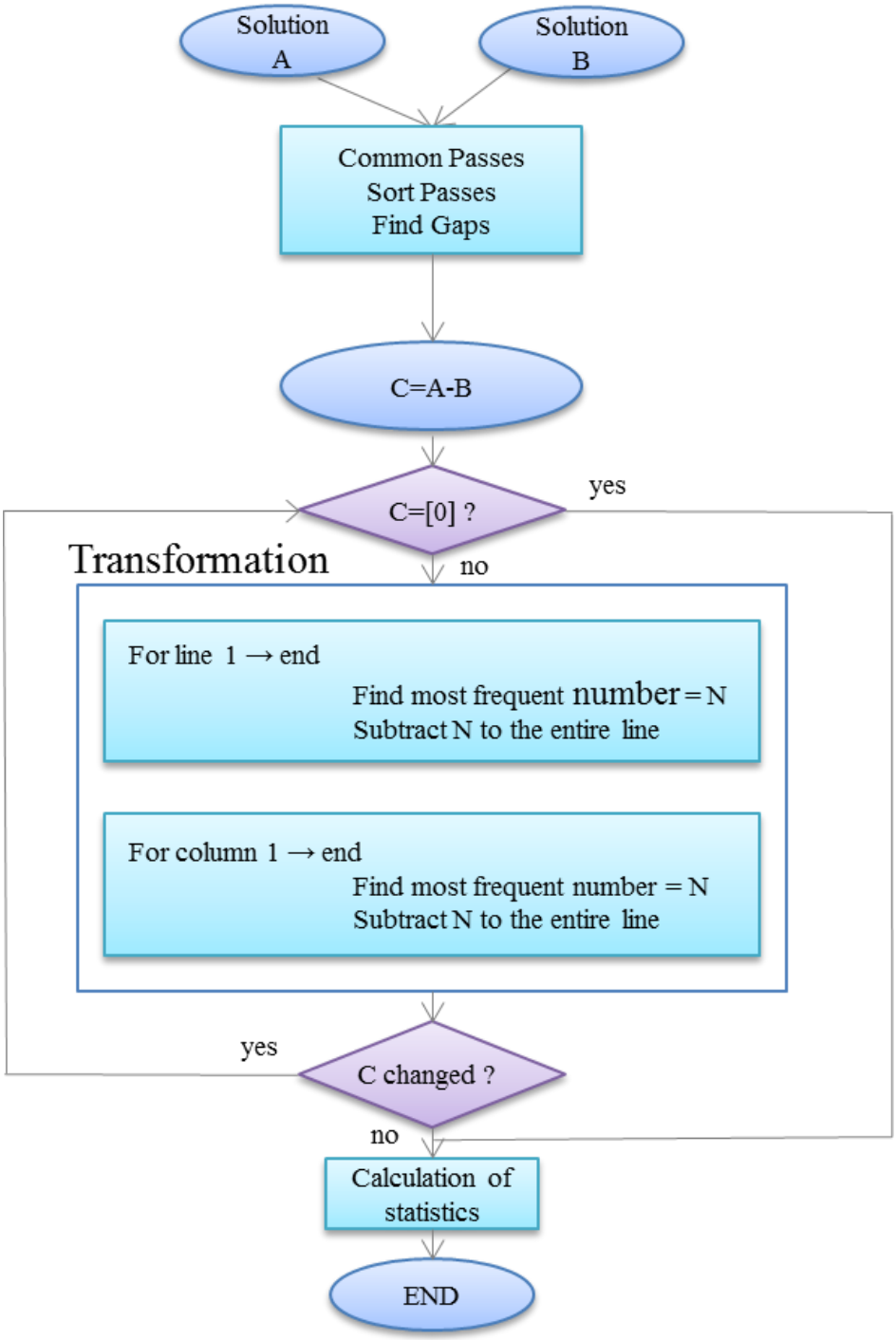

Fig. 5.22: Steps of the procedure to perform integer ambiguity matrices comparison

This tool is a way to detect the cells (i.e. station-satellite pairs) that have disagreements among two solutions and specify their difference (in integer numbers). Having such information is helpful to identify and solve potential problems in the AR processing.

The figure Fig. 5.23 is showing an example for AR success rates and AR comparison overlaps, using the algorithm described, for GPS and Galileo. The AR comparison is an indicator of the overall AR disagreement from one day to another. The overall AR disagreement for GPS is

around 4% and for Galileo is 7%. It is obvious that ideally with a flawless ambiguity fixing, the AR comparisons should be at 0%.

The reason behind these AR comparison percentages has not been found with certainty. Probable reasons might be:

- Some errors in the AR process: e.g. from a wrong WL AR, from undetected cycle slips, for wrong NL AR etc.
- Some models used might not be fully appropriate; The fact that Galileo AR percentages are lower and AR comparisons are higher than GPS might be due to the fact that the Galileo ANTEX values are not provided from the IGS until that point. For the Galileo POD calculation ANTEX values from GPS were also considered for Galileo.
- Some undetected errors in the processing routines: either in GINS and DYNAMO, or in the AR matrices comparison routine itself.

The same logic can be applied when doing PPP or PPP-AR processing. The only difference in these cases is that since only a single station is processed, instead of a matrix, two vectors of integer values are compared.

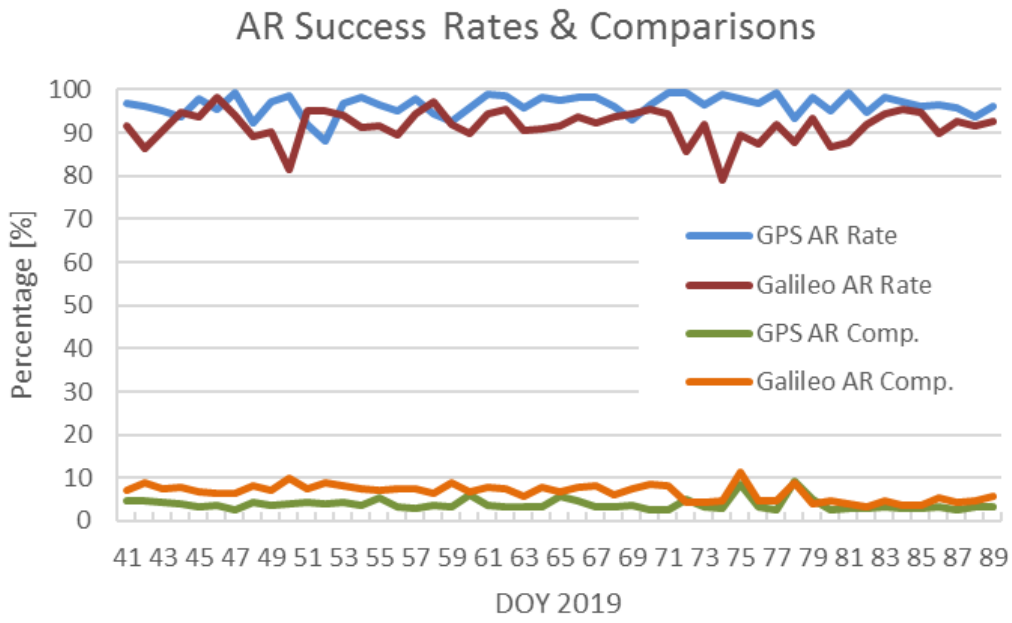

Fig. 5.23: AR success percentages and AR comparisons (Period: GPS weeks 2040 - 2046)

This AR matrices comparison tool was initially created and implemented using the MATLAB software. Later it was transferred and adapted in FORTRAN language from the CNES/CLS AC. It is now used as a tool for AR validation within the AC operational routine.

5.6 Conclusions

In this chapter, the second step of zero-difference method for fixing the phase ambiguities is executed for the Galileo system combined with GPS measurements in a Multi-GNSS POD solution. The integer property of the Galileo phase clocks is demonstrated. Both orbit overlaps and orbit validation using SLR validation methods showed that there is an improvement mainly in the normal and the along track direction.

Even with an incomplete constellation, Galileo ambiguity fixing success percentage is around 90%, a result that is nearly as good as for the GPS system.

These results indicated that in the zero-difference Galileo phase observations can be fixed at the same level as GPS. This is a promising result showing that it may be possible to perform precise positioning using these Galileo orbit and clock products (e.g. PPP and PPP-AR).

After this work, the CNES/CLS IGS AC has announced in the IGS workshop in Wuhan, China the delivery of weekly Galileo precise orbits, IRC clocks and WL satellite biases starting from October 2018 (Loyer, et al., 2018).

In the following chapter we will investigate the performance of Galileo-only, GPS-only and Multi-GNSS precise positioning.

The results and conclusions of this Chapter have been used in the following publications and communications:

- Article: "*Improving Galileo orbit determination using zero-difference ambiguity fixing in a Multi-GNSS processing"* (2019) Advances in Space Research, 63 2952–2963, doi: 10.1016/j.asr.2018.08.035
- Poster: "*Galileo Precise Orbit Determination using zero-difference ambiguity fixing in a Multi-GNSS processing: First results"* EGU 2018, Vienna, Austria
- Presentation: *"Improving Galileo Orbit Determination using zero-difference ambiguity fixing in a Multi-GNSS processing"* ION 2018, Miami, USA
- Poster: "*Improving Galileo Orbit Determination using zero-difference ambiguity fixing in a Multi-GNSS processing"* IGS Workshop 2018, Wuhan, China
- Presentation: *"Galileo un-differenced "integer" products: method, results and perspectives"* IGS Workshop 2018, Wuhan, China

6. Precise Point Positioning

6.1 Introduction

The Precise Point Positioning (PPP) method (Zumberge, et al., 1997) is a well-known and widely used method for positioning using zero-differences Pseudorange and carrier phase observations. This method is used for calculating the coordinates of a station without the need of a reference station near as a control station. Instead, satellite orbits and clocks estimated through a global network of reference stations are used (Kouba, 2009).

The PPP technique has been extensively used since decades for geodetic and other scientific applications. It has been validated through numerous scientific applications for the GPS system; e.g. for static positioning (Lescarmontier, et al., 2012), kinematic positioning (Fund, et al., 2012), time transfer (Petit, et al., 2015) etc.

Since last decade, PPP with ambiguity resolution (PPP-AR) was progressively used either by calculating uncalibrated phase delays (Ge, et al., 2008) or by applying the zero-difference method (Laurichesse & Mercier, 2007). Few IGS ACs are delivering products that allow PPP-AR: e.g. CNES/CLS, Wuhan University and the Center for Orbit Determination in Europe (CODE). Future demands for precise positioning with AR have led to the foundation of the IGS PPP-AR working group (Banville, Simon; IGS, 2018).

Since 2010, the CNES/CLS AC is using the zero-difference method of performing post-processed PPP-AR also known as “Integer PPP” (IPPP) (Laurichesse, et al., 2009) (Fund, et al., 2012) for the GPS system. The algorithms needed are implemented in the GINS software.

With the weekly delivery of Galileo precise orbits and IRC products it became possible to study and validate the precise positioning through the PPP and PPP-AR techniques. In this chapter the following questions are addressed:

- Can the techniques of PPP and PPP-AR be performed for Galileo? What is their resulting accuracy?
- What is the precise positioning comparison of GPS and Galileo?
- What is the global performance of PPP and PPP-AR with Galileo-only, GPS-only and Multi-GNSS (GPS + Galileo)?
- Can the inclusion of Galileo system benefit the current situation of positioning with GPS?

Since the beginning of 2019, Galileo system is comprising 22 operational satellites and 2 satellites in elliptical orbit. The full constellation is only 4 satellites away to be complete. The interest now is to speculate if Galileo can contribute or improve the existing precise positioning accuracy and whether geodetic scientific applications can benefit from it.

6.2 PPP with Ambiguity Resolution

The PPP method has been used in numerous applications for scientific applications as described in Chapter 2. The PPP accuracy is reaching the highest levels once the carrier phase ambiguities are resolved; the so-called PPP-AR or Integer PPP. In order to apply this method for PPP, orbit and clock products as well as satellite biases must be coherent. In the present thesis the products are taken from the CNES-CLS AC (GRG/GRM products).

Recent studies about Multi-GNSS PPP and PPP-AR including Galileo mostly deal with real-time processing (e.g. (Li, et al., 2017) (Xiao, et al., 2019) (Xia, et al., 2018) etc.). In these cases, the interest is focused on the convergence time. Nonetheless, there are no relevant publications so far about post-processed PPP and PPP-AR studies.

The way for performing PPP and PPP-AR with CNES/CLS products is the zero-difference method. The general idea of the PPP-AR method is presented in Fig. 6.1. The CNES/CLS AC is taking data from the global network of IGS stations and after computations, is delivering weekly the WL satellite biases (μ^s)[8], precise satellite orbits and IRC. These data are delivered weekly and can be found in the IGS portal under the name 'GRM'. These data are essential in order to fix the WL ambiguity and later the NL ambiguity on the user's side:

- The WL satellite biases are given to be used during the pre-processing phase, to decorrelate the terms $N^s_{wl,r}$ and $\mu_r(t)$ and to solve for the WL ambiguities.
- Precise satellite orbits are used to give information about the geometrical distance (ρ^s_r) and the IRC products give information about the satellite clocks (δt^s) adjusted to $\pm n$ NL integers ($N^s_{r,i}$). The IRC are giving the relative relation of the NL integers among the satellites (See Fig. 5.18 (b)).

The users then may use these data as inputs together with their RINEX observation file and compute their position in PPP-AR mode. The zero-difference method for PPP and PPP-AR processing is shown in Fig. 6.2. It is partially similar to the global processing when performing POD with two step approaches. The difference in this case (or with other AR methods) is that

[8] The WL satellite biases are available inside the header of CNES/CLS AC 'grm' .clk files or online: ftp://ftpsedr.cls.fr/pub/igsac/Wide_lane_GAL_satellite_biais.wsb

at this point the global network of stations is not needed. The users can perform AR using only their RINEX file.

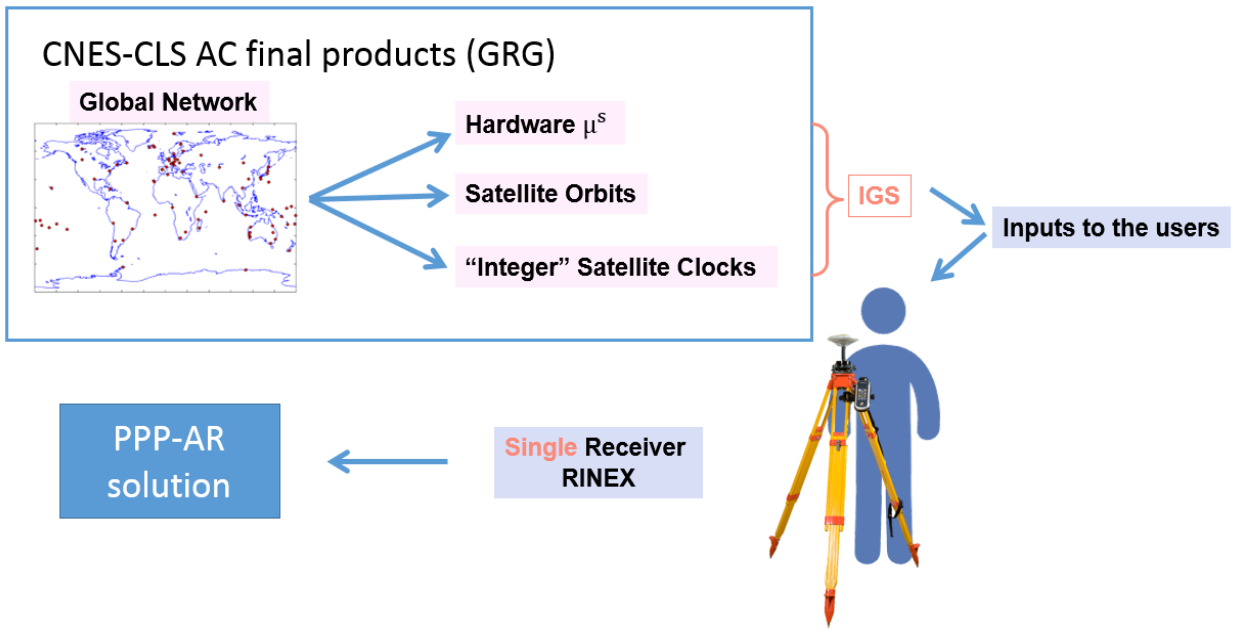

Fig. 6.1: The PPP-AR method using data from the CNES/CLS AC

For the experimentation, one week of data (11-17/02/2019) is chosen. During that period, 31 GPS satellites and 24 Galileo satellites (including the ecliptic E14 and E18) were processed. A network of 65 IGS MGEX stations was examined.

The GRGS software used were PRAIRIE, GINS and EXE-PPP. The software EXE-PPP is a tool designed from the CNES/CLS AC and GRGS group. It gets RINEX files as inputs, performs PPP or PPP-AR according to the user's needs and preferences and delivers positioning results. Nevertheless, this tool had to be changed and adapted to the current needs for Galileo PPP and PPP-AR as well as Multi-GNSS PPP and PPP-AR. All changes were made with the cooperation of the GRGS team in order to adjust the software to perform all types of possible combinations of GPS, Galileo and GLONASS for PPP and GPS and Galileo for PPP-AR.

All models and processing parameters are shown in Tab. 6.1. These settings are considered as default in EXE-PPP but they can be changed to the user's needs.

For the positioning estimation it was chosen to perform post-processed Kinematic positioning, estimating one set of coordinates for every 300 sec. The choice of this setting was made because the kinematic processing is used frequently by the scientific community to show in a dynamical way the potential motion of the stations (e.g. when computing the motion of a GNSS Buoy or examining the displacements following an earthquake). For "static" stations it gives access to displacements and errors at short periods (lower than one day).

	GPS	Galileo
Processing strategy		
Number of satellites	31	24 (incl. E14, E18)
Arc duration	24 h	
Measurements Stepsize	30 sec	
Elevation mask	8°	
Measurement weights	Code: 0.6 m Phase: 0.0035 m	
GNSS system weights	GPS=Galileo	
Models		
Antenna phase center corrections	ANTEX14	
Troposphere model	VMF + GPT2 (Böhm, et al., 2014)	
Ionosphere model	Ionosphere-free combination & second order corrections (Hernández-Pajares, et al., 2007)	
Reference frame	ITRF 2014 (Altamimi, et al., 2016)	
Attitude model	(Kouba, 2008)	(GSA, 2017)
Solid earth tides, polar tides, ocean loading effects	Oceanic tide: FES2012	
	Oceanic pole tide: (Desai, 2002)	
Ocean loading effects	FES2012 (Carrère, et al., 2012)	
Phase windup	(Kouba, 2008)	
Estimated Parameters		
Troposphere	1 ZTD / 2 h	
	1 pair of gradients (E, N) / day	
Inter-system biases	1 / station	
Ambiguities	1 / pass (float solution)	
Station coordinates and clock	One ENU set each 300 sec	

Tab. 6.1: Models applied for PPP-AR during the Multi-GNSS processing

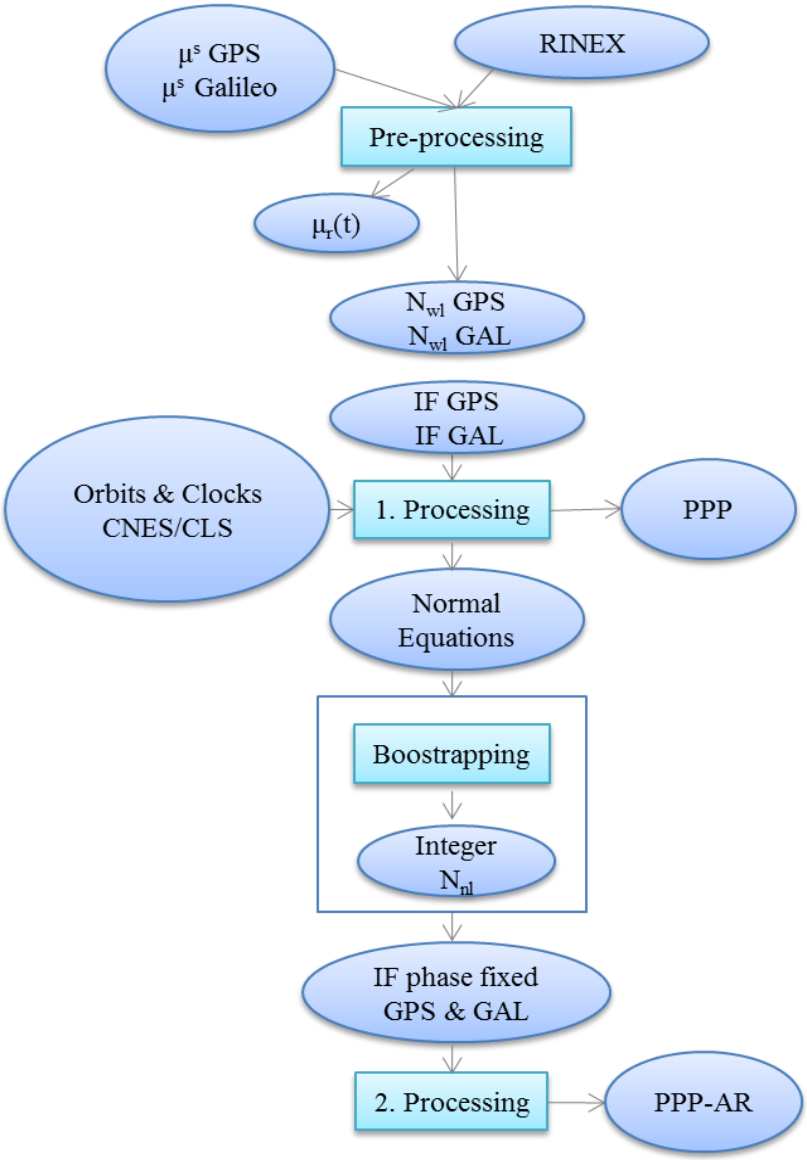

Fig. 6.2: Steps of the procedure to perform PPP and PPP-AR of carrier phase measurements for a combined Multi-GNSS solution

The following graphs (See Fig. 6.3 to Fig. 6.8) are showing some examples of PPP and PPP-AR positioning in detail for the BRUX station for all six scenarios: Galileo-only, GPS-only and Multi-GNSS (GPS + Galileo) in either PPP or PPP-AR mode. On the left-hand side it is shown the repeatability of the positioning for every 300 sec in the East (E), North (N) and Up (U) directions. On the right-hand side the points are represented in histograms and the 1 σ standard deviation values are given with respect to the mean value for every direction. The differences among PPP and PPP-AR solutions show the level of improvement that can be made when carrier phase ambiguities are solved.

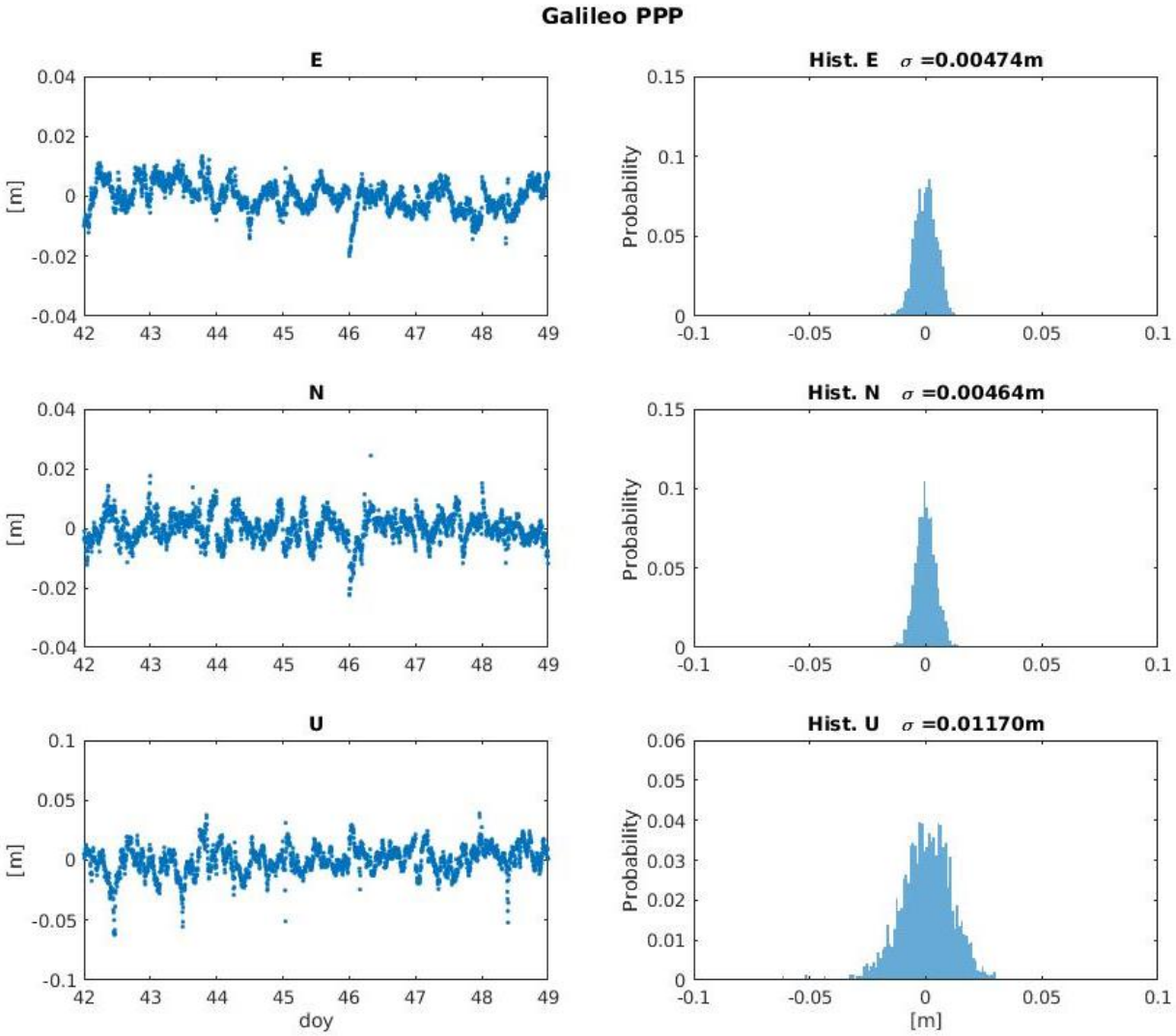

Fig. 6.3: Galileo-only PPP solutions of BRUX station in East (E), North (N) and Up (U) components (left) and their respective histograms with 1 σ values (right)

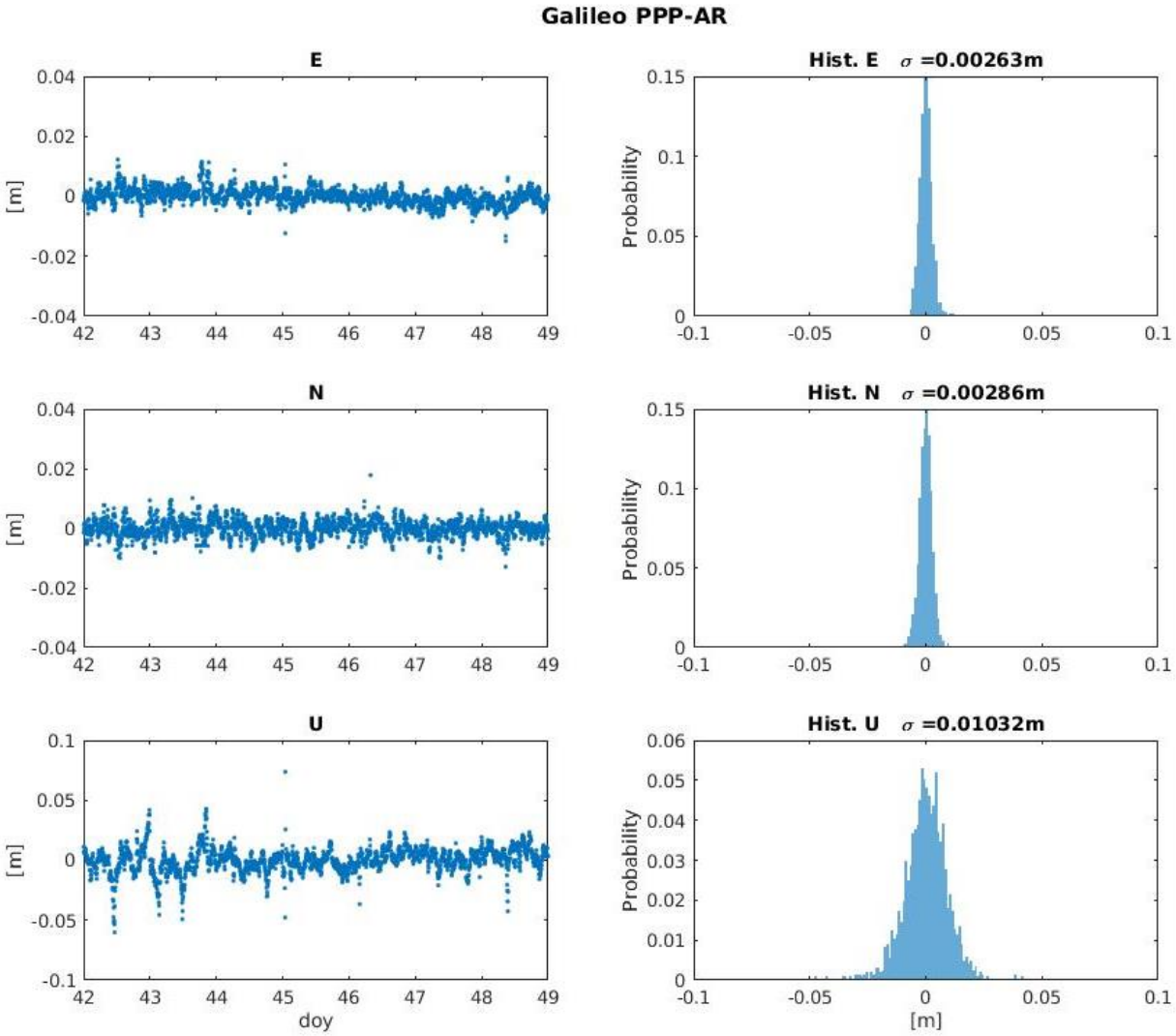

Fig. 6.4: Galileo-only PPP-AR solutions of BRUX station in East (E), North (N) and Up (U) components (left) and their respective histograms with 1 σ values (right)

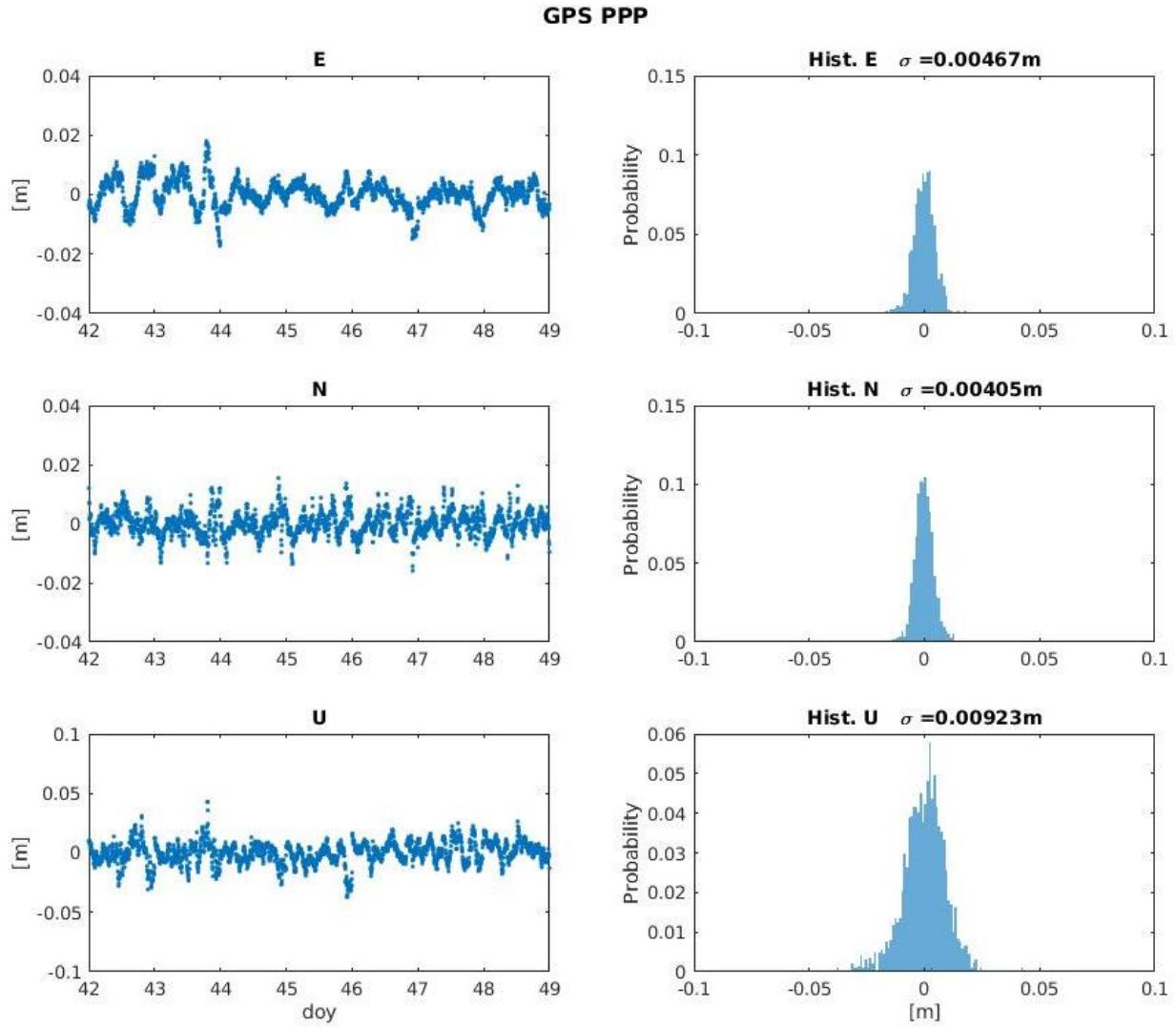

Fig. 6.5: GPS-only PPP solutions of BRUX station in East (E), North (N) and Up (U) components (left) and their respective histograms with 1 σ values (right)

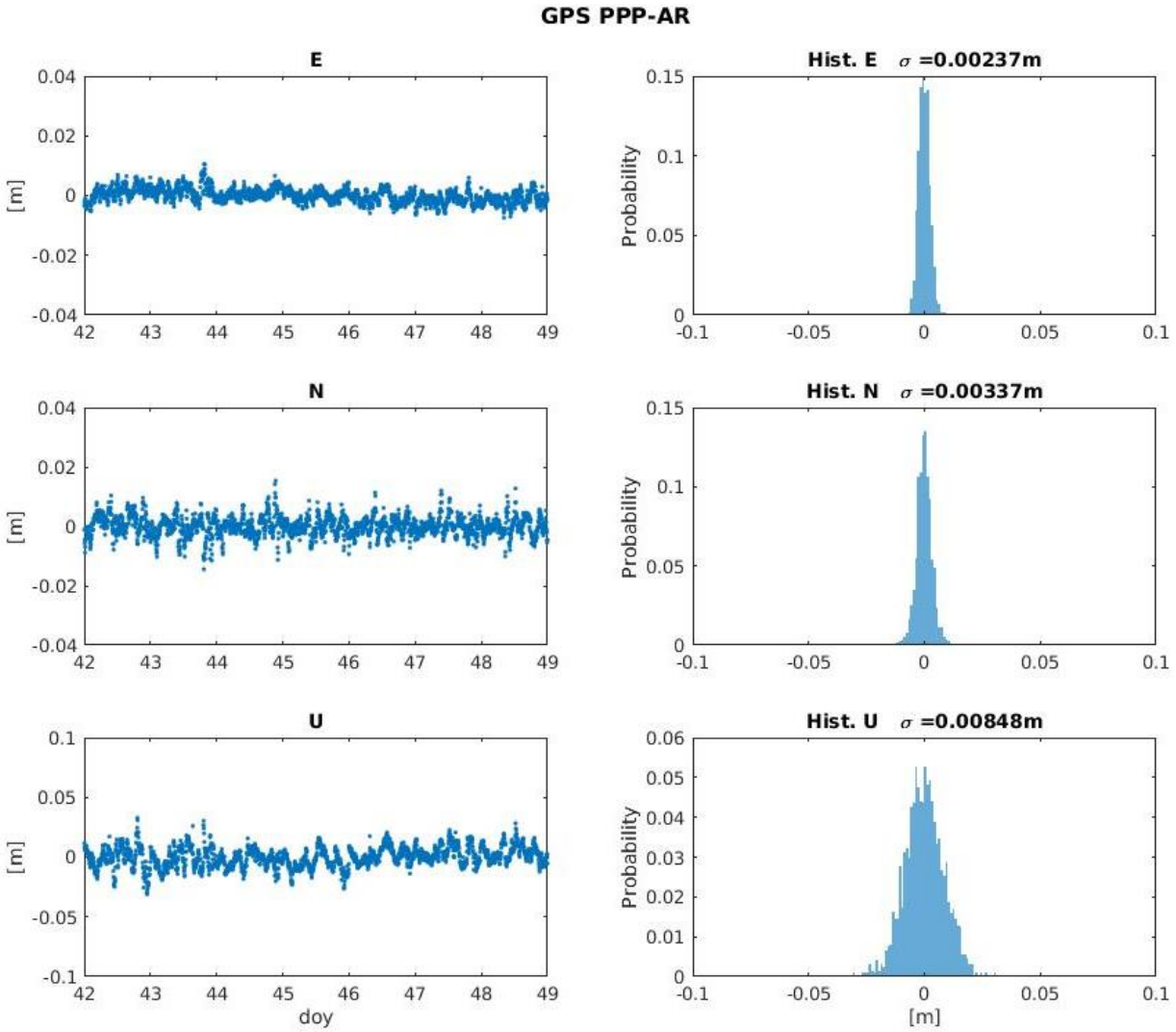

Fig. 6.6: GPS-only PPP-AR solutions of BRUX station in East (E), North (N) and Up (U) components (left) and their respective histograms with 1 σ values (right)

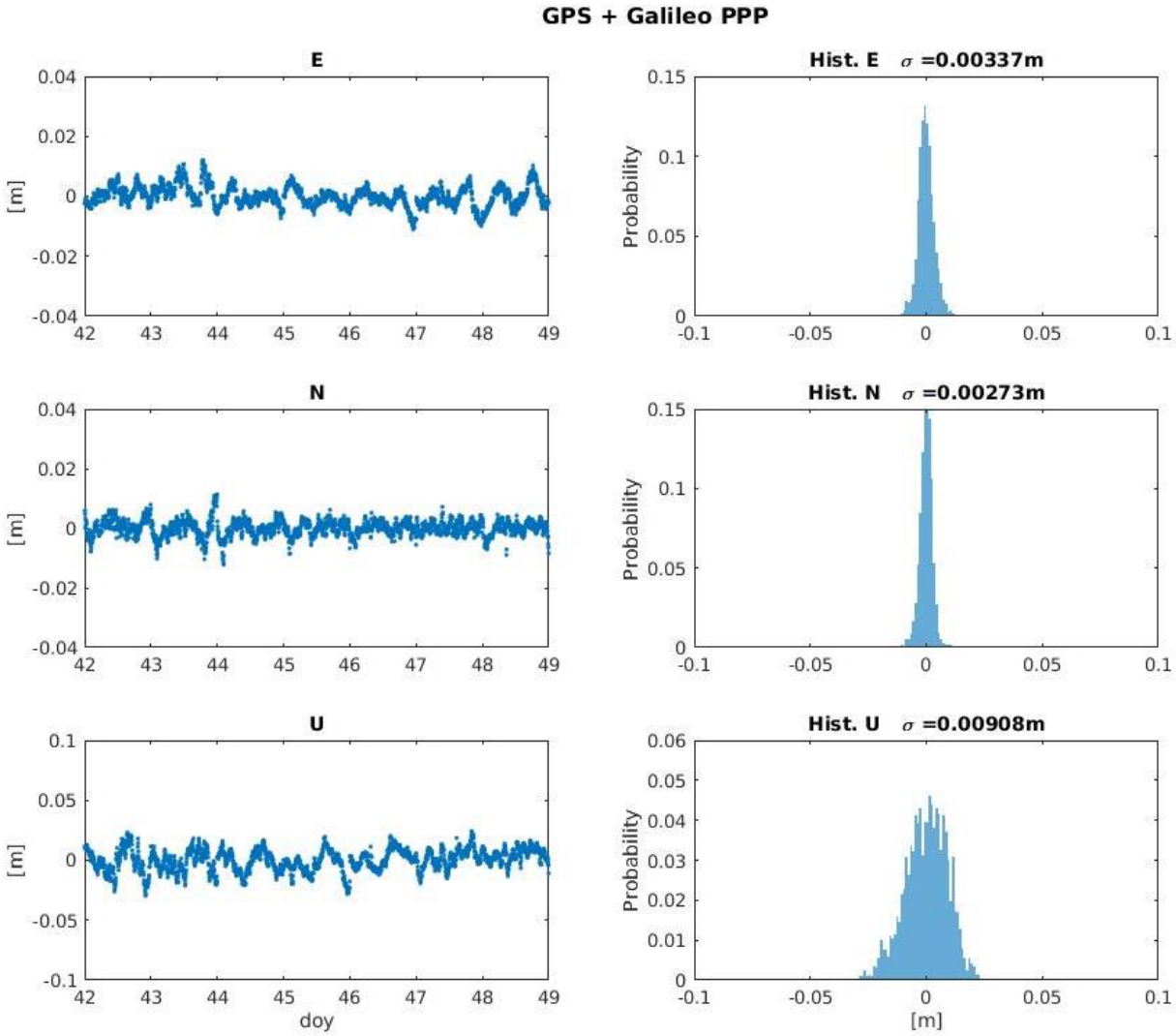

Fig. 6.7: Multi-GNSS PPP solutions of BRUX station in East (E), North (N) and Up (U) components (left) and their respective histograms with 1 σ values (right)

It is interesting to notice that certain irregularities of the repeatability patterns in the PPP solutions do almost disappear in PPP-AR solutions. For example, in Fig. 6.7 there is a little jump at the end of DOY 043 for North and East directions. This jump is certainly coming from the contribution of the GPS system (also seen in Fig. 6.5 of around 2 cm in East and 1 cm in North) to the Multi-GNSS solution. Nevertheless, it is seen that in Fig. 6.8 (adding ambiguity fixing) this jump is reduced to less than 0.5 cm.

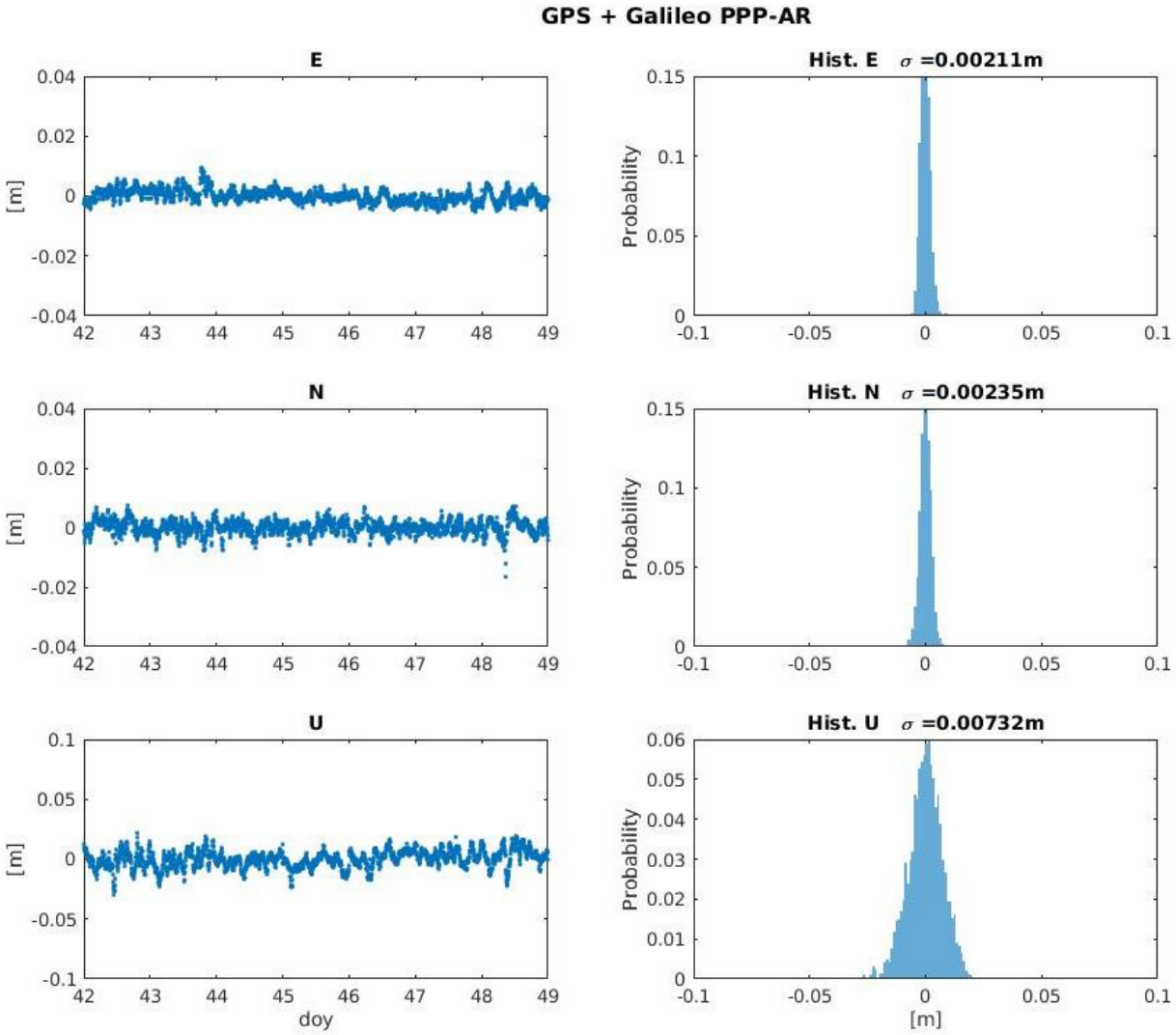

Fig. 6.8: Multi-GNSS PPP-AR solutions of BRUX station in East (E), North (N) and Up (U) components (left) and their respective histograms with 1 σ values (right)

The importance of AR in precise positioning is also seen in Fig. 6.9 to Fig. 6.11. In these graphs the individual solutions are grouped per system and are compared with respect to the processing modes (i.e. PPP or PPP-AR). Generally, it is seen that jumps or spurious signals in the PPP solution do no longer appear when performing PPP-AR processing. The PPP-AR mode is showing smoother and more linear than the PPP mode. Another example is the one seen for Galileo-only (see Fig. 6.9) around DOY 046. There is a downward jump of around 2 cm for East and North directions that is eliminated for the PPP-AR mode.

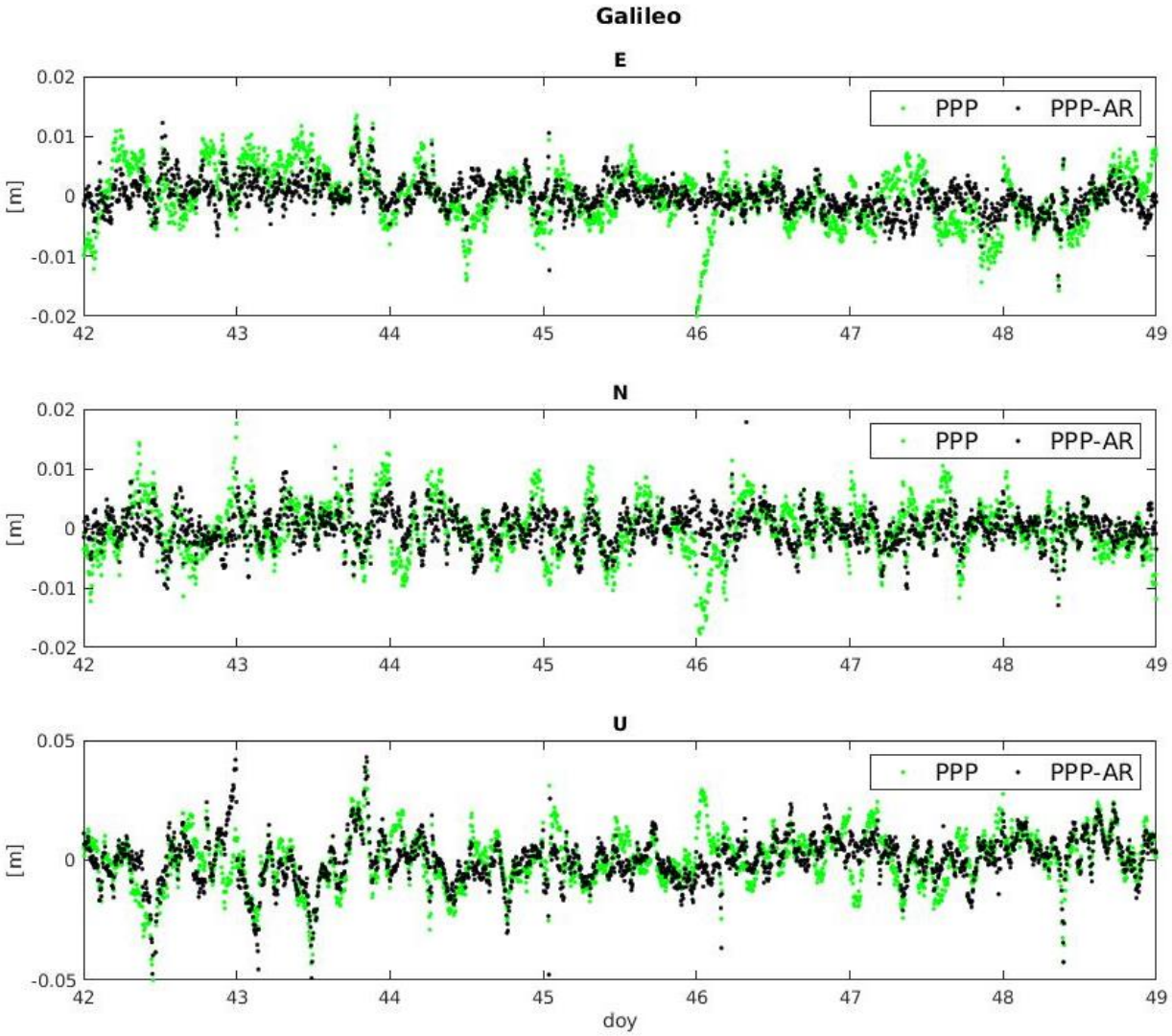

Fig. 6.9: Comparison of PPP and PPP-AR solutions for Galileo-only solution for BRUX station

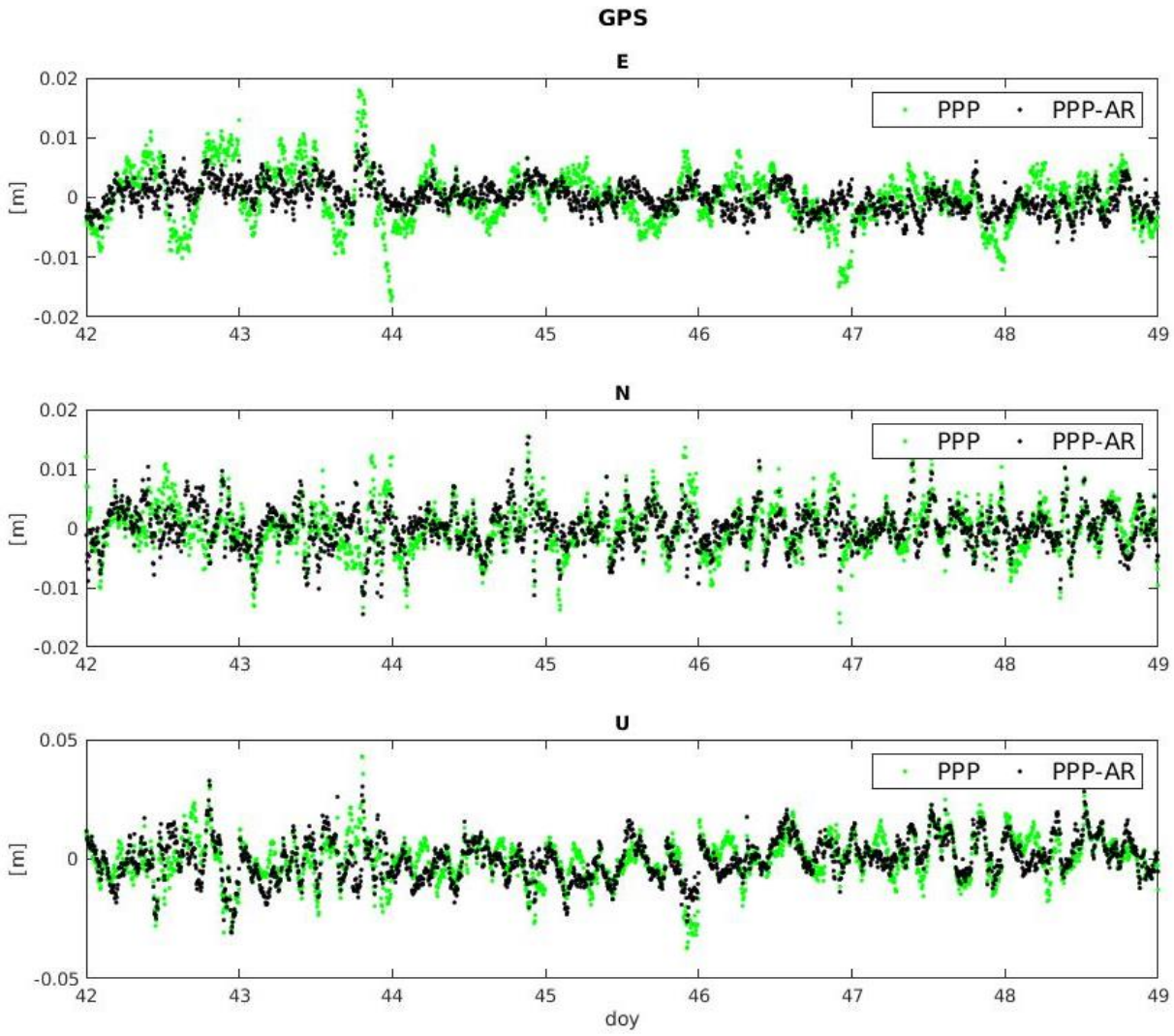

Fig. 6.10: Comparison of PPP and PPP-AR solutions for GPS-only solution for BRUX station

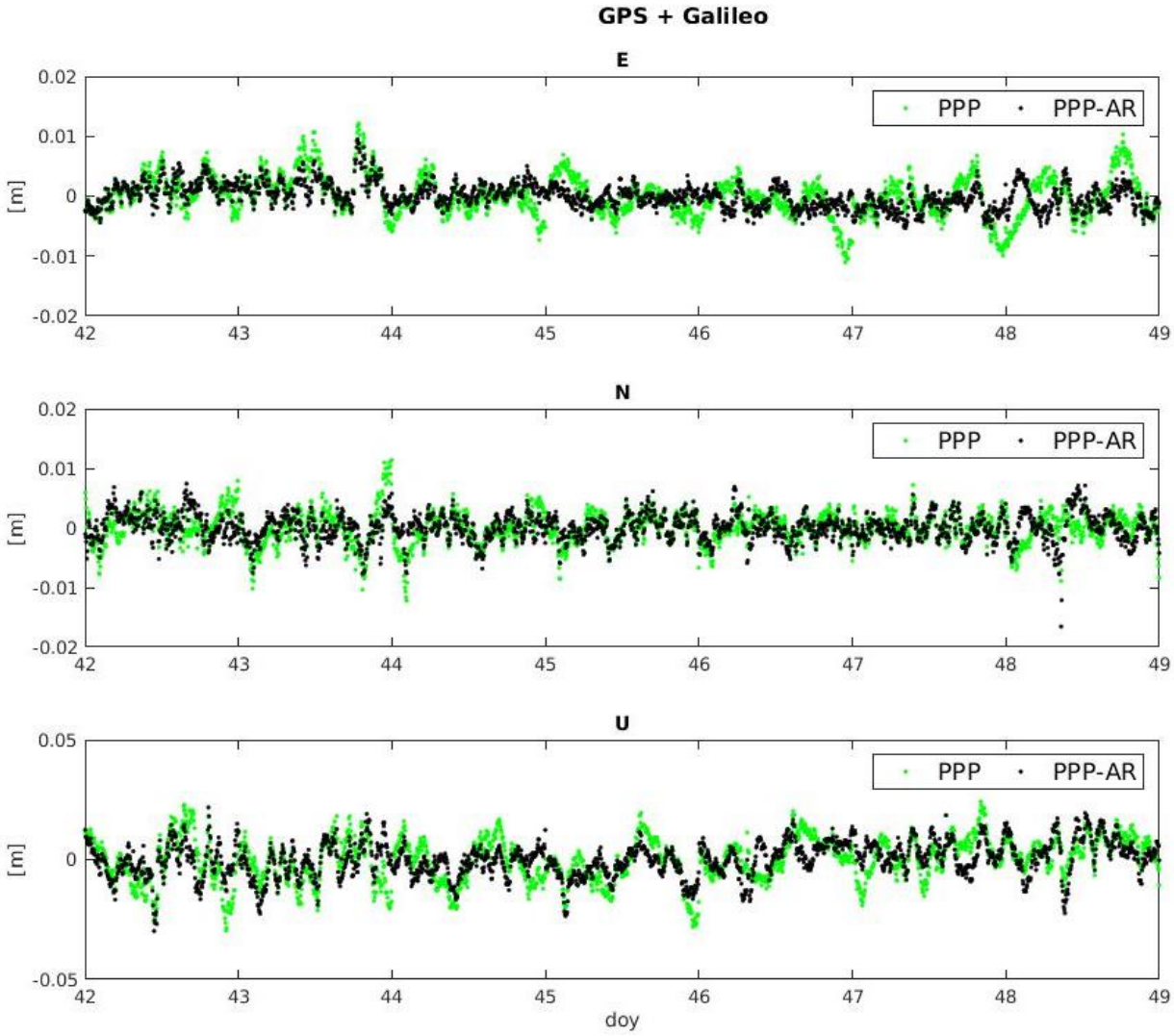

Fig. 6.11: Comparison of PPP and PPP-AR solutions for Multi-GNSS solution for BRUX station

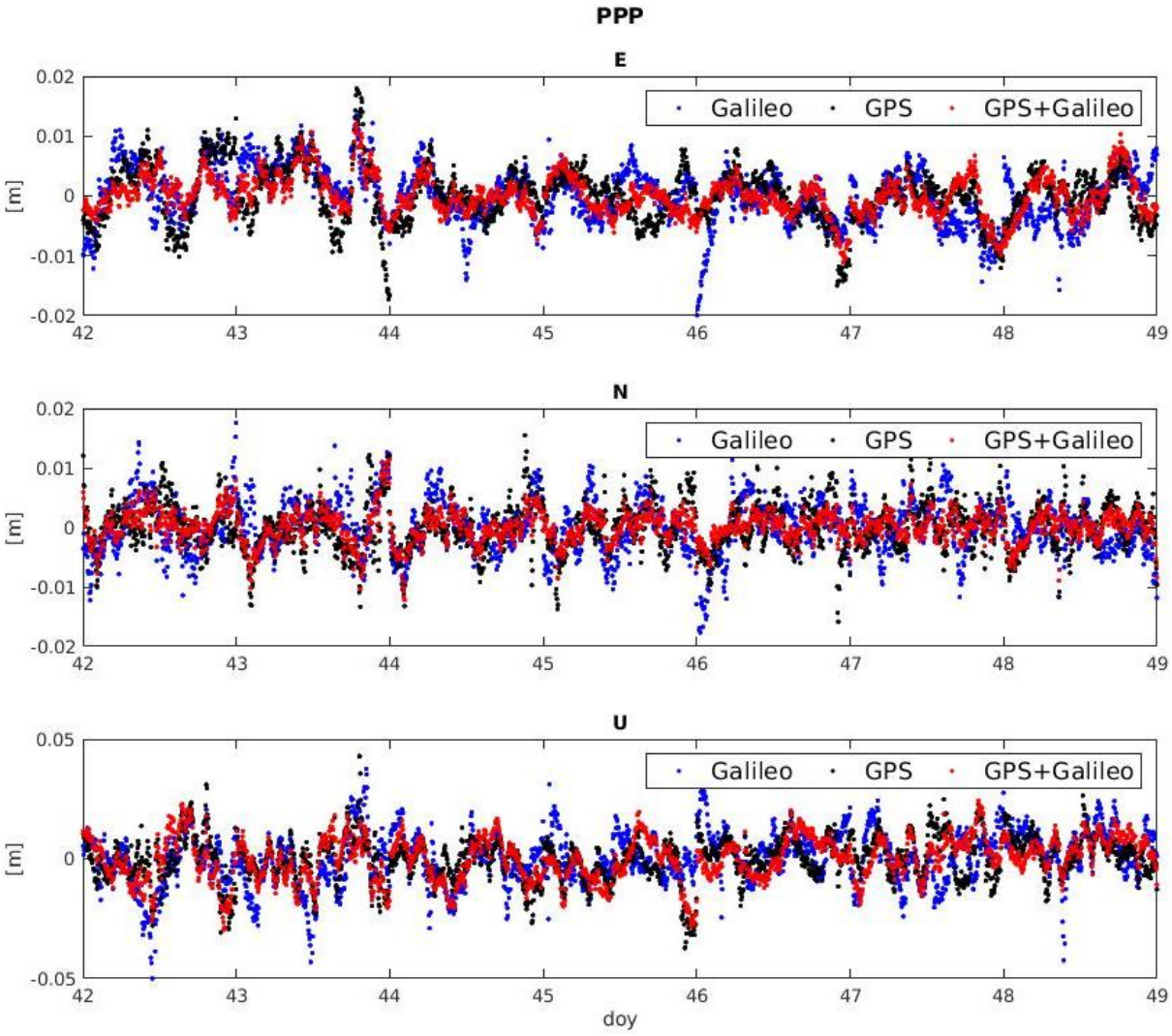

Fig. 6.12: Comparison of all constellations of PPP solution for BRUX station

In Fig. 6.12 and Fig. 6.13 the timeseries are grouped according to the processing mode and are shown for all the three cases. It is seen that for the PPP mode all three cases show the same behavior of fluctuations especially in the East and North directions. A reason why this is happening could be the tropospheric delays that can be common to all cases. In the PPP-AR graph it is observed that the Multi-GNSS timeseries is slightly more linear in East and North components. In the Up component the fluctuations are mitigated: for example, around DOY 043 the fluctuations seen for Galileo-only and GPS-only are decreased in the Multi-GNSS constellation.

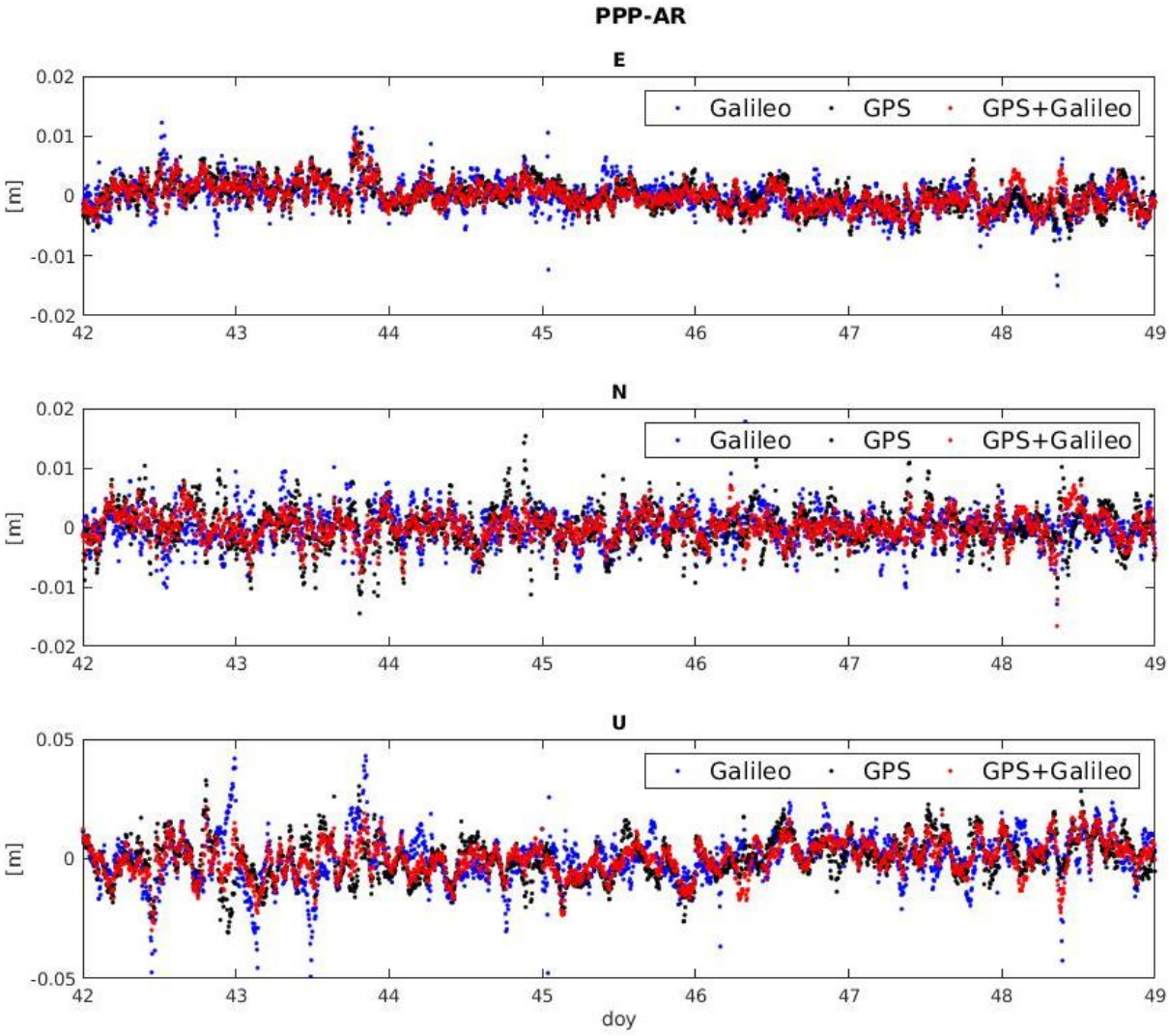

Fig. 6.13: Comparison of all constellations of PPP-AR solution for BRUX station

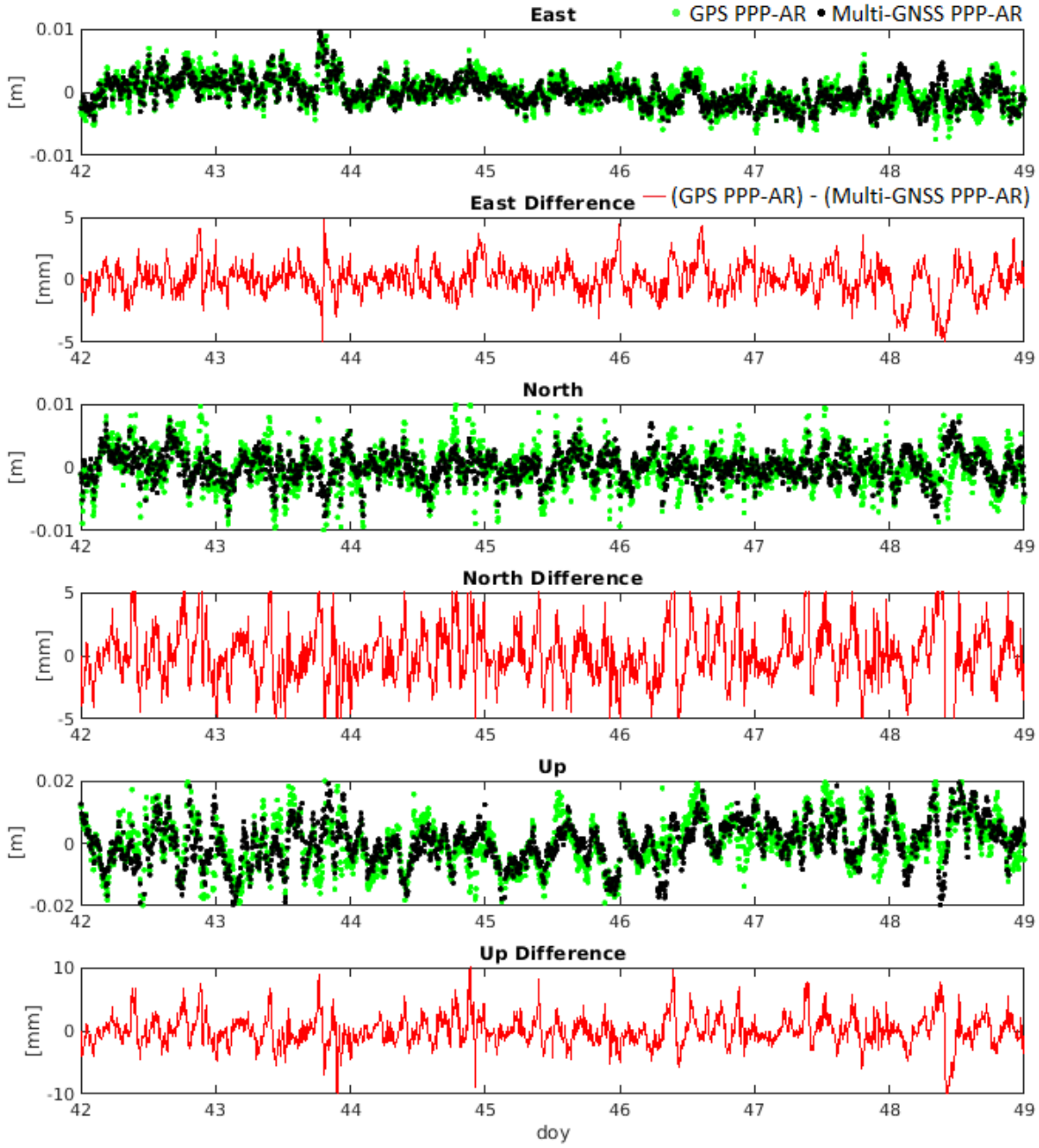

Fig. 6.14: Comparison between GPS PPP-AR and Multi-GNSS and their differences for BRUX station.

In Fig. 6.14 it is shown a comparison between the current precise positioning possibilities using GPS PPP-AR and the precise positioning when including Galileo system in a Multi-GNSS PPP-AR mode. For each direction the timeseries are compared and their difference is computed below. It is noticeable that with the Multi-GNSS PPP-AR mode the timeseries appear slightly more linear for the Up and the East component and well more linear for the north component. The overall RMS of the differences are: 1.31 mm for the difference in East, 2.44 mm for the difference in North and 5.64 mm for the difference in Up.

In Tab. 6.1 the percentages of AR for the example of BRUX station are given. It is seen that overall for this particular week, station and processing strategy, the percentages for Galileo are slightly higher than the ones of GPS.

BRUX		042	043	044	045	046	047	048
AR [%]	Galileo	95.24	100	100	97.67	100	100	95.45
AR [%]	GPS	98.63	91.67	91.30	98.44	100	98.48	94.03

Tab. 6.2: Ambiguity resolution percentages for Galileo and GPS systems for BRUX station

The 1 σ values of the above histograms for BRUX and another two examples of stations (CAS1 and NYA) for PPP and PPP-AR are gathered in the following Tables:

BRUX		East (mm)	North (mm)	Up (mm)
Galileo	PPP	4.7	4.6	11.7
	PPP-AR	2.6	2.9	10.3
GPS	PPP	4.7	4.1	9.2
	PPP-AR	2.4	3.4	8.5
Multi-GNSS	PPP	3.4	2.7	9.1
	PPP-AR	2.1	2.4	7.3

Tab. 6.3: 1 σ values of PPP and PPP-AR for BRUX station

CAS1		East (mm)	North (mm)	Up (mm)
Galileo	PPP	7.1	6.8	16.6
	PPP-AR	4.2	5.2	15.6
GPS	PPP	6.4	6.8	15.2
	PPP-AR	3.8	5.2	14.3
Multi-GNSS	PPP	4.6	4.5	11.3
	PPP-AR	3.1	3.7	10.3

Tab. 6.4: 1 σ values of PPP and PPP-AR for CAS1 station

NYA2		East (mm)	North (mm)	Up (mm)
Galileo	PPP	4.9	5.0	15.5
	PPP-AR	2.8	2.9	13.9
GPS	PPP	4.2	4.1	16.0
	PPP-AR	2.4	2.2	11.7
Multi-GNSS	PPP	3.3	3.1	10.3
	PPP-AR	2.5	2.1	9.8

Tab. 6.5: 1 σ values of PPP and PPP-AR for NYA2 station

From the numbers in the tables it is seen that when fixing the ambiguities, the positioning is ameliorated. For the example of BRUX station:

- In Galileo-only, the improvement reaches 45% in East, 40% in North and 12% in Up.
- In GPS-only, the improvement reaches 49% in East, around 20% in North and around 10% in Up.
- In the Multi-GNSS solution, the improvement reaches 40% in East, around 10% in North and around 20% in Up.

The reason behind the improvement when performing PPP-AR is that when the ambiguities are fixed and known they are no longer parameters to be estimated. Therefore, the system of equations has the same amount of measurements but less unknown parameters. Hence, the degree of freedom of the system of equations is lower. This means that the de-correlation and estimation of the parameters for Tropospheric effects, station clocks and station coordinates becomes easier and more accurate. The following Tab. 6.6 shows an example of the number of parameters and the number of measurements for DOY 042 of BRUX station. For the number of phase fixed measurements and parameters approximate numbers are given due to the fact that sometimes few ambiguities are not fixed so they remain in the PPP-AR system of equations.

BRUX DOY 042		Unknown Parameters	# Parameters	# Measurements
Galileo	PPP	$x_r, y_r, z_r, t_r, T, N_{GAL}$	~ 3800	~ 27000
	PPP-AR	x_r, y_r, z_r, t_r, T	~ 3758	
GPS	PPP	$x_r, y_r, z_r, t_r, T, N_{GAL}$	~ 3833	~ 20000
	PPP-AR	x_r, y_r, z_r, t_r, T	~ 3758	
Multi-GNSS	PPP	$x_r, y_r, z_r, t_r, T, N_{GPS}, N_{GAL}, ISB$	~ 3876	~ 47000
	PPP-AR	$x_r, y_r, z_r, t_r, T, ISB$	~ 3759	

Tab. 6.6: An example of number of parameters and measurements for BRUX station

Where for each of the unknown parameters' terms the following numbers of parameters are added to the system of equations:

- x_r, y_r, z_r: Cartesian station coordinates. They are $3 \times n_{epochs}$. In our example with the 300 sec observation sampling: $3 \times 288 = 864$ parameters.
- t_r: GNSS station receiver clock. Calculated for each stepsize. In our example is 2880 parameters.
- T: Tropospheric parameters. They include the zenithal tropospheric bias that brings 12 parameters (one parameter every 2 h) and 2 more parameters for the tropospheric gradient for North and East.
- N_{GPS}, N_{GAL}: undifferenced ambiguity terms for GPS and Galileo. In our example is 75 parameters for GPS and 42 parameters for Galileo respectively.
- ISB: Inter-system bias between GPS and Galileo system. In our processing it is one parameter.

In the case of Multi-GNSS PPP-AR processing, the system of equations is using nearly double the measurements compared to Galileo-only or GPS-only solutions. Furthermore, for the number of unknown parameters only one extra parameter is added; the ISB. Hence the ratio between measurements and unknowns is more favorable for an accurate solution (i.e. lower degree of freedom, better de-correlation of the unknown parameters). This is mainly the reason why the combined positioning with AR gives better positioning results than each system separately.

6.3 PPP and PPP-AR on a global network

The graphs of the previous part give some indications:

- The PPP-AR mode gives better accuracy for the timeseries than the PPP mode.
- Galileo gives similar accuracy as GPS
- The use of Galileo can improve the current precise positioning situation using GPS in a PPP-AR mode.
- The use of Galileo can bring corrections at the level of few mm to the GPS-only kinematic positioning.

Nevertheless, the graphs shown in detail referred to a very small specimen of stations. It was considered important to process a network of the IGS stations used in MGEX. In this was it can be investigated whether these assumptions are valid globally and whether there are any potential geographical dependencies that affect the positioning accuracy.

Similarly to the previous experiment, the same week of data (11-17/02/2019) is chosen. All 65 MGEX stations were tested within a post-processed kinematic positioning with 300 sec observation sampling.

The following figures (See Fig. 6.15 to Fig. 6.20) show the overall network performance of the 1 σ values (as computed from the histograms similar to

Fig. 6.3 to Fig. 6.8) as well and the global RMS values (the RMS of all the values plotted) for each of the six scenarios for East, North and Up components.

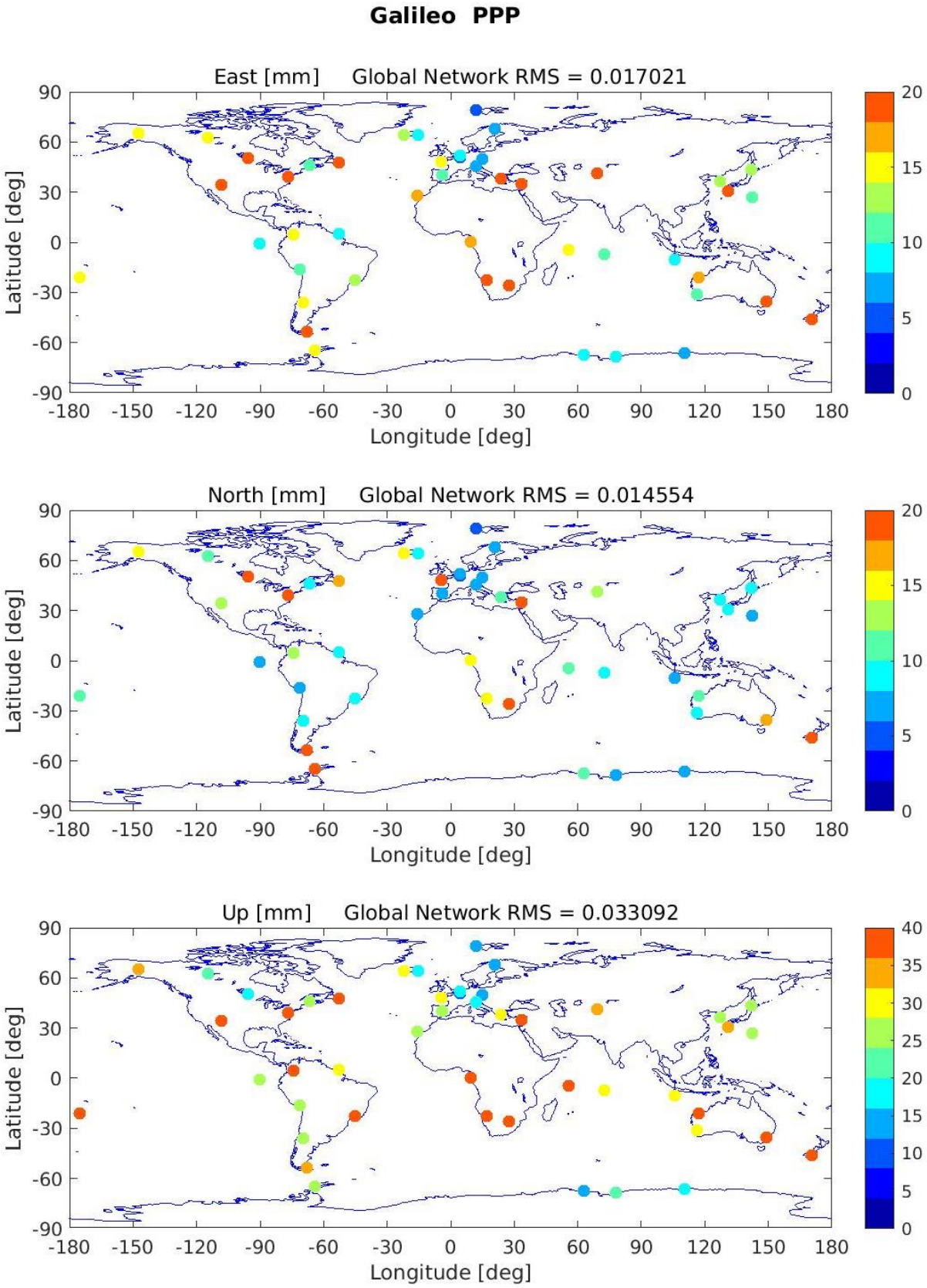

Fig. 6.15: Galileo PPP solutions for the network of IGS stations in East, North and Up components and their global RMS (in [m])

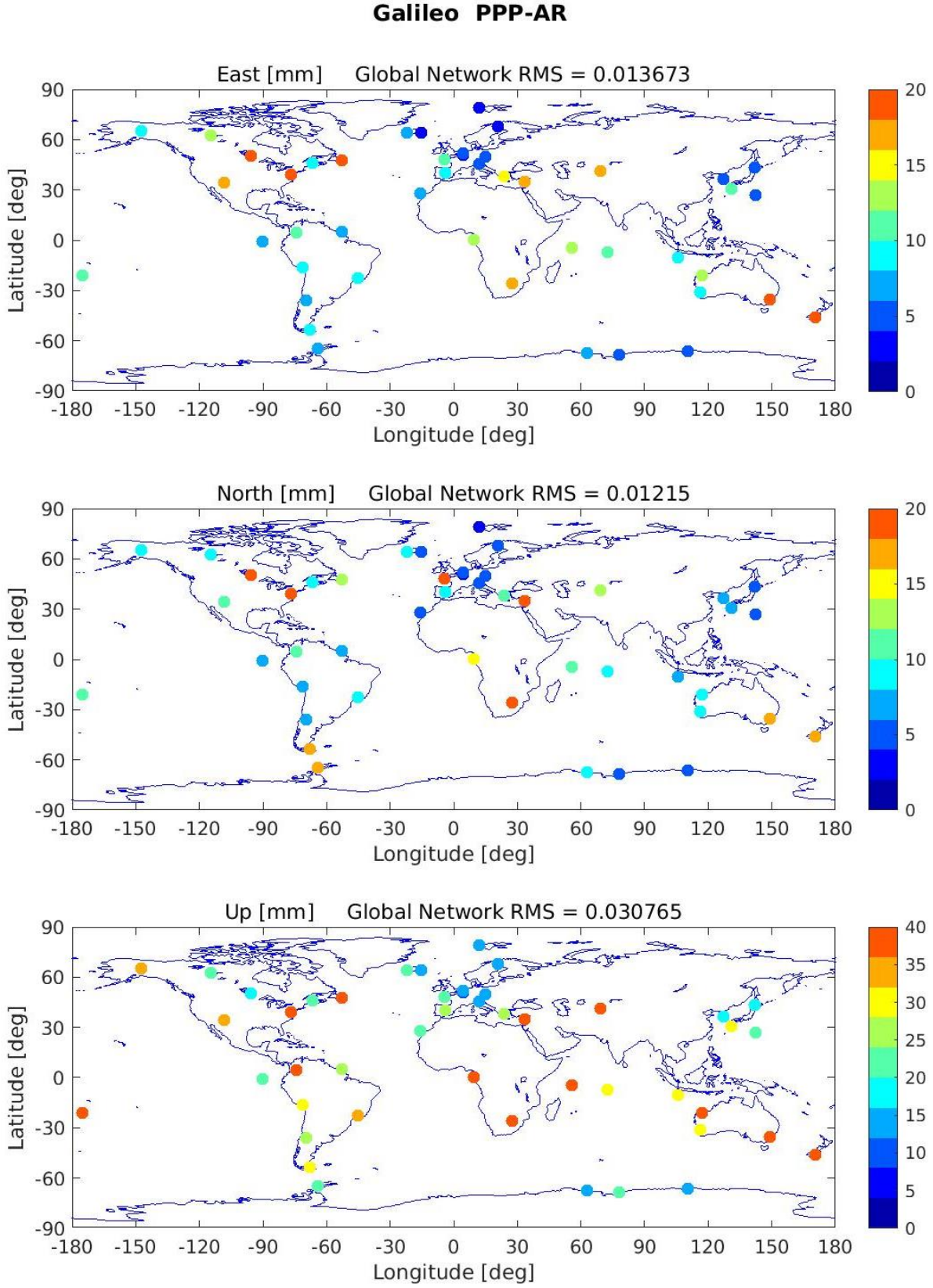

Fig. 6.16: Galileo PPP-AR solutions for the network of IGS stations in East, North and Up components and their global RMS (in [m])

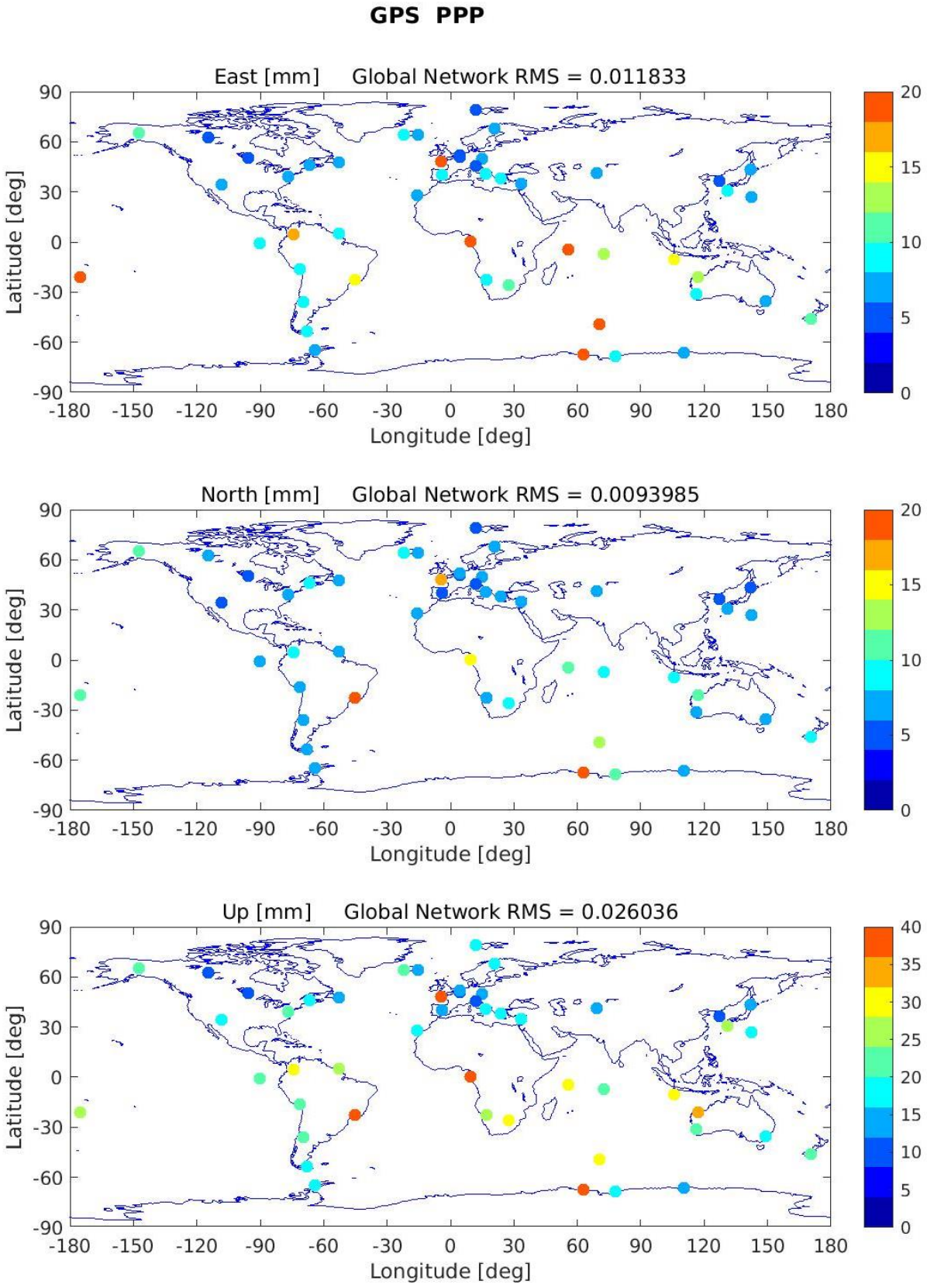

Fig. 6.17: GPS PPP solutions for the network of IGS stations in East, North and Up components and their global RMS (in [m])

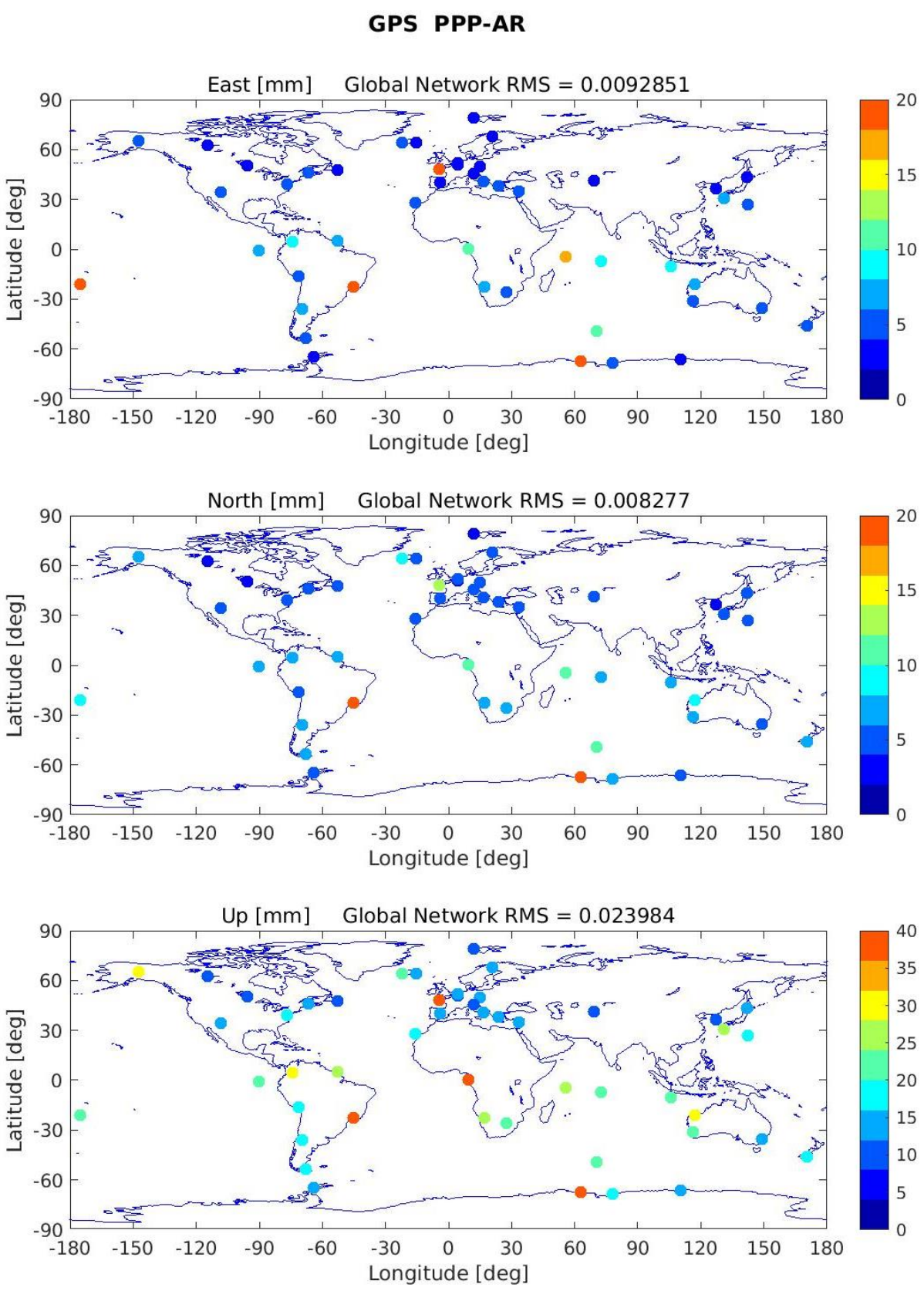

Fig. 6.18: GPS PPP-AR solutions for the network of IGS stations in East, North and Up components and their global RMS (in [m])

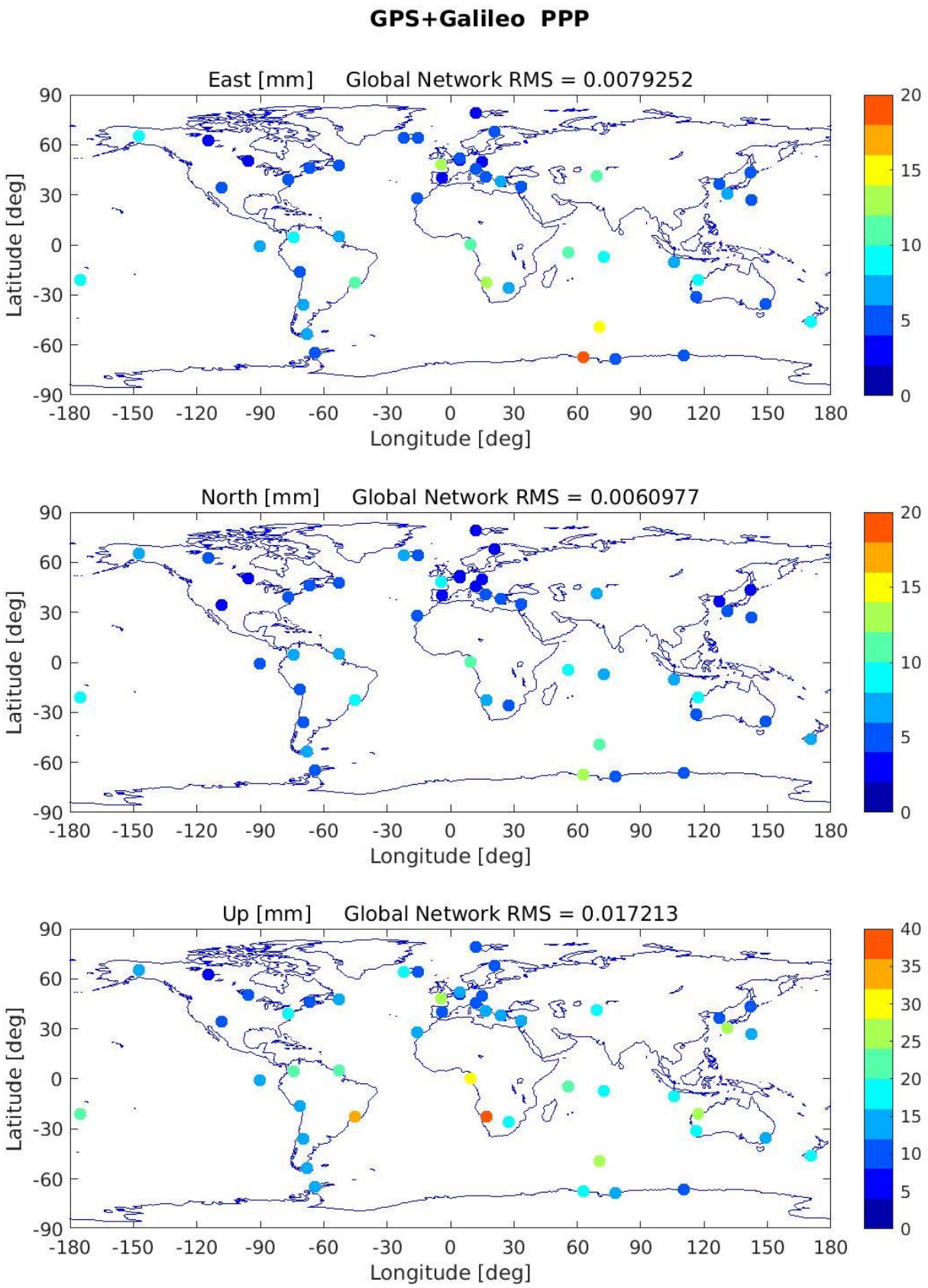

Fig. 6.19: GPS + Galileo PPP solutions for the network of IGS stations in East, North and Up components and their global RMS (in [m])

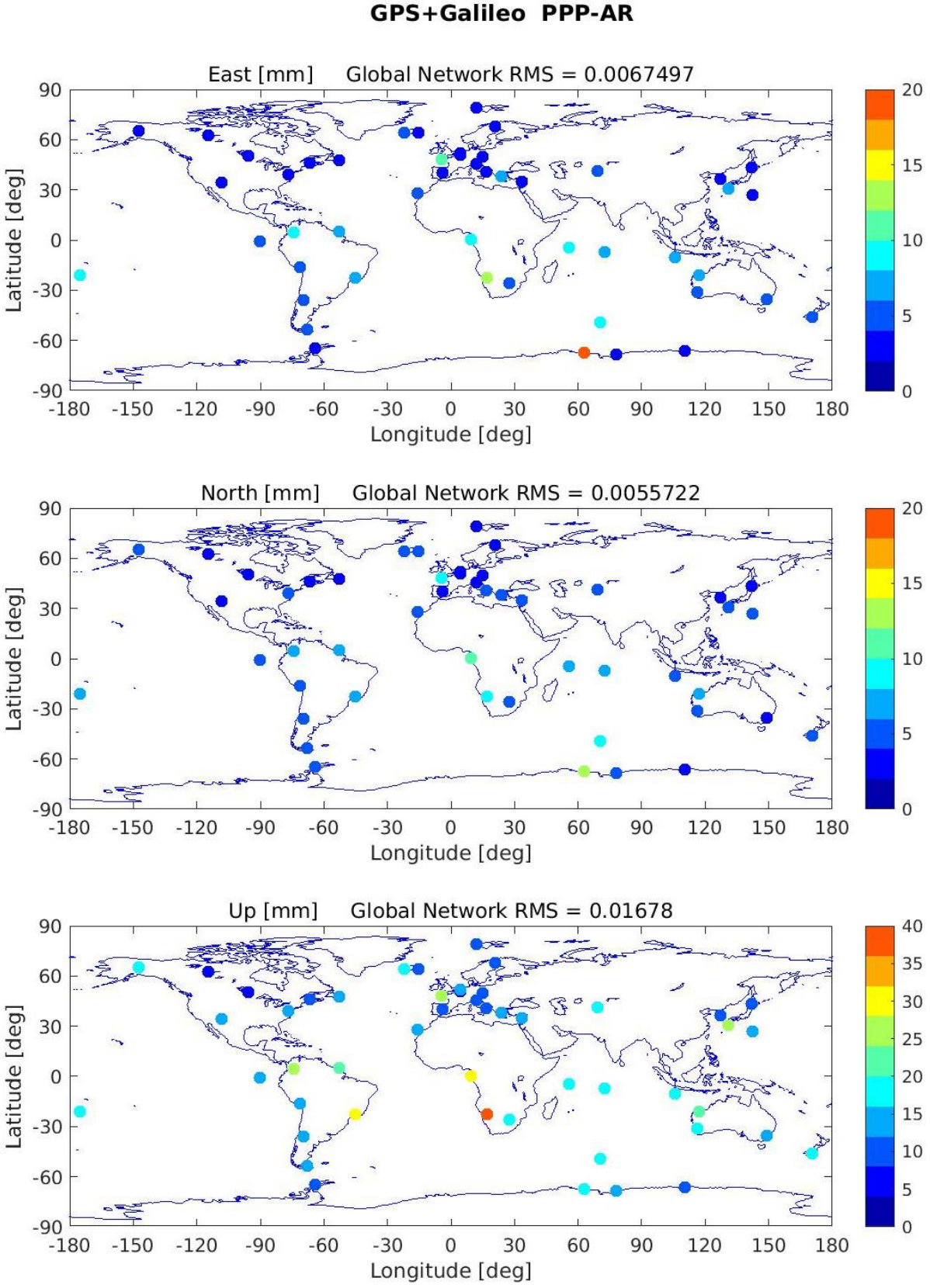

Fig. 6.20: GPS + Galileo PPP-AR solutions for the network of IGS stations in East, North and Up components and their global RMS (in [m])

From the plots it was not possible to observe any geographical pattern. It is clear that level of accuracy achieved varies slightly for each individual station. This could be because of several parameters such as: multipath, misleading station ANTEX parameters (i.e. for Galileo station antenna ANTEX files are not yet provided so therefore the GPS station antenna ANTEX files were used), etc. Nevertheless, for the Multi-GNSS PPP-AR global graphs it is seen a better homogeneity among the stations (i.e. more blue points).

The following Tab. 6.7 is giving the mean value of all AR percentages for the entire network and the mean value for the whole week of processing. It is justified that in general the Galileo percentages are a little higher than the GPS ones.

Network RMS		042	043	044	045	046	047	048	RMS
AR [%]	Galileo	90.71	95.38	95.39	95.56	96.16	95.67	89.39	94.07
AR [%]	GPS	93.55	92.25	89.85	93.90	94.09	94.54	89.62	92.56

Tab. 6.7: Ambiguity resolution percentages for Galileo and GPS systems for the global network of MGEX stations.

In Tab. 6.8 are gathered the RMS values in the three directions from the global maps. Ambiguity resolution improves the solution about 1-3 mm in East and North directions (i.e. around 10% - 20%) and about 0-2 mm in Up direction (2% - 10%). As it is clearly seen adding Galileo to the constellation can improve the positioning globally both for PPP and PPP-AR modes. Even the PPP mode of Multi-GNSS gives better repeatability than the GPS PPP-AR (which is considered as the best case that can be achieved until now).

By comparing GPS PPP-AR positioning to the Multi-GNSS PPP-AR, it is seen that the use of Galileo is improving the positioning by around 3 mm (28%) in East, around 3 mm (33%) in North and around 7mm (30%) in Up directions.

Global Network		East (mm)	North (mm)	Up (mm)
Galileo	PPP	17.0	14.6	33.1
	PPP-AR	13.7	12.2	30.8
GPS	PPP	11.8	9.4	26.0
	PPP-AR	9.3	8.3	24.0
Multi-GNSS	PPP	7.9	6.1	17.2
	PPP-AR	6.7	5.6	16.8

Tab. 6.8: 1 σ values of PPP and PPP-AR for the Global Network of stations

All these conclude that the quality of measurements is similar for the two systems. In general, it is seen that the level of accuracy from Galileo-only solutions is nearly comparable to the one of GPS-only solutions. The Multi-GNSS solutions for both PPP and PPP-AR give much better results than both systems individually. This can be explained by two facts: Firstly, with Multi-GNSS solution there is nearly double the number of satellites, therefore double the number of

measurements of similar good quality. Secondly, a better geometry of measurements is helping to decorrelate the positioning parameters.

It is interesting to observe that even though the Galileo only solution is not better than the GPS only solution, when using both systems the combined solution is improved with respect to the GPS only one. This means that adding Galileo is ameliorating the overall performance of positioning both in PPP as well as in PPP-AR mode.

It is expected that once the Galileo constellation is complete, the accuracy of PPP and PPP-AR respectively will improve.

6.4 Conclusions

The Galileo constellation permits already a PPP-AR solution. In this chapter we examined the results of post-processed kinematic PPP and PPP-AR using Galileo-only, GPS-only and Multi-GNSS (GPS + Galileo) constellations. The interest is to examine the accuracy for each GNSS system individually but also of their combination. Results show that Galileo-only positioning accuracy is nearly at the same level of accuracy as GPS-only. In addition, it is shown that the use of Galileo system -even uncompleted- improves the performance of the GPS positioning giving mm level repeatability. The contribution of Galileo ameliorates the positioning accuracy around 30% in all directions (comparison GPS PPP-AR and Multi-GNSS PPP-AR).

This proves that the Galileo constellation together with GPS will give improved precise positioning with respect to the current GPS-only. In the future it is anticipated that geoscience applications will make use of an improved Multi-GNSS (GPS + Galileo) solution.

The results and conclusions of this Chapter have been used in the following publications and communications:

- Express Letter: *"Performance of Galileo-only kinematic PPP and PPP-AR solutions"* (2019) Earth, Planets and Space, 71: 76, doi: 10.1186/s40623-019-1055-1
- Article: "*PPP and PPP-AR kinematic post-processed performance of GPS and Galileo"* (2019) Remote Sensing (under review)
- Presentation: *"Galileo Precise Positioning with Ambiguity Resolution and its contribution to Earth Rotation solutions*" 7th International Colloquium Scientific and Fundamental Aspects of GNSS 2019, Zurich, Switzerland. Award for the best presentation of the 'Geodesy' session.

7. Conclusions and Suggestions

7.1 Conclusions in English

The GNSS systems are widely used since decades, not only for navigation and positioning purposes but also for high precision positioning scientific applications. In the frame of GGOS, the GNSS systems are an important space geodesy technique that can benefit to numerous scientific areas: e.g. realization and densification of reference frames, Earth rotation studies, geohazard applications, sea level surveys, climate research, time & frequency transfer, etc.

Up until recently, the GPS system was extensively used for precise positioning applications needed for geodetic and scientific purposes. The new European system Galileo, that is under completion, is designed to be compatible with GPS. In this thesis we examined the potentiality to use the combination of GPS and Galileo in a Multi-GNSS formation in order to improve the accuracy of precise positioning.

The first issue to be resolved was to perform Galileo precise orbit determination. It is known that the more precise and exact are the satellite orbits and clocks the more accurate the positioning results can be. One of the key issues to improve the satellite orbit quality is the resolution of the ambiguities of phase measurements. The zero-difference method for ambiguity resolutions, proposed and used by the CNES/CLS AC is examined and applied to Galileo observations. This method consists of two steps: the resolution of the Wide-Lane ambiguity after the formulation of the Melbourne-Wübbena linear combination and the resolution of the Narrow-Lane ambiguity after the formulation of the Ionosphere-free linear combination.

For the first step the main conclusion is that the Galileo fractional biases μ^s are very stable over long periods of time. Their values are extracted and can be used for processing by the users. Some small variations are seen that are related to the constellation repeatability and satellite planes. There fluctuations (around 0.1 cycle WL) caused probably from multipath effects, do not pose problems for the WL AR. The Galileo satellite biases are observed in the same way from all receiver manufacturers, in contrast to the GPS system. The Galileo satellite biases are now weekly calculated and provided from the CNES/CLS AC to the users.

For the second step it was at first decided to combine Galileo measurements with float phase ambiguities with GPS measurements with fixed phase ambiguities. The reason for this strategy was the too low number of Galileo satellites at that time. The success rates of NL ambiguity fixing for Galileo and GPS reached well over 90%. Both GPS and Galileo orbit overlaps showed an improvement of around 50% between the orbit overlaps with float phase ambiguities and fixed phase ambiguities respectively. In addition, the integer property was demonstrated in the GPS and Galileo integer recovery clock overlaps. Furthermore, the results were also validated through SLR residuals. All validation methods showed an improvement on the normal and along track directions of the orbits.

Moreover, a new validation method was introduced that is performing ambiguity matrices comparisons. Results showed that even though the success rates of ambiguity fixing reach well over 90% there is still some disagreements when comparing the AR solutions from overlapping arcs. This is an indication that further improvements in the processing, models or algorithms are needed.

After the successful improvement of the Galileo orbits within a Multi-GNSS processing, the CNES/CLS AC started the delivery of precise orbit, clock products and satellite biases. The positioning capabilities of these products have been tested with of PPP and PPP-AR methods for post-processed kinematic solutions for Galileo-only, GPS-only and Multi-GNSS (GPS + Galileo) constellations. Results showed that Galileo-only positioning accuracy is nearly at the same level of accuracy as GPS-only. The use of Galileo system improves the performance of the GPS positioning giving mm level repeatability. Comparisons of the previous GPS PPP-AR positioning with the new Multi-GNSS PPP-AR shows improvements around 30% for East, North and Up directions.

This proves that the Galileo constellation together with GPS will give improved precise positioning with respect to the current GPS-only. In the future it is anticipated that geoscience applications will make use of an even improved Multi-GNSS (GPS + Galileo) solution, once the constellation of Galileo will be completed.

All in all, these results and conclusions show that scientific applications can benefit from a Multi-GNSS precise positioning when including the Galileo system.

7.2 Suggestions for future work

In the present dissertation, efforts were made in order to perform Multi-GNSS precise positioning with Galileo and GPS. These results represent a big step towards precise positioning using the GNSS systems. However, research about this topic does not stop here. Further

research can be done for improvement and further investigations. Some ideas are presented below for anyone that is interested in the present research topic:

- Further research is needed for the PCO/PCV information on the receiver's side for the corrections on the Galileo frequencies, namely E5a that was used in the present dissertation. This kind of information is quite important because it is used as a correction for the geometry term ρ_r^s.
- Studies related to the intersystem biases could also be helpful in order to investigate the reason behind these station cases that were seen where the hypothesis of a stable ISB are not valid. What could be the reasons behind and what is their impact to the positioning accuracy.
- Studies about what could be the impact of Galileo on the realization of ITRF with respect to station coordinates and frame scale. This can be studies as a part of the REPRO3 campaign.
- Calculation of Earth Orientation Parameters in a Multi-GNSS processing and investigation whether the Galileo system can contribute to the solutions calculated from the CNES/CLS Analysis Centers and delivered to the IERS.
- Analysis of the correlated errors seen in spectral analysis of the Earth Rotation solutions like spikes or the draconitic effect. Can Galileo reduce those errors which affect GPS?
- Further improvement of the already existing algorithms: e.g. for solar radiation pressure, satellite attitude, box and wings model etc.

7.3 Conclusions en Français

Les systèmes GNSS sont largement utilisés depuis des décennies, non seulement pour la navigation et le positionnement, mais également pour des applications scientifiques de positionnement précis. Dans le cadre de GGOS, les systèmes GNSS constituent une technique importante de géodésie spatiale pouvant bénéficier à de nombreux domaines scientifiques comme la réalisation de repères de référence, l'étude de la rotation de la Terre, la prévention des risques naturels, l'étude du niveau de la mer, la recherche sur le climat, etc.

Jusqu'à récemment, le système GPS était largement utilisé pour des applications de positionnement précis à des fins géodésiques et scientifiques. Le nouveau système européen Galileo, en cours d'achèvement, est conçu pour être compatible avec le GPS. Dans cette thèse, nous avons examiné le potentiel d'utilisation et de combinaison des mesures GPS et des mesures Galileo dans une traitement multi-GNSS afin d'améliorer la précision du positionnement précis.

La première question à résoudre consistait à effectuer une détermination précise de l'orbite de Galileo. Il est connu que plus les orbites et les horloges des satellites sont connues avec

précision et exactitude, plus les résultats de positionnement sont fiables. L'un des problèmes clés pour améliorer la qualité de l'orbite des satellites est la résolution des ambiguïtés des mesures de phase. La méthode de résolution des ambiguïtés au niveau des mesures non-différenciées, proposée et utilisée par le Centre d'Analyse CNES / CLS, est examinée pour Galileo. Cette méthode comprend deux étapes : la résolution de l'ambiguïté Wide-Lane après la formulation de la combinaison linéaire Melbourne-Wübbena et la résolution de l'ambiguïté Narrow-Lane après la formulation de la combinaison linéaire Ionosphère-free.

Pour la première étape, la conclusion principale est que les valeurs des biais wide lane μ^S des satellites Galileo sont très stables sur de longues périodes. Leurs valeurs sont diffusées et peuvent être utilisées pour le traitement par les utilisateurs. On observe quelques petites variations liées à la géométrie et à la répétabilité de la constellation. Les fluctuations (environ 0,1 cycle WL) dues probablement à des effets de trajets multiples ne posent aucun problème pour la résolution des ambiguïtés WL. Les biais de satellite Galileo sont cohérent tous les fabricants de récepteurs, avec plus d'homogénéité que pour le système GPS. Les biais des satellites Galileo sont aujourd'hui calculés et diffusés chaque semaine par le Centre d'Analyse CNES / CLS.

Pour la deuxième étape, il a été décidé de combiner les mesures Galileo avec les ambiguïtés de phase flottantes avec des mesures GPS avec des ambiguïtés des fixés. La raison de cette stratégie de traitement est le faible nombre de satellites Galileo à l'époque du démarrage de cette thèse. Les taux de réussite de la détermination de l'ambiguïté NL pour Galileo et GPS ont largement dépassé les 90%. Les recouvrements d'orbite entre GPS et Galileo ont montré une amélioration d'environ 50% de la qualité des recouvrements d'orbite entre les solutions avec des ambiguïtés de phase flottantes et celles avec des ambiguïtés de phase fixées, en particulier dans les directions normales et tangentielles. De plus, la propriété entière a été démontrée dans les recouvrements d'horloge pour les horloges GPS et Galileo. Les résultats ont également été validés à l'aide des résidus des mesures SLR disponibles pour Galileo.

En parallèle, une nouvelle méthode de validation a été introduite, qui consiste à comparer directement les matrices d'ambiguïtés. Les résultats ont montré que même si les taux de réussite de la résolution des ambiguïtés dépassent largement les 90%, il subsiste quelques désaccords lors de la comparaison des solutions d'AR entre deux arcs consécutifs. Cela indique que d'autres améliorations du traitement, des modèles ou des algorithmes seront nécessaires dans le futur

Après l'amélioration réussie des orbites Galileo dans le cadre d'un traitement multi-GNSS, le Centre d'Analyse CNES / CLS a commencé à délivrer les produits précis des orbites et des horloges des satellites. Les capacités de positionnement de ces produits ont été testées avec des solutions cinématiques en PPP et PPP-AR pour les constellations Galileo uniquement, GPS uniquement et Multi-GNSS (GPS + Galileo). Les résultats ont montré que la précision de positionnement de Galileo seul atteint pratiquement celui du GPS. L'utilisation du système Galileo améliore les performances du positionnement GPS en offrant une répétabilité au niveau

millimétrique. Les comparaisons des traitements PPP-AR GPS et GPS+Galileo montrent des améliorations d'environ 30% pour les directions Est, Nord et Verticale.

Nous avons prouvé que l'utilisation des mesures de la constellation Galileo, associée au GPS, améliorera la précision du positionnement par rapport au GPS actuel. Le déploiement complet de la constellation Galileo devrait permettre d'améliorer encore la performance des traitements hybrides ce qui bénéficiera à tous les utilisateurs.

En synthèse, ces travaux montrent que les usages scientifiques des GNSS bénéficieront de l'inclusion des données du système Galileo.

7.4 Suggestions de travaux futurs

Dans la présente thèse, des efforts ont été déployés pour réaliser un positionnement précis multi-GNSS en combinant les mesures Galileo et GPS. Ces résultats représentent un grand pas en avant vers un positionnement précis avec les systèmes GNSS. Cependant, les recherches sur ce sujet ne s'arrêtent pas là. Des recherches supplémentaires peuvent être effectuées pour améliorer et approfondir les résultats. Quelques idées sont présentées ci-dessous pour toute personne intéressée par le sujet de recherche actuel :

- Il est nécessaire de poursuivre les recherches sur les informations PCO / PCV côté récepteur pour les corrections sur les fréquences Galileo, à savoir E5a, qui ont été utilisées dans le présent mémoire. Ce type d'information est particulièrement important car il impacte directement le terme géométrique ρ_r^s du modèle de mesure
- Des études sur les biais inter-systèmes pourraient également s'avérer utiles afin de déterminer la raison derrière ces cas de stations observés où l'hypothèse d'un biais inter-système stable n'est pas valide. Quelles pourraient être les raisons sous-jacentes et quel est leur impact sur la précision de positionnement.
- Outre Galileo, un autre nouveau système GNSS sera bientôt totalement déployé : le système chinois Beidou. Il serait également intéressant d'étudier l'applicabilité de la méthode de la zéro-différence pour résoudre les ambiguïtés et de valider de la même manière l'avantage de traiter simultanément trois systèmes GNSS.
- Calcul des paramètres d'orientation de la Terre dans un traitement multi-GNSS et recherche de la capacité du système Galileo à contribuer aux solutions calculées à partir du CA et livrées à l'IERS.
- Nouvelle amélioration des algorithmes existants : par ex. pour la pression de rayonnement solaire, l'attitude du satellite, le box and wings model etc.

Bibliography

Altamimi, Z., Rebischung, P., Métivier, L., & Collilieux, X. (2016). ITRF2014: A new release of the International Terrestrial Reference Frame modeling nonlinear station motions. *Journal of Geophysical Research Solid Earth, 121*(8), 6109-6131.

Altamimi, Z. (2018). *Fondement des Conventions IERS: Systèmes de Référence Terrestres.* Retrieved from www5.obs-mip.fr/wp-content-omp/uploads/sites/28/2018/10/02_RefTerrestre_Altamimi.pdf

Arnold, D., Meindl, M., Beutler, G., Dach, R., Schaer, S., Lutz, S., Prange, L., Sosnica, K., Mervart, L., & Jäggi, A. (2015). CODE's new solar radiation pressure model for GNSS orbit determination. *Journal of Geodesy, 89*(10.1007/s00190-015-0814-4), 775-791.

Banville, S., Santerrel, R., Cocard, M., & Langley, R. (2008). Satellite and Receiver Phase Bias Calibration for Undifferenced Ambiguity Resolution. *Proceedings Institute of Navigation, National Technical Meeting*, (pp. 711-719). San Diego, CA, USA.

Banville, Simon; IGS. (2018). *Precise Point Positioning with Ambiguity Resolution Charter and Membership.* Retrieved from https://kb.igs.org/hc/en-us/articles/360020571631-Precise-Point-Positioning-with-Ambiguity-Resolution-Charter-and-Membership

Bock, Y., & Melgar, D. (2016). Physical applications of GPS geodesy: a review. *Reports on Progress in Physics, 79*. doi:10.1088/0034-4885/79/10/106801

Böhm, J., Möller, G., Schindelegger, M., Pain, G., & Weber, R. (2014). Development of an improved empirical model for slant delays in the troposphere (GPT2w). *GPS Solutions, 19*, 433 - 441.

Bossler, J., Goad, C., & Bender, P. (1980). Using the global positioning system (GPS) for geodetic positioning. *Bull. Géod., 54*, pp. 553-563.

Bunge, M. (1998). *The Scientific Approach - Philosophy of Science: Volume 1, From Problem to Theory.* (Routledge ed., Vols. ISBN 978-0-765-80413-6). New York. doi: 10.4324/9781315126371

Carrère, L., Lyard, M., Cancet, M., Guillot, A., & Roblou, L. (2012). FES2012: A new global tidal model taking advantage of nearly 20 years of altimetry. Venice, Italy: Proceedings of the 20 Years of Progress in Radar Altimetry Symposium.

CLS, (2018). Documentation utilisateur du programme Prairie (in French) CLS-GEO-NT-18-001. *CLS-Géodésie*.

CNES/CLS. (2017). Retrieved 2017, from https://igsac-cnes.cls.fr/

Cormen, T., Leiserson, C., Rivest, R., & Stein, C. (2001). *Introduction to Algorithms* (Vol. Second Edition). MIT Press and McGraw-Hill. doi:ISBN 0-262-03293-7

Desai, S. (2002). Observing the pole tide with satellite altimetry. *Journal of Geophysical Research, 107*(C11), 7-1-7-13. doi:10.1029/2001JC001224

ESA, Sanz Subirana, J., Juan Zornoza, J., & Hernández-Pajares, M. (2013). *GNSS Data Processing: Volume I: Fundamentals and Algorithms* (Vols. ISBN 978-92-9221-886-7). Leiden: K. Fletcher.

ESA. (2014). *Navipedia - Galileo IOV Satellites.* Retrieved 2019, from https://gssc.esa.int/navipedia/index.php/Galileo_IOV_Satellites

ESA. (2017). *Satellite anatomy*. Retrieved 2017, from http://www.esa.int/Our_Activities/Navigation/Galileo/Satellite_anatomy

ESA. (2019). *Four New Galileos Join Europe's Largest Satellite Constellation*. Retrieved 2019, from https://www.esa.int/Our_Activities/Navigation/Four_new_Galileos_join_Europe_s_largest_satellite_constellation

ESPI, Sitruk, A., & Plattard, S. (2017). *The Governance of Galileo* (Vol. 62). Vienna: European Space Policy Institute. Retrieved from https://espi.or.at/files/news/documents/Rep62_online_170203_1142.pdf

Fund, F., Perosanz, F., Testut, L., & Loyer, S. (2012, September). An Integer Precise Point Positionins technique for sea surface observations using a GPS buoy. *Advances in Space Research, 51*, pp. 1311-1322. doi:10.1016/j.asr.2012.09.028

Ge, M., Gendt, M., Rothacher, M., Shi, C., & Liu, J. (2008). Resolution of GPS Carrier-Phase Ambiguities in Precise Point Positioning (PPP) with Daily Observations. *Journal of Geodesy, 82*, 389-399. doi:10.1007/s00190-007-0187-4

GGOS. (2007). *The Global Geodetic Observing System - Assessing Geohazards and Reducing Disaste*. Retrieved 2019, from http://www.iag-ggos.org/library/promotion/ggos_and_geohazards_flyer_online.pdf.

GGOS. (2016a). *Global Geodetic Observing System*. Retrieved 2019, from http://www.ggos.org/en/about/ggos-infos/

GGOS. (2016b). *Unified Height System*. Retrieved 2019, from http://www.ggos.org/en/focus-areas/unified-height-system/

GGOS. (2016c). *Geohazards*. Retrieved 2019, from http://www.ggos.org/en/focus-areas/geohazards/

GGOS. (2016d). *Sea Level Change, Variability and Forecasting*. Retrieved 2019, from http://www.ggos.org/en/focus-areas/sea-level-change-variability-and-forecasting/

GGOS. (2016e). *Sea Level Change, Variability and Forecasting.* Retrieved 2019, from http://www.ggos.org/en/focus-areas/sea-level-change-variability-and-forecasting/

GGOS. (n.d.). *The Global Geodetic Observing System*. Retrieved 2019a, from http://www.iag-ggos.org/about_geodesy/the_three_pillars.php

GRGS. (n.d.). *GRGS-Groupe de Recherche de Géodésie Spatiale*. Retrieved 2019, from https://grgs.obs-mip.fr/

GSA. (2016). *Galileo Initial Services: Galileo Goes Live*. Retrieved 2019, from https://www.gsa.europa.eu/system/files/documents/initial_services_factsheet.pdf

GSA. (2017). *Galileo Satellite Metadata*. Retrieved Nov 2017, from https://www.gsc-europa.eu/support-to-developers/galileo-satellite-metadata

GSA. (2018). *Galileo Initial Services*. Retrieved 2019, from https://www.gsa.europa.eu/galileo/services/initial-services

GSA. (2018). *Galileo Services*. Retrieved 2019, from https://www.gsa.europa.eu/galileo/services

GSA. (n.d.). *Active user notifications*. Retrieved 2019, from https://www.gsc-europa.eu/system-status/user-notifications

Håkansson, M., Jensen, A., Horemuz, M., & Hedling, G. (2017). Review of code and phase biases in multi-GNSS positioning. *GPS Solutions, 21*, 849-860. doi:10.1007/s10291-016-0572-7

Hernández-Pajares, M., Juan, J., Sanz, J., & Orús, R. (2007). Second-order ionospheric term in GPS: Implementation and impact on geodetic estimates. *Journal of Geophysical Research, 112*. doi:10.1029/2006JB004707

Hofmann-Wellenhof, B., Lichtenegger, H., & Wasle, E. (2008). *GNSS-Global Navigation Satellite Systems GPS, GLONASS, Galileo and more.* Vienna: Springer-Velag Wien.

Hugentobler, U. (2013). ESPACE 2: Satellite Navigation - Lecture Notes of MSc ESPACE. Munich: IAPG Presentation.

IAG. (n.d.). *IAG: A Constituent Association of the International Union of Geodesy and Geophysics*. Retrieved 2019, from http://www.iag-aig.org/templates_img/iagbrochure.pdf

IAG. (n.d.). *International Association of Geodesy... advancing geodesy...* Retrieved 2019, from http://www.iag-aig.org/index.php

IAG. (n.d.). *What is Geodesy?* Retrieved 2019, from http://www.iag-aig.org/templates_img/iagbooklet.pdf

IGS. (2010). *Tracking Network*. (IGS) Retrieved 03 2015, from http://igscb.jpl.nasa.gov/network/netindex.html

IGS. (2011). *International Global Navigation Satellite Systems Service Multi-GNSS Experiment - Call for participation*. Retrieved from ftp://igs.org/pub/resource/pubs/IGS%20M-GEX%20VF.pdf

IGS. (2013). *RINEX The Receiver Independent Exchange Format - Version 3.02.* Retrieved April 2015, from ftp://igs.org/pub/data/format/rinex302.pdf

IGS. (2017). *Charter for IGS Analysis Centers and Associate Analysis Centers*. Retrieved 2019, from https://kb.igs.org/hc/en-us/articles/202346467-Charter-for-IGS-Analysis-Centers-and-Associate-Analysis-Centers

IGS. (2017b). *Strategic Plan 2013-2016*. Retrieved from https://kb.igs.org/hc/en-us/articles/201747733-Strategic-Plan-2013-2016

IGS. (2018). *The Multi-GNSS Working Group*. Retrieved 2019, from http://mgex.igs.org/IGS_MGEX_MGWG.php

IGS. (2019). *Final Orbits (AC solutions compared to IGS Final)*. Retrieved from acc.igs.org/media/Gmt_sum_final_all_orb_smooth_ALL.gif

IGS Central Bureau. (2013). International GNSS Service strategic plan 2013-2016. *Tech. Report., Jet Propulsion Laboratory*.

IGS/MGEX. (2019). *MGEX Product Analysis*. Retrieved from http://mgex.igs.org/analysis/

Kouba, J. (2008). A simplified yaw-attitude model for eclipsing GPS satellites. *GPS Solutions, 13*, 1-12. doi:10.1007/s10291-008-0092-1

Kouba, J. (2009). *A GUIDE TO USING INTERNATIONAL GNSS SERVICE (IGS) PRODUCTS.* Retrieved 2019, from http://acc.igs.org/UsingIGSProductsVer21.pdf

Laurichesse, D., & Mercier, F. (2007). Integer ambiguity resolution on undifferenced GPS phase measurements and its application to PPP. *ION GNSS 2007 20th international technical meeting of the satellite division, 25-28 Sept 2007*, (pp. 839-848). Fort Worth, TX.

Laurichesse, D., Mercier, F., Berthias, J., Broca, P., & Cerri, L. (2009). Integer ambiguity resolution on undifferenced GPS phase measurements and its application to PPP and satellite precise orbit determination. *Navigation, Journal of the Institute Of Navigation, 2*, 135-149.

Lescarmontier, L., Legrésy, B., Coleman, R., Perosanz, F., Mayet, C., & Testut, L. (2012). Vibrations of Mertz Glacier ice tongue, East Antarctica. *Journal of Glaciology, 58*(210), pp. 665-676, doi: 10.3189/2012JoG11J089.

Li, X., Li, X., Yuan, Y., Zhang, K., Zhang, X., & Wickert, J. (2017). Multi-GNSS phase delay estimation and PPP ambiguity resolution: GPS, BDS, GLONASS, Galileo. *Journal of Geodesy, 92*(6), pp. 579-608. doi:10.1007/s00190-017-1081-3

Loyer, S., Perosanz, F., Mercier, F., Capdeville, H., & Marty, J. (2012). Zero-difference GPS ambiguity resolution at CNES-CLS IGS analysis center. *Journal of Geodesy*, 991-1003. doi:10.1007/s00190-012-0559-2

Loyer, S., Perosanz, F., Versini, L., Katsigianni, G., Mercier, F., & Mezerette, A. (2018, Oct.). *CNES/CLS IGS Analysis center: recent activities, Poster at IGS Workshop 2018.* Retrieved from http://www.igs.org/assets/pdf/IGSWS-2018-PS01-03.pdf

Marty, J. C. (2013). Algorithmic documentation of the GINS software. Retrieved from http://grgs.obs-mip.fr/recherche/logiciels

Melbourne, W. (1985). The case for ranging in GPS based geodetic system. *1st international symposium on precise positioning with the global positioning system. U.S. Department of Commerce*, (pp. 373-386). Rockville, MD.

Mercier, F., & Laurichesse, D. (2007). Receiver/Payload hardware biases stability requirements for undifferenced Widelane ambiguity blocking. *Scientific and fundamental aspects of the Galileo program.* Toulouse, France.

Montenbruck, O., Hauschild, A., & Hessels, U. (2011). Characterization of GPS/GIOVE sensor stations in the CONGO network. *GPS Solutions, 15*(3), pp. 193–205, doi: 10.1007/s10291-010-0182-8.

Montenbruck, O., Steigenberger, P., Prange, L., Deng, Z., Zhao, Q., Perosanz, F., Romero, I., Noll, C., Stürze, A., Weber, G., Schmidt, R., MacLeod, K., & Schaer, S. (2017). The Multi-GNSS Experiment (MGEX) of the International GNSS Service (IGS) - Achievements, prospects and challenges. *Advances in Space Research, 59*(7), 1671-1697. doi:10.1016/j.asr.2017.01.011

NOAA. (2018). *What is geodesy?* Retrieved 2019, from https://oceanservice.noaa.gov/facts/geodesy.html

Odijk, D., Teunissen, P., & Huis, L. (2012). First results of mixed GPS+GIOVE single-frequency RTK in Australia. *Journal of Spatial Science, 57*(1), pp. 3-18, doi: 10.1080/14498596.2012.679247.

Paziewski, J., & Wielgosz, P. (2015). Accounting for Galileo–GPS inter-system biases in precise satellite positioning. *Journal of Geodesy, 89*, pp. 81-93, doi: 10.1007/s00190-014-0763-3.

Petit, G., Kanj, A., Loyer, S., Delporte, J., Mercier, F., & Perosanz, F. (2015). 1 x 10^-16 frequency transfer by GPS PPP with integer ambiguity resolution. *Metrologia, 52*, pp. 301-309. doi:10.1088/0026-1394/52/2/301

Remondi, B. (1985). PERFORMING CENTIMETER-LEVEL SURVEYS IN SECONDS WITH GPS CARRIER PHASE: INITIAL RESULTS. *NAVIGATION, Journal of The Institute of Navigation, 32*(4), pp. 386-400.

Sośnica, K., Prange, L., Kaźmierski, K., Bury, G., Drożdżewski, M., Zajdel, R., & Hadas, T. (2017). Validation of Galileo orbits using SLR with a focus on satellites launched into incorrect orbital planes. *Journal of Geodesy*, 131-148. doi:10.1007/s00190-017-1050-x

Steigenberger, P., Hugentobler, U., Loyer, S., Perosanz, F., Prange, L., Dach, R., Uhlemann, M., Gendt, G., & Montenbruck, O. (2014). Galileo orbit and clock quality of the IGS Multi-GNSS Experiment. *Advances in Space Research*. doi:10.1016/j.asr.2014.06.030

Teunissen, P., & Montenbruck, O. (2017). *Handbook of Global Navigation* (ISBN: 978-3-319-42926-7 ed.). Springer. doi:10.1007/978-3-319-42928-1

Uhlemann, M., Gendt, G., Ramatschi, M., & Deng, Z. (2016). GFZ global multi-GNSS network and data processing results. *IAG 150 Years*, 673-679. doi:10.1007/1345_2015_120

UN. (2012). *United Nations Programme on Space Applications.* Retrieved from http://www.unoosa.org/pdf/publications/ST_SPACE_52_Rev1.pdf

UN. (2018). *European GNSS and Earth Observation: A promising convergence for sustainable development.* Retrieved from https://www.gsa.europa.eu/newsroom/news/european-gnss-and-earth-observation-promising-convergence-sustainable-development

UN. (2019). *UN-GGIM: Aims and Objectives*. Retrieved from http://ggim.un.org

UN. (n.d.). *The Sustainable Development Agenda*. Retrieved 2019, from https://www.un.org/sustainabledevelopment/development-agenda/

US Department of Transportation. (2008). *GLOBAL POSITIONING SYSTEM WIDE AREA AUGMENTATION SYSTEM (WAAS) PERFORMANCE STANDARD.* Retrieved 2019, from https://www.gps.gov/technical/ps/2008-WAAS-performance-standard.pdf

Verhagen, S. (2005). *The GNSS integer ambiguities: estimation and validation.* Delft: NCG, Nederlandse Commissie voor Geodesie, Netherlands Geodetic Commission, 2005. Retrieved from https://repository.tudelft.nl/islandora/object/uuid:07c6f2be-3a70-42aa-97b3-894a5770454d/datastream/OBJ

Wübbena, G. (1985). Software developments for geodetic positioning with GPS using TI-4100 code and carrier measurements. *1st international symposium on precise positioning with the global positioning system. U.S. Department of Commerce*, (pp. 403-412). Rockville, MD.

Xia, F., Ye, S., Xia, P., Zhao, L., Jiang, N., Chen, D., & Hu, G. (2018). Assessing the latest performance of Galileo-only PPP and the contribution of Galileo to Multi-GNSS PPP. *Advances in Space Research, 63*(9), pp. 2784-2795. doi:10.1016/j.asr.2018.06.008

Xiao, G., Li, P., Sui, L., Heck, B., & Schuh, H. (2019). Estimating and assessing Galileo satellite fractional cycle bias for PPP ambiguity resolution. *GPS Solutions, 23*(3). doi:10.1007/s10291-018-0793-z

Zajdel, R., Sośnica, K., & Bury, G. (2017). A new online service for the validation of Multi-GNSS orbits using SLR. *Remote Sensing*. doi:10.3390/rs9101049

Zumberge, J., Heflin, M., Jefferson, D., Watkins, M., & Webb, F. (1997, March 10). Precise point positioning for the efficient and robust analysis of GPS data from large networks. *Journal of Geophysical Research*(102), pp. 5005-5017. doi:0148-0227/97/96JB-03860$09.00

Table of Figures

Table of Tables

Appendix I

In this appendix they are presented two examples of AR matrices solution comparison method. For simplicity, these examples represent 3x3 matrices (i.e. 3 satellites and 3 stations, hence 9 common passes) and no 'gaps' as explained in Fig. 5.20.

Example 1

Let us assume that we have a matrix C (3x3) (for simplicity- it is the same for bigger matrices), that 'agrees with' a zero matrix. We then define elements -integer non-zero numbers- a, b, c, d, e and f where a<b<c<d<e<f (also for simplicity, the order can be changed without changing the result).

We will count the number of non-zero elements and the number of zero elements at the end of every loop. We will stop the iterations when C can no longer be changed (i.e. $C_n = C_{n-1}$)[9] and when the percentage of non-zero values (P value) is not changing. The arrows help to indicate at which row or column is done the processing.

C=

a+d	a+e	a+f
b+d	b+e	b+f
c+d	c+e	c+f

C_0:
9 non-zero elements
0 zero elements

C=

a+d-(a+d)=0	a+e-(a+d)	a+f-(a+d)
b+d	b+e	b+f
c+d	c+e	c+f

8 non-zero elements
1 zero element

[9] The n index is showing the iteration number.

C=

0	e-d	f-d
b+d-(b+d)=0	b+e-(b+d)	b+f-(b+d)
c+d	c+e	c+f

7 non-zero elements
2 zero element

C=

0	e-d	f-d
0	e-d	f-d
c+d-(c+d)=0	c+e-(c+d)	c+f-(c+d)

6 non-zero elements
3 zero element

C=

0	e-d	f-d
0	e-d	f-d
0	e-d	f-d

6 non-zero elements
3 zero element

C=

0	e-d-(e-d)=0	f-d
0	e-d-(e-d)=0	f-d
0	e-d-(e-d)=0	f-d

3 non-zero elements
6 zero element

C=

0	0	f-d-(f-d)=0
0	0	f-d-(f-d)=0
0	0	f-d-(f-d)=0

C_1:
0 non-zero elements
9 zero element

After C_1 the matrix cannot change anymore (i.e. if we perform C_2 it will be equal to C_1) and is a zero matrix. This is the final solution: P=0%

Example 2

Let us assume now that we have a matrix C (3x3) that does not 'agree with' a zero matrix. Now, we will be substitute random elements and we will put x and y elements that do not agree with (x≠b+f , y≠c+e).

C=

a+d	a+e	a+f
b+d	b+e	x
c+d	y	c+f

C_0:
9 non-zero elements
0 zero elements
P=100%

C=

a+d-(a+d)=0	a+e-(a+d)	a+f-(a+d)
b+d	b+e	x
c+d	y	c+f

8 non-zero elements
1 zero elements

C=

0	e-d	f-d
b+d-(b+d)=0	b+e-(b+d)	x-(b+d)
c+d	y	c+f

7 non-zero elements
2 zero elements

C=

0	e-d	f-d
0	e-d	x-(b+d)
c+d-y	y-y=0	c+f-y

6 non-zero elements
3 zero elements

C=

0	e-d	f-d
0	e-d	x-(b+d)
c+d-y	0	c+f-y

6 non-zero elements
3 zero elements
no changes

C=

0	e-d-(e-d)=0	f-d
0	e-d-(e-d)=0	x-(b+d)
c+d-y	0-(e-d)	c+f-y

5 non-zero elements
4 zero elements

C=

0	0	f-d-(c+f-y)
0	0	x-(b+d)-(c+f-y)
c+d-y	d-e	c+f-y-(c+f-y)=0

C_1:
4 non-zero elements
5 zero elements
$C_1 \neq C_0$: the process continues

C=

0	0	f-d-(c+f-y)
0	0	x-(b+d)-(c+f-y)
c+d-y	d-e	0

4 non-zero elements
5 zero elements
no changes

C=

0	0	f-d-(c+f-y)
0	0	x-(b+d)-(c+f-y)
c+d-y	d-e	0

4 non-zero elements
5 zero elements
no changes

C=

0	0	f-d-(c+f-y)
0	0	x-(b+d)-(c+f-y)
c+d-y-(d-e)	d-e-(d-e)=0	0-(d-e)

4 non-zero elements
5 zero elements

C=

0	0	f-d-(c+f-y)
0	0	x-(b+d)-(c+f-y)
c-y+e	0	e-d

4 non-zero elements
5 zero elements
no changes

C=

0	0	f-d-(c+f-y)
0	0	x-(b+d)-(c+f-y)
c-y+e	0	e-d

4 non-zero elements
5 zero elements
no changes

C=

0	0	f-d-(c+f-y)-(e-d)
0	0	x-(b+d)-(c+f-y)-(e-d)
c-y+e	0	e-d-(e-d)=0

C_2:
3 non-zero elements
6 zero elements
$C_2 \neq C_1$: the process continues

For the following iterations only the ones that do change the matrix are shown for brevity. The arrows help to show were the change is happening and to which row or column the processing takes place. The order of row and column changes is kept the same.

C=

0	0	y-e-c-(y-e-c)=0
0	0	x-b-c-f+y-e-(y-e-c)
c-y+e	0	0-(y-e-c)

C_3:
3 non-zero elements
6 zero elements
$C_3 \neq C_2$: the process continues

C=

0	0	0
0	0	x-b-f
c-y+e-(c-y+e)=0	0-(c-y+e)	c-y+e-(c-y+e)=0

C_4:
2 non-zero elements
7 zero elements
$C_4 \neq C_3$: the process continues

After C_4 the matrix transformation continues. There are no changes in the next transformation for any row or column. The C_5 matrix is made as:

C=

0	0	0
0	0	x-(b+f)=x’
0	y-(c+e)=y’	0

C_5:
2 non-zero elements
7 zero elements
$C_5 = C_4$: the process stops
P=22%

If we define: x’= x-(b+f) and y’= y-(c+e), we observe that the non-zero values are at the exact same places in the matrix in the beginning at C_0, therefore we can know the places of the disagreements. Another remark is that the values x’ and y’ show the difference (in integers) with respect to the C matrix that transforms to a zero matrix (see in Example 1: x and y substitute b+f and c+e respectively). These two properties are very useful in practice to examine where and by how much AR differences are occurring and to identify potential problems (e.g. when a particular station or satellite has elevated P% of disagreements).

Generalization

This processing is the same for any kind of size of matrix consisting of any kind of integer numbers. The general case can be written adding together Latin alphabet characters in the columns and Greek alphabet characters in the lines. The following notation example assumes that characters are non-zero.

C=

a+α	a+β	a+γ	a+δ	…	…	a+θ	…	…	a+ω
b+α	b+β	b+γ	b+δ	…	b+η	…	…	…	b+ω
c+α	c+β	c+γ	c+δ	…	…	…	c+ι	…	c+ω
…	…	…	…	…	…	…	…	…	…
z+α	z+β	z+γ	z+δ	…	…	…	z+ι	…	z+ω

C_0:

zxω non-zero elements

0 zero elements

After completing the first iteration (**$C_{0,5}$**) for the lines we will have at least one zero in every line. Therefore, the non-zero elements will be minimum (zxω–z). Note that the Latin numbers vanish.

C=

α-θ	β-θ	γ-θ	δ-θ	…		0		…	ω-θ
α-η	β-η	γ-η	δ-η	…	0			…	ω-η
α-ι	β-ι	γ-ι	δ-ι	…			0	…	ω-ι
…									…
α-ι	β-ι	γ-ι	δ-ι	…			0	…	ω-ι

$C_{0,5}$:

(zxω-z) non-zero elements

z zero elements

After completing the columns (**C_1**) we will have at least (zxω–ω) respectively. Consequently, most of the letters will be eliminated until the transformation cannot continue any further. This proves that after any finished transformation the total number of non-zero elements is either eliminated (i.e. the transformation must continue) or the same as the previous iteration (i.e. the transformation is completed).

Appendix II

In this appendix it is presented the general noise computations used in GNSS processing when forming linear combinations. The errors are calculated by extracting the noise amplification factors (Hugentobler, 2013).

In GNSS processing linear combinations are used to generate new observables. The general linear combination (O_3) among two observables (O_1, O_2) is written as:

$$O_3 = \alpha_1 O_1 + \alpha_2 O_2 \tag{AII.1}$$

using coefficients α_1 and α_2. Without restrictions, it may be defined that these coefficients fulfill the following condition:

$$\alpha_1 + \alpha_2 = 1 \tag{AII.2}$$

The noise of the amplification factors is then calculated as follows:

$$\sigma(O_3) = \sqrt{(\alpha_1 \sigma(O_1))^2 + (\alpha_2 \sigma(O_2))^2} \tag{AII.3}$$

In cases that we assume that the noise of O_1 and O_2 are similar (i.e. $\sigma(O)$) the previous equation becomes:

$$\sigma(O_3) = \sqrt{(\alpha_1)^2 + (\alpha_2)^2}\sigma(O) \tag{AII.4}$$

These are valid for every kind of linear combination of observations: with code, carrier phases, single differences, double differences, undifferenced etc.

Appendix III

`t` :observation type	`C` = pseudorange,	`L` = carrier phase,	`D` = doppler,	`S` = signal strength)
`n` :band / frequency	`1, 2,...,8`			
`a` : attribute	tracking mode or channel, e.g., `I`, `Q`, etc			

Appendix A: Observation code explanation (as given in Rinex 3.02) (IGS, 2013)

GNSS System	Freq. Band /Frequency	Channel or Code	Observation Codes			
			Pseudo Range	Carrier Phase	Doppler	Signal Strength
GPS	L1/1575.42	C/A	C1C	L1C	D1C	S1C
		L1C (D)	C1S	L1S	D1S	S1S
		L1C (P)	C1L	L1L	D1L	S1L
		L1C (D+P)	C1X	L1X	D1X	S1X
		P	C1P	L1P	D1P	S1P
		Z-tracking and similar (AS on)	C1W	L1W	D1W	S1W
		Y	C1Y	L1Y	D1Y	S1Y
		M	C1M	L1M	D1M	S1M
		codeless		L1N	D1N	S1N
	L2/1227.60	C/A	C2C	L2C	D2C	S2C
		L1(C/A)+(P2-P1) (semi-codeless)	C2D	L2D	D2D	S2D
		L2C (M)	C2S	L2S	D2S	S2S
		L2C (L)	C2L	L2L	D2L	S2L
		L2C (M+L)	C2X	L2X	D2X	S2X
		P	C2P	L2P	D2P	S2P
		Z-tracking and similar (AS on)	C2W	L2W	D2W	S2W
		Y	C2Y	L2Y	D2Y	S2Y
		M	C2M	L2M	D2M	S2M
		codeless		L2N	D2N	S2N
	L5/1176.45	I	C5I	L5I	D5I	S5I
		Q	C5Q	L5Q	D5Q	S5Q
		I+Q	C5X	L5X	D5X	S5X

Appendix B: Rinex 3.02 observation codes for GPS (IGS, 2013)

GNSS System	Freq. Band /Frequency	Channel or Code	Observation Codes			
			Pseudo Range	Carrier Phase	Doppler	Signal Strength
Galileo	E1 / 1575.42	A PRS	C1A	L1A	D1A	S1A
		B I/NAV OS/CS/SoL	C1B	L1B	D1B	S1B
		C no data	C1C	L1C	D1C	S1C
		B+C	C1X	L1X	D1X	S1X
		A+B+C	C1Z	L1Z	D1Z	S1Z
	E5a / 1176.45	I F/NAV OS	C5I	L5I	D5I	S5I
		Q no data	C5Q	L5Q	D5Q	S5Q
		I+Q	C5X	L5X	D5X	S5X
	E5b / 1207.140	I I/NAV OS/CS/SoL	C7I	L7I	D7I	S7I
		Q no data	C7Q	L7Q	D7Q	S7Q
		I+Q	C7X	L7X	D7X	S7X
	E5(E5a+E5b) / 1191.795	I	C8I	L8I	D8I	S8I
		Q	C8Q	L8Q	D8Q	S8Q
		I+Q	C8X	L8X	D8X	S8X
	E6 / 1278.75	A PRS	C6A	L6A	D6A	S6A
		B C/NAV CS	C6B	L6B	D6B	S6B
		C no data	C6C	L6C	D6C	S6C
		B+C	C6X	L6X	D6X	S6X
		A+B+C	C6Z	L6Z	D6Z	S6Z

Appendix C: Rinex 3.02 observation codes for Galileo (IGS, 2013)